Alexander Schnabel, BSc

Material Compatibility Studies for Low Temperature PEM-FC Subsystems

MASTERARBEIT

zur Erlangung des akademischen Grades
Diplom-Ingenieur
Masterstudium Technische Physik

eingereicht an der
Technischen Universität Graz

Betreuer:
Ao.Univ.-Prof. Dipl.-Ing. Dr.techn. tit.Univ.-Prof. Günther Leising
Institut für Festkörperphysik

Graz, Juni 2016

ACKNOWLEDGEMENT

This Master Thesis was carried out at AVL List GmbH and at the Institute of Solid State Physics, Graz University of Technology.

I would like to thank my supervisor Prof. Günther Leising for his great advise and support.

For AVL, I would like to address special thanks to Tomas Dehne for his kind support and thank Susanne Mahler and her team from the chemistry lab for support.

Alexander Schnabel

Eidesstattliche Erklärung

Ich erkläre an Eides statt, dass ich die vorliegende Arbeit selbstständig verfasst, andere als die angegebenen Quellen/Hilfsmittel nicht benutzt, und die den benutzten Quellen wörtlich und inhaltlich entnommenen Stellen als solche kenntlich gemacht habe. Das in TUGRAZonline hochgeladene Textdokument ist mit der vorliegenden Masterarbeit identisch.

Graz, am _____ _____

Datum Unterschrift

Contents

1 Introduction

Low Temperature Polymer Electrolyte Membrane Fuel Cell (LT-PEM-FC) systems are the most suitable candidates for electrical energy sources for mobile applications. Some of their advantages are: high power density, rapid start-up, high efficiency, good transient response, the absence of corrosive liquid electrolytes and low operating temperature [1, 2]. However, there are still significant physical and chemical questions to be clarified especially concerning performance degradation of fuel cell systems over time. Contaminants which can be leached out of system materials by gas/water streams or be produced by corrosion of metallic components can reduce the performance of the fuel cell system or lead to safety issues.

To face the safety topic that is related to the coolant conductivity a test system for material compatibility for the coolant circuit of a LT-PEM-FC was built up, which was conducted at AVL List GmbH. Further optimization and evaluation of this test system was needed and this was the initial motivation for this thesis. The *fundamental part* includes basics of LT-PEM-FCs and typical system design for automotive applications. Sources and effects of contaminants on LT-PEM-FCs related to the coolant circuit and to the gas circuits are discussed. After basics of conductivity measurements and conductivity effects in aqueous solutions, a model for calculation of CO_2 induced conductivity increase in pure water under various conditions is presented. In the *experimental part* the design of the test system, measurement procedure and evaluation method are described. An analysis of the reference measurements in combination with aftertreatment of possible ion sources in the system is carried out. This also includes employment of a CO_2 degassing procedure. Evaluation of the testbed with reference materials is performed. It includes analysis of leachant solutions and mass loss determination of the samples. This experiments are complemented by various leaching tests, degassing tests, corrosion tests and optical investigation of sample surfaces. An outlook is given towards a possible test system for material compatibility for the gas circuits of a LT-PEM-FC system.

2 Fundamentals

2.1 Function principle of a PEMFC

A fuel cell is a galvanic cell which directly converts chemical energy to electrical energy (DC electricity). This also is true for a battery in discharge mode. The main difference between batteries and fuel cells is that in batteries the conversion and the fuel storage happens at the same place within the cell. In a fuel cell the storage and conversion are separated, the fuel is permanently supplied from external sources. In fuel cells oxidation of hydrogen and reduction of oxygen happens at the electrodes which are not undergoing chemical changes in normal operation. In batteries diffusion of ions changes the electrodes in chemical composition. The following reactions happen at the anode and the cathode at the same time

$$2\,H_2 \longrightarrow 4\,H^+ + 4\,e^- \tag{1}$$

$$O_2 + 4\,H^+ + 4\,e^- \longrightarrow 2\,H_2O \tag{2}$$

and the overall reaction is therefore

$$2\,H_2 + O_2 \longrightarrow 2\,H_2O \tag{3}$$

The difference to the classical oxyhydrogen reaction is that the oxidation of hydrogen and the reduction of oxygen are spatially separated. No direct electron transfer takes place [3]. This separation is realized by the electrolyte which is also the distinguishing feature of different fuel cell types. In case of the polymer electrolyte membrane fuel cell (PEMFC) this electrolyte is a proton (H^+) conducting polymer. In Figure 1 the basic principle of a PEMFC with air as oxygen source is shown. The reactions in Equation 1 and 2 happen at the interface of the H^+ conducting membrane (electrolyte), the catalyst particles and the electrically conductive electrode. Electrons are forced to take the path over an external circuit because the membrane is electrically insulating. Hydrogen ions travel through the membrane and combine with the reduced oxygen to produce water. Water, excess oxygen and nitrogen are removed by the air stream at the cathode side. Also heat is generated by entropic heat of reactions. The irreversible heat of electrochemical reactions, heat from the ohmic resistances and condensation of water vapor [4, 1].

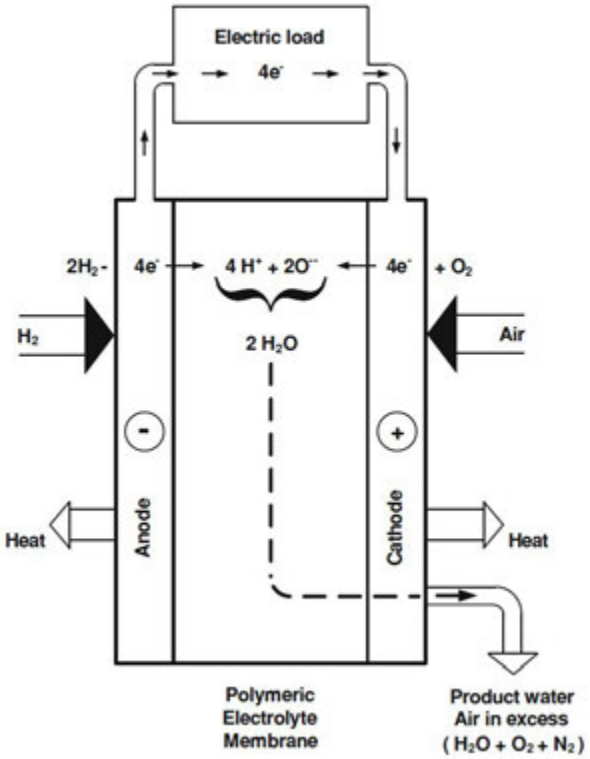

Figure 1: PEM fuel cell - basic principle [5]

2.1.1 Thermodynamics

To show possible efficiencies of a fuel cell some thermodynamic aspects are discussed. The change of Gibbs free-energy equals the maximum useful work (electricity output) from reaction, because in an electrochemical reaction no expansive work $P\Delta V$ is involved. Therefore it can be associated with an electrochemical potential E by

$$\Delta G = -nFE \tag{4}$$

where n is the number of exchanged electrons and F is the Faraday constant (96 500 As/mol). The energy entering the reaction corresponds to the enthalpy, also called the *heating value* of hydrogen. This depends on the physical state after the reaction where the *upper heating value* (UHV) corresponds to product water in the liquid phase and the *lower heating value* (LHV) to the gaseous phase [5, 3]:

$$\text{UHV: } H_2 + \tfrac{1}{2}\,O_2 \longrightarrow H_2O(l) \;.....\Delta H_{UHV}\text{=-285.8 kJ/mol}$$
$$\text{LHV: } H_2 + \tfrac{1}{2}\,O_2 \longrightarrow H_2O(g) \;.....\Delta H_{LHV}\text{=-241.8 kJ/mol}$$

The maximum theoretical cell voltage is E^0 =1.23 V which can be calculated via Equation 4 and the change in free energy at 25 °C and 1 atm ΔG^0=−237.4 kJ/mol. The

total thermal energy available is ΔH. From the Gibbs-Helmholtz equation the relation between ΔG and ΔH can be obtained

$$\Delta G = \Delta H - T\Delta S \tag{5}$$

The entropic heat ΔS is representative of the entropy change of the electrochemical reaction which has to be removed (or supplied when the sign is positive) [4]. It is the part of chemical energy that cannot converted to useful work. As entropy of the overall reaction (Equation 3) is negative ΔG gets less negative, therefore available electrical output is reduced. The equation also indicates that the theoretical potential is reduced when temperature is increased, but thermodynamic parameters do not change significantly up to 100 °C which is not exceeded by low temperature PEM fuel cells (see below).

Efficiencies

The *theoretical efficiency* η_{th} can be calculated by the relation of useful output energy to input of chemical energy (related to the upper heating value)

$$\eta_{th} = \frac{\Delta G}{\Delta H} = \frac{237.4}{285.8} = 83\,\% \tag{6}$$

it describes a situation with infinitesimal small current which plays no role practically. A more realistic value is the *electrical efficiency* η_{el} which takes into account the dependence of cell voltage on current drawn

$$\eta_{el} = \frac{E(j)}{\frac{-\Delta H}{zF}} \tag{7}$$

where polarization losses[1] are included in E(j). It is usually related to the lower heating value (LHV) to be comparable to other systems like the internal combustion engine [3]. Peak efficiencies of PEM fuel cell stacks can be up to 70 % (LHV).

2.1.2 Main cell components

In Figure 2 the main components of a PEM fuel cell are shown. The combination of the polymer membrane with the catalyst layer and the gas diffusion layer is called membrane electrode assembly (MEA). The latter is sandwiched between two bipolar plates which act as current collectors. In case of a multicell configuration (fuel cell stack), it connects

[1]Different kinds of polarization- or voltage losses occour in fuel cells: (1) Kinetics of the electrochemical reactions, (2) Internal electrical and ionic resistance, (3) Difficulties in getting the reactants to reaction sites, (4) Internal (stray) currents, (5) Crossover of reactants [6]

the anode from one cell to the cathode of the adjacent cell. Also channels for gas flow are provided by the bipolar plates.

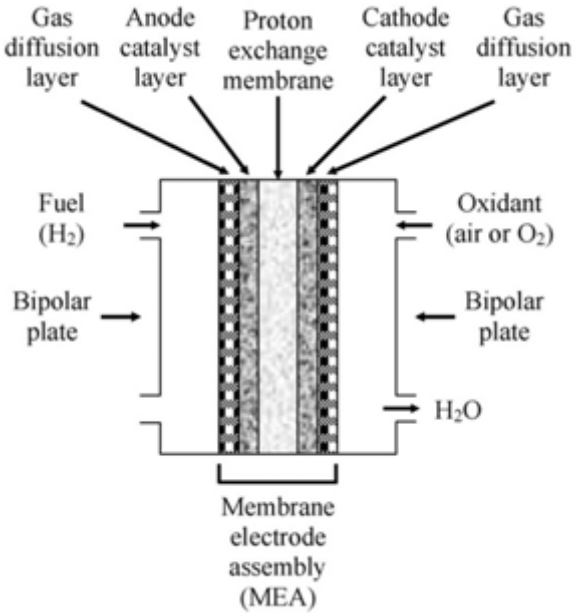

Figure 2: PEM fuel cell - membrane electrode assembly [7]

Membrane

The heart of a PEM fuel cell is the polymer electrolyte membrane. Beside its ability to transfer protons from the anode to the cathode it has to be chemically and physically stable in the PEM fuel cell environment [6, 5]. Typically these membranes are made of *perfluorocarbonsulfonic acid* (PSA), which is a copolymer of tetrafluorethylene (TFE) and various types of of perfluorosulfonate monomers. Nafion^{TM} (DuPont) is the most well-known membrane material, see Figure 3(a). The PTFE like backbone is responsible for good chemical and mechanical stability next to its highly hydrophobic characteristics. The ionic bound SO_3H groups are highly hydrophilic and tend to cluster within the hydrophobic regions leading to "water channels" within the membrane (if sufficient water is present).

The transport of protons in these membranes is shown by the simplified picture in Figure 3(b) and is assumed to be carried out by (i) surface diffusion mechanism occurring close to the pore wall (low water activity), (ii) a bulk diffusion where the protons diffuse predominantly via the Grotthuss mechanism[2] (high water activity), but (iii) the H_3O^+

[2]This **proton transport mechanism** is described in Section 2.4.3

ion also undergoes traditional mass diffusion (*en masse* diffusion) [8]. The mobility of protons in the "bulk water" phase is much higher than in the "surface water" phase [8]. Conductivity is a strong function of water content of the membrane which ranges between 0.01 S/cm and 0.2 S/cm for hydrated membranes [5], which further means that stack performance depends on the proper humidification of the membrane.

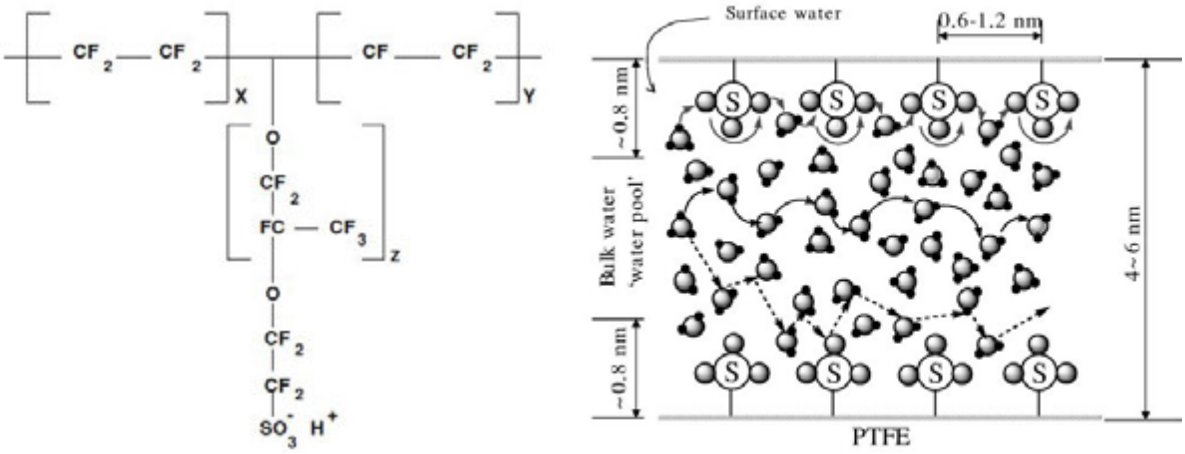

(a) Structure of PFSA polymer [5]

(b) Proton transport in Nafion [8]

Figure 3: Structure and charge transport of Nafion membranes

2.1.3 Operating conditions

Typical operating conditions for low temperature PEM fuel cells are shown in Table 1 which are only briefly discussed. These values are rather typical values than strict boundaries. Of course the stoichiometric ratios (reactant flow rate provided/consumption rate by reaction) have to be appropriate to provide sufficient fuel. As pressure increases the cell potential increases. Also with increasing temperature the cell potential increases (although theoretical cell potential decreases) up to an optimum temperature which is between 60 °C and 80 °C for most membrane types of low temperature PEM fuel cells [6, 3, 1]. At higher temperatures catalyst- and membrane degradation can reduce stack performance while lower temperatures negatively influence reaction kinetics and may lead to flooding by condensation. Also humidification of both reactants can be necessary to maintain high proton conductivity as mentioned above.

Table 1: Typical PEM fuel cell operating conditions [6]

Operating parameter	Typical ranges
Pressure	H_2/Air: Ambient to 4 bar
Temperature	50 °C to 90 °C
Stoichiometric ratio	H_2: 1 to 1.2
	O_2: 1.2 to 1.5
	Air: 1.6 to 2.5
Humidity of reactants	H_2: 0 % to 125 %
	O_2/Air: 0 % to 100 %

2.2 LT-PEM fuel cell systems for automotive applications

A fuel cell system (FCS) is the combination of a fuel cell stack with all components needed to generate electricity. These subsystems are called balance of plant (BOP). In Figure 4, a general scheme of an automotive FCS with its interfaces to environment is shown. It further indicates that generated water and heat are partly recovered and that the subsystems need to optimize stack operation in terms of reactant feeding, temperature control and humidification [6, 9]. As discribed in Section 2.1.2 and 2.1.3 proper humidification and temperature level significantly influence stack performance.

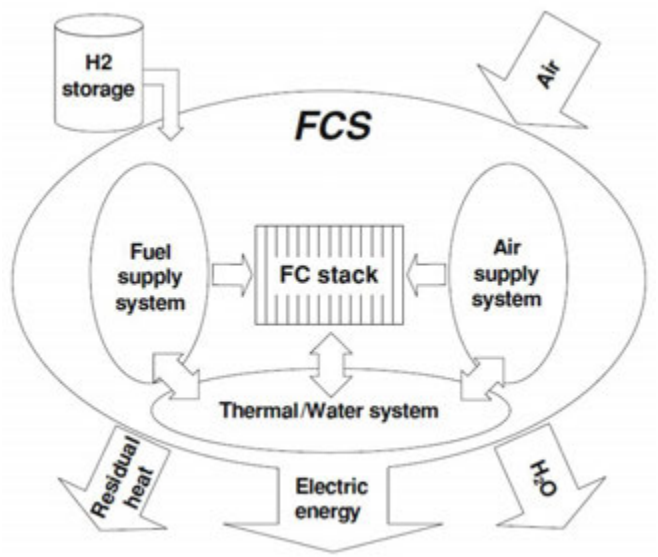

Figure 4: General scheme of a PEMFC system for vehicles [9]

A flow schematic of an up-to-date PEM fuel cell system configuration can be seen in Figure 5. This system does not reflect the design of any manufacturer but it is a selection of various designs [10].

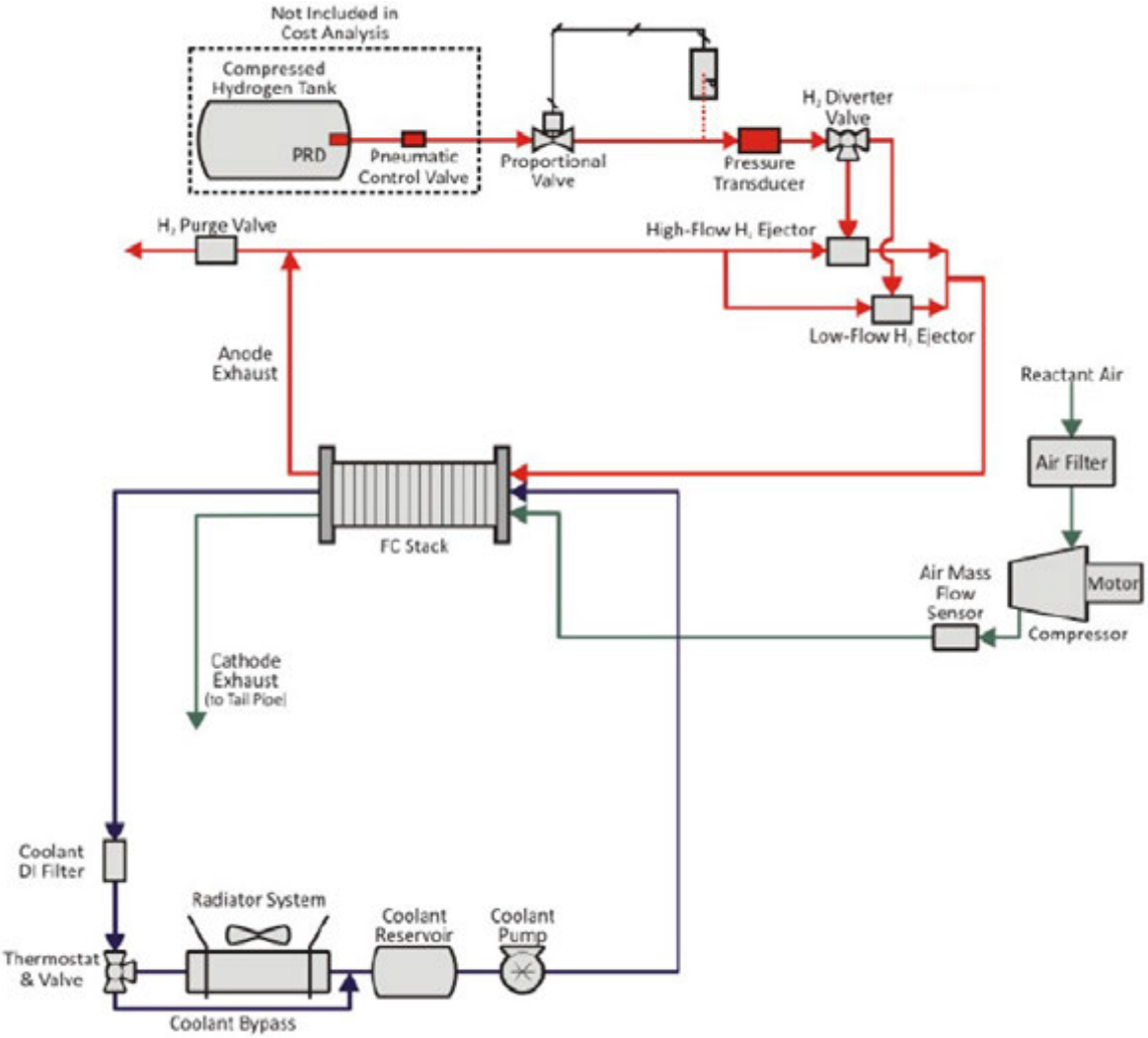

Figure 5: Flow schematic of an automotive PEMFC system [10]

2.2.1 Gas circuits

The Hydrogen is stored in a pressurized tank (e.g. 5.64 kg hydrogen at 70 MPa for the Hyundai ix35 Fuel Cell from 2015). The pressure usually is reduced in a first step to about 2 MPa to 3 MPa and in a second step to hydrogen supply pressure which is typically up to 1 MPa. Finally the hydrogen is injected into the anode of the stack at up to 0.3 MPa. In this system the hydrogen is supplied in *recirculation mode*[3] where recirculation is realized by two ejectors (high-flow and low-flow). The anode compartment needs to be periodically purged to remove accumulated (i) nitrogen which diffuses from the cathode to the anode side, (ii) water droplets caused by critical operating con-

[3]Other possible supply modes would be *dead-end mode* or *flow-through mode* [6]

ditions and (iii) traces of impurities which are usually contained in (reformed) hydrogen.

The cathode side in this system is supplied with oxygen from air. To achieve the oxygen concentrations needed on the cathode surface at all load points a blower or compressor is needed [9]. If pressures higher than 0.2 MPa are needed an additional expander is used in some cases[4] to partly recover the energy of pressurized air [9]. The air used in a PEM fuel cell stack needs to be free of catalyst poisoning substances. Traces of contaminants (see Table 2) can reduce efficiency and durability, therefore oil free compressors and filtration are required.

2.2.2 Coolant circuit

As mentioned in Section 2.1 heat is created in a low temperature PEM fuel cell stack which needs to be removed. The temperature of the stack effects the water management. As described in Section 2.1.2, the proton conductivity of the membrane (and therefore fuel cell stack performance) depends the humidity level. The amount of generated water changes with the load point and the water content of the membrane further depends on pressure and humidity level of hydrogen and air. Therefore the temperature has to be adjusted to each load point. For powers of typical automotive systems ($\geq$ 80 kW electrical output power) this is usually done by liquid cooling. In these systems cooling is very challenging because of high power densities and the small temperature difference to ambient compared to internal combustion engines. Furthermore, heat removal by reactants and product streams is almost negligible, this means heat powers equal to the generated electrical power or even more have to be removed by the cooling system [1, 2]. This fact can be seen by the large radiators which are normally used in PEM fuel cell cars.

Keeping ionic content of coolant low

Additional efforts are needed for maintaining the conductivity of the coolant at a low level. This is a very important safety issue in operation of a PEM fuel cell car because the coolant is in permanent contact with life parts (bipolar plates) of the stack. Next to the use of large amounts of ion exchange resin, special coolants are used. It was reported that in mixtures of DI water and ethylene glycol with (special) antioxidant additives the amount of ion exchange resin can be reduced significantly [1]. Also other

[4]For automotive fuel cell systems it has to be evaluated if the increase in efficiency is enough to justify the extra space needed for the expander

alternative coolants were investigated like (i) nanoparticle based mixtures of glycol/DI water with the ability of self-deionizing, (ii) dielectric coolants like kerosenic hydrocarbon which don´t need ion exchange resin at all [1, 2]. Possible impacts of increased coolant conductivity are discussed in more detail in Section 2.3.2 because of being also part of the section about LT-PEM fuel cells and contamination.

2.3 LT-PEM fuel cell systems: Contamination

The contamination topic can be structured as shown in Figure 6. The solid filled parts denote the main focus of this work. A closer look will be taken on the contamination of the cooling circuit of a LT-PEM fuel cell system, the possible sources and impacts of contaminants will be discussed.

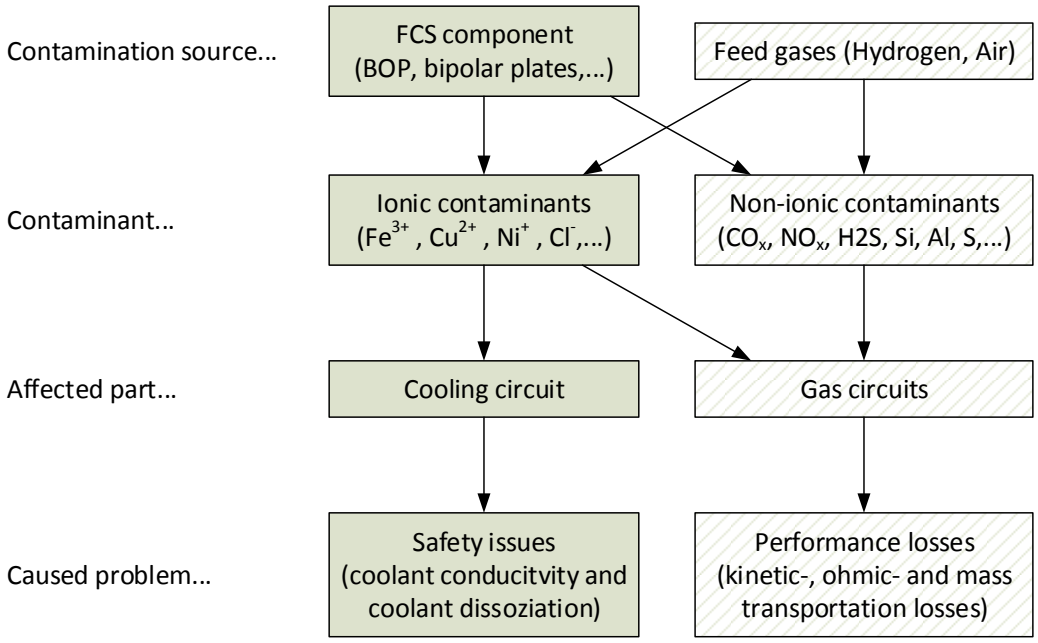

Figure 6: An overview of LT-PEM fuel cells and contamination; The main focus of this work is filled solid

The components and materials used in the cooling circuit and its ionic and non-ionic emissions will be a main point. Also the gas side contamination needs to be reviewed. On the one hand it gives a full picture of the contamination topic, on the other hand this work will close with an outlook towards a possible test system for the gas circuits (see Section 7).

2.3.1 Contamination sources

In Table 2 an overview of sources and possible contaminants can be seen. These species were reported to decrease the performance of LT-PEM fuel cell systems [7]. The ionic species which origin from components within the coolant loop are able to cause serious issues which will be described below.

Table 2: Overview of sources and common species known as PEM fuel cell contaminants [7]

Source	Contaminants
Air	NO_x, CO_x, SO_x, H_2S, O_3, and NH_3
Reformed hydrogen	CO, CO_2, H_2S and NH_3
Bipolar plates	Fe^{3+}, Cr^{3+}, Cu^{2+}, Ni^{2+}
Nafion® membrane	Na^{+}, Ca^{2+}
Gaskets	Si
Coolant, DI water	Si, Al, S, K, Fe, Cu, Cl, V, Cr
Battlefield emissions	SO_2, NO_2, CO, benzene, propane
Compressors	Oils

Balance of plant as contamination source

When designing a LT-PEM fuel system, great attention has to be payed on the material mix of the selected components. Beside the desired functional properties of all the used materials, their ability of emitting unwanted species has to be taken into account. Depending on the surface properties of these components and the environment (e.g. temperature, humidity, acidity,...) inside these components more or less contaminants can be leached out or be produced by physical or chemical effects.

As already mentioned the *leaching properties of polymers* are very important due to their widespread use. There is a huge variety of different additives used to achieve certain chemical or physical properties. These added materials can be divided into three main categories: Functional-, filling- and reinforcing materials [11]. In Table 3 common additives for polyamides (PA) are shown, which are widely used thermoplastics in the automotive industry.

For example the species Al, B, Si, and Ca are commonly found in glass fiber reinforcement additives (alumina borosilicate- and soda lime glasses). Additionally the monomer itself can emerge as contaminant. In case of the aliphatic polymer PA 6 the residual (after polymerization) monomer caprolactam and in the case of PA 66 the monomers hexamethylenediamine/adipic acid may be present [11]. For PA 6 the residual monomer acts as an efficient plasticizer. In Table 4 examples for identified leachants of automotive plastics are shown:

Corrosion of metallic components also plays an important role. Even at low corrosion rates which are acceptable from the mechanical point of view, ions are produced which can increase coolant conductivity (see Section 2.3.2) or change properties of the MEA [7]. Surface properties (e.g. roughness, composition) of stainless steels, especially at welded joints need to be considered carefully, proper treatment is mandatory to maintain corrosion resistance.

Table 3: A selection of additives in polyamides [11]

Category	Additive, Material	Property
Functional	Aromatic amines, Phosphite,	Antioxidants
	Hindered phenols (e.g. BHT)	Antioxidants
	Soot	UV-Stabilizer, Colour
	Organic pigments	Colour
	Antimony oxide, Melamine derivate,	Flame retardant
	Phosphates	Flame retardant
	Elastomers (e.g. EPDM, EVA)	Impact strengh
Filling	SiO_2, Chalk, Mica	Tensile strength, Hardness, Surface properties
	Metals (Al, Steel, Bronze, Pb, Zn, Cu, Ni)	Heat deflection temperature (HDT), Conductivity
Reinforcing	Glass fibre	Tensile strength , hardness , HDT, Creep resistance , Chemical- and hydrolysis resistance
	Carbon fibre	Anti-friction, thermal- and electrical conductivity

Table 4: Examples for identified leachants of standard automotive plastics. More polymer materials and details can be found in work [12, 13]

Material	Anions	Elements	Organics
PA, PPA, PBT	Cl^-, NO_2^-, NO_3^-,	Na, Si, B,	Caprolactam (-tetramer, -hexamer)
PPS, PSU	SO_4^{2-}, F^-	Ca, Al, K,	DCTDD, Benzoic Acid
		Cu, P	Nylon 6.10 cyclic dimer

Hydrogen as contamination source

The world wide purity "standard" for supplied hydrogen for the automotive PEM-FC application is 5.0, therefore almost no contaminants enter the anode at all. In the case of using hydrogen with less purity contaminants such as CO, CO_2, H_2S and NH_3 may be present. These contaminants come from the hydrogen production process, in which usually natural gas (CH_4) or hydrocarbons (C_xH_x) are reformed to a hydrogen-rich gas. This reformate usually consists of 40 % to 70 % H_2, 15 % to 25 % CO_2, 1 % to 5 % CO, traces of N_2, water vapor and sulfur compounds. As NH_3 is used as a tracer gas in natural gas pipelines, also NH_3 impurities can be found in the reformate [7].

Airborne contaminants

Normally, the oxygen of air is used to feed the fuel cell stack. For the cathode side possible contaminants are NO_x, SO_x, CO, CO_2, NH_3. These contaminants mainly origin from automotive and industrial exhaust gases.

Other contamination sources

Other possible contaminants come from fuel cell stack components like bipolar plates, seals and membranes. Here impurities like metal ions can be produced by corrosion of metallic stack components. Nonmetallic ions can be found which are connected to degradation mechanisms of the membrane. Silicon was identified as a contaminant which can be leached out of seals [7, 2]. Oxidation of ethylene glycol was reported to create ionic species [1, 2].

2.3.2 Impacts and mechanisms: cooling circuit

As already mentioned in Section 2.2.2, in an automotive LT-PEMFC system the cooling liquid is in permanent contact to live parts of the fuel cell stack. It passes the coolant channels within the bipolar plates, which usually have no insulating layer. In such vehicles electrical powers up to 150 kW and voltages in the range of 200 V to 500 V are common. This is an important safety issue in the operation of a PEM fuel cell car. Ion exchange resins are used to keep the conductivity low [1]. Temperatures up to 90 °C, high flow rates (e.g. 250 l/min) in combination with deionized (DI) water or glycol/DI water mixtures with low conductivities (lack of ions) are very inviting conditions for ions or other substances to get leached out and increase the coolant conductivity or the amount of non-ionic impurities. As mentioned above degradation of ethylene glycol was also found to increase coolant conductivity [1, 2]. If the coolant becomes electrically conductive leakage currents start to flow and the following problems can occur [1]:

1. *Charging of components* which are in contact to the cooling loop (safety issue)
2. *Coolant electrolysis* (safety issue)
3. *Reduced stack efficiency*
4. *Degradation of bipolar plates*

Therefore its conductivity has to be monitored and maintained low, which means below 100 μS/cm [2]. A typical upper limit for an automotive LT-PEMFC system is at 20 μS/cm. If the conductivity is higher, the safety system has to turn off the car.

2.3.3 Impacts and mechanisms: gas circuits

Due to operating conditions such as temperatures from 50 °C to 90 °C and humidities up to 125 % (see Table 1), LT-PEM fuel cells are very susceptible for contamination. Impurities in the feed streams can reduce the durability of PEMFCs significantly. Table 2 shows an overview of sources and possible contaminants which can be present at the gas streams. All the contamination processes happen at the MEA by influencing its hydrophobicity or hydrophilicity, reducing active surface area of the catalyst layer, modifying proton transportation or affecting water transport properties. One of the strongest degradation effects is the loss of active catalyst surface [7]. Three main types of voltage losses were found which can be caused by contaminants:

1. *Kinetic losses* which are related to the loss of active surface area of the catalyst. The contaminant physically or chemically adsorbs on the catalyst layer, therefore competing with the hydrogen or the oxygen for the active sites of the catalyst.

2. *Ohmic losses* caused by worsened charge transportation properties of cell components. This can be an effect on the ionic or on the electronic charge charge transportation path.

3. *Mass transportation losses* due to changes in hydrophobicity and structure of gas diffusion layer, the polymer membrane and catalyst layer.

Carbon monoxide (CO) is one of the most famous examples of toxic substances for catalysts of low temperature fuel cells. It adsorbs on the Pt catalyst sites and therefore reduces the active surface area. This is a well studied effect which can be influenced by the concentration of CO in the feed gas, operating conditions (e.g. temperature, pressure, exposure time, ...) and type of catalyst.
Cationic contaminants are able to reduce the available SO_3^- sites for protons of the membrane (Nafion), therefore increasing the ohmic resistance and the water content of the latter at the same time.
Transition metal ions and other contaminants could be attached or deposited on the gas diffusion layer changing surface properties such as hydrophobicity and hydrophilicity. Further details regarding contamination effects and mechanisms at the gas circuits can be found in literature [7].

2.4 Conductivity measurement

Conductivity measurement is a very common approach for determining the ionic content of aqueous solutions. The more ions a solution contains the higher the conductivity. Therefore it's an indication for water purity, although non-ionic impurities like oils and other organic substances cannot be detected.
Applying a voltage between two electrodes immersed in an ion containing solution, a current starts to flow. The ions act as charge carriers for the electron charge because electrons cannot flow through water [14]. In the following sections basic transport properties for ions in aqueous solutions will be discussed.

2.4.1 Basics

The movement of solvated[5] ions through an aqueous solution happens at a velocity v_{max}, where the electric force is equal to the friction force

$$ze_0\vec{E} = 6\pi\eta r_I \vec{v}_{max} \tag{8}$$

with **Stokes' Law** on the right side. Therefore the velocity of the ion is

$$\vec{v}_{max} = \frac{ze_0\vec{E}}{6\pi\eta r_I} \tag{9}$$

The higher the charge ze_0 of the ions and the higher the electric field $\vec{E}$, the higher the velocity. The higher the viscosity η of the fluid and the larger the radius r_I of the solvated ions, the slower the ions will move [15]. The current is proportional to the ion content according to

$$i = \frac{dQ^+}{dt} + \frac{dQ^-}{dt} = Ae_0(n^+z^+v^+ + n^-z^-v^-) \tag{10}$$

with the number n^+, the charge z^+ and the velocity v^+ of the ions. The product describes the number of ions passing through a surface A per time. For each ion type a summand has to be added. Because of Eq. 9, the current is proportional to $\vec{E}$ and therefore to the voltage drop across the ion conductor

$$i = GU \tag{11}$$

[5]Solvated ions: The molecules of the solvent interact with the molecules of the solute. In case of an aqueous solution the (charged) ions are surrounded by water dipoles, here the term "hydrated" is used instead of solvated.

where the **conductance G** is not only a function of the number and type of ions and the viscosity η but also of the wetted surface area of the two electrodes and their distance. The viscosity is strongly dependent on the temperature T. The unit of conductance is $\Omega^{-1} = 1\,\text{Siemens}$, which is the inversion of resistance R.

2.4.2 Measuring the conductance of electrolyte solutions

When measuring the conductance of an electrolyte solution one would assume a linear relation between voltage and current because of Eq. 11. But this is indeed not the case because a conducting metal with mobile electrons immersed in an aqueous solution attracts unsymmetrical water molecules. Also the charged ions in the solution attract water dipoles. Both of the latter effects build up an insulating layer. This capacitor-like arrangement is called electric double layer (Helmholtz double layer, see Figure 7).

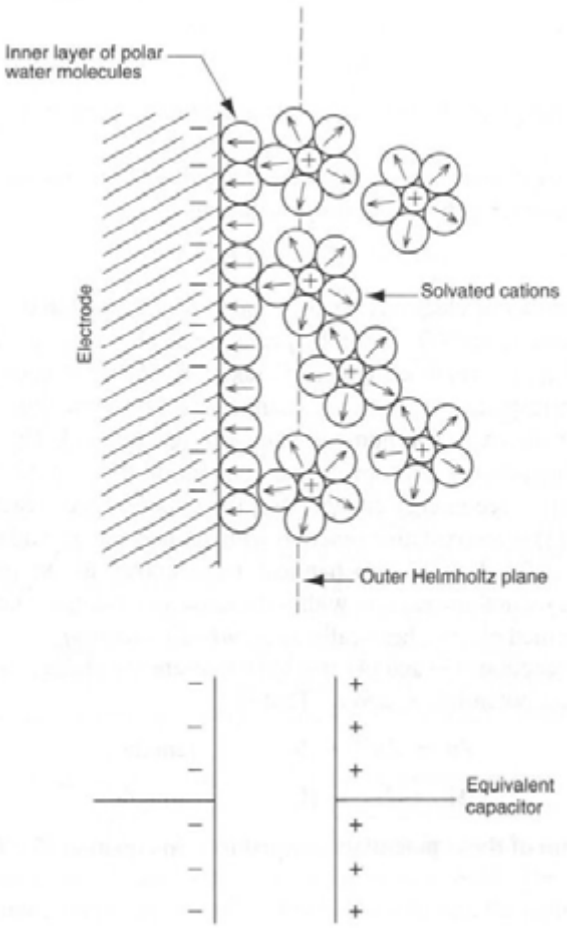

Figure 7: The Helmholtz double layer and the equivalent capacitor [16]

A certain threshold voltage (decomposition voltage) has to be reached, before a current starts to flow. This problem can be overcome if an alternating current is applied, where the double layer capacitance gets charged and discharged as the voltage changes sign. Now a linear current-voltage characteristic can be observed (see Figure 8).

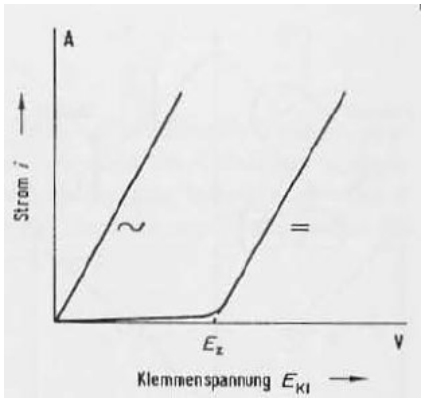

Figure 8: Electrolysis current as a function of voltage for AC(∼) and DC(=); E_Z...Decomposition voltage [15]

The equivalent circuit of an electrolysis cell is shown in Figure 9. The resistance R_E of the electrolyte is in series with the two capacitors C_D^+ (C_D^-) of the electrolyte-electrode junctions. In parallel to the capacitors there are the resistances of the electrodes.

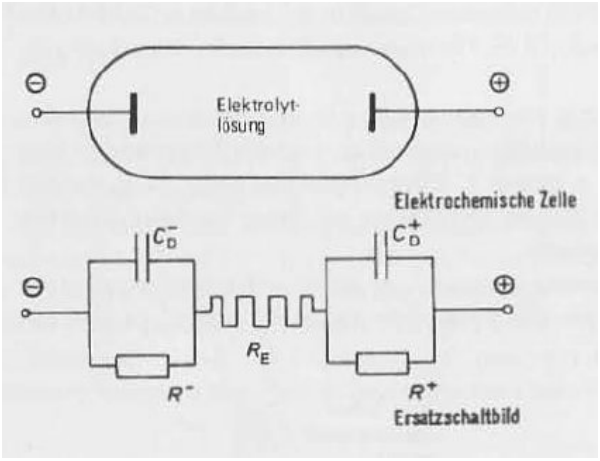

Figure 9: The equivalent circuit of an electrolysis cell [15]

The reactance of a capacitor is

$$X_C = \frac{1}{\omega C} \tag{12}$$

Therefore if one wants to minimize this contribution, high frequencies and large capacities should be achieved. In practical applications, frequencies up to 50 kHz and

platinized electrodes are used. The latter can increase the surface area by a factor of 1000 due to finely distributed platinum particles [15]. However, as an industrial standard for low conductivity measurements in pure water and ultrapure water applications usually stainless steel or titanium electrodes are used.

2.4.3 Conductivity

To get a material specific constant which is independent of the measurement geometry, the specific conductance or **conductivity $\boldsymbol{\kappa}$**

$$\kappa = \frac{1}{\rho} = G\frac{l}{A} \tag{13}$$

is defined which is the inverse of the resistivity. The unit of conductivity reads as S/cm. It can be determined by measuring the conductance between two electrodes with a distance l of 1 cm and a surface area A of 1 cm^2 each.
In practice the geometry of a certain measuring cell is not exactly defined. Therefore the cell constant $G^* = l/A$ is determined by using a standard solution of known conductivity. So this value can be seen as calibration factor for a certain measuring cell. By multiplying it with the actual conductance we get the conductivity

$$\kappa = G \cdot G^* \tag{14}$$

Although every ion contributes to the conductivity, there are certain species of ions which have a greater influence. This is caused by the mobility and the size of the ions. As a parameter for their relative contribution to the total conductivity the **Molar conductivity $\boldsymbol{\Lambda^0}$** is defined

$$\Lambda^0 = \frac{\kappa}{c} \tag{15}$$

where c is the molar concentration (mol/l) of the electrolyte in the solvent. In Table 5 common ionic species and their molar conductance in pure water are shown. The proton and the hydroxide have a much greater influence than the other examples. Both are hydrated[6] and show similar radii as hydrated metal ions, therefore their contribution should also be similar [15].

[6]Hydrated ions: The (charged) ions are surrounded by water dipoles, see section 2.4.1.

Table 5: Molar conductivities of common ionic species at 298 K in pure water [17]

Ion	Λ^0 (Scm^2/mol)
H^+	349,8
Li^+	38,7
Na^+	50,1
K^+	73,5
OH^-	198,6
F^-	55,4
Cl^-	76,8
$HCO3^-$	44,5

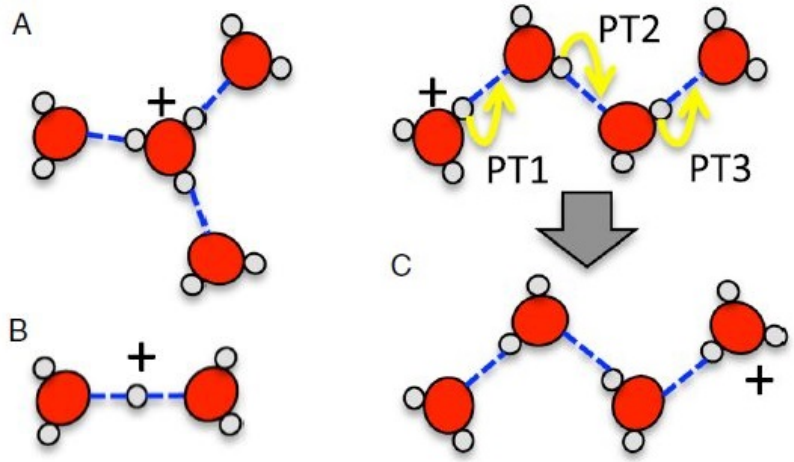

Figure 10: Excess proton as (A) Eigen cation (hydrated Hydronium ion) and as (B) Zundel cation; (C) The subsequent proton transfer PT1-PT3 along the hydrogen bonds in water [18]

This effect can be explained by the **proton transport mechanism**. An excess proton in water can exist either as an "Eigen" (hydrated hydronium ion H_3O^+) or as "Zundel" cation, see Figure 10 A and B [18]. Once the proton is bound to a water molecule, all the hydrogen atoms are equivalent to each other, comparable to the NH_3 structure. As shown in Figure 10 C, it further undergoes a stepwise hopping process from one water molecule to the other. These tunneling process happens along the hydrogen bounds in water. In the case of OH^- the proton hops from a water molecule to the OH^- ion. The details of hopping transport mechanisms are still subject of discussion [19].

2.4.4 Total dissolved solids - conductivity

The TDS (total disssolved solids) value is the total amount of cations, anions and solid agglomerates in a solution. Usually the TDS value of solution is measured by evaporation of a certain volume of the solution and weighing the residuals (gravimetric analysis).

Within certain boundaries, the TDS value can be calculated from conductivity by formulas [20] such as

$$TDS = 0.65\kappa_{25} \tag{16}$$

where κ_{25} is the reference conductivity at 25 °C. The conversion factor can vary between 0.5 and 0.9 mg L^{-1} (μS cm^{-1})$^{-1}$, depending on the type of ions in the solution, some examples are shown in Table 6. For reliable TDS values the conversion factor has to be validated empirically by comparing conductivity to gravimetric TDS results. During TDS measurements via a constant conversion factor the type of ions in the system should not change as well as the amount of non-ionic species. For an unknown aqueous system the fourmula above can give a rough estimation with an error of at least 30 % [20].

Table 6: TDS conversion factors for different salts [21]

Salt	Conductivity equivalent	TDS-Faktor
NaCl	1 mg/L TDS = 2,04 μS/cm	0,49
Na_2SO_4	1 mg/L TDS = 1,49 μS/cm	0,67
$CaSO_4$	1 mg/L TDS = 1,36 μS/cm	0,74
$NaHCO_3$	1 mg/L TDS = 1,06 μS/cm	0,91

2.5 The CO_2 - Water System

The Conductivity of ultrapure water exposed to air changes from 0.055 µS/cm to approximately 1 µS/cm at T=25 °C, depending on the actual CO_2 concentration which was at 360 ppm in air in 1995. Ambient concentrations of CO_2 vary between 380 ppm and 410 ppm [22]. These are usually measured outdoors, indoor concentrations can reach levels up to 2000 ppm, depending on ventilation and the amount of people or other CO_2 sources present. CO_2 is the only one of the primary species in ambient air contributing to this increase in conductivity, all other components do not form ionic species [23].

2.5.1 Calculation model

A model is presented to calculate the conductivity increase of pure water which is exposed to ambient air. The following calculation should provide an estimation for this difference and may help to understand the underlying processes. Similar calculations can be found in work [23] and [24]. CO_2 reacts with water to carbonic acid H_2CO_3 which immediately dissociates to ionic species

$$\mathrm{CO_2(aq) + H_2O(l) \longleftrightarrow H_2CO_3 \longleftrightarrow H^+ + HCO_3^-} \tag{17}$$

$$\mathrm{HCO_3^- \longleftrightarrow H^+ + CO_3^{2-}} \tag{18}$$

$$\mathrm{H_2O \longleftrightarrow H^+ + OH^-} \tag{19}$$

with the dissociation constants

$$K_1 = \frac{\left[\mathrm{H^+}\right]\left[\mathrm{HCO_3^-}\right]}{\left[\mathrm{CO_2(aq)}\right]} = 4.45 \times 10^{-7} \tag{20}$$

$$K_2 = \frac{\left[H^+\right]\left[\mathrm{CO_3^{2-}}\right]}{\left[\mathrm{HCO_3^-}\right]} = 4.69 \times 10^{-11} \tag{21}$$

$$K_W = \left[H^+\right]\left[\mathrm{OH^-}\right] = 1.00 \times 10^{-14} \tag{22}$$

which are valid for 25 °C. Based on the Kohlrausch law the conductivity κ can be written as

$$\kappa = 10^{-3} \sum_i \Lambda_i^0 c_i \tag{23}$$

where Λ_i^0 is the molar conductivity (Scm^2/mol) and c_i the concentration (mol/l) of ion i and the factor 10^{-3} corrects the mole/l to mole/cm^3. The sum goes over all ions and in case of the CO_2 H_2O-Water-System one gets

$$\kappa = 10^{-3} \cdot \left(\Lambda^0_{H^+} \left[H^+\right] + \Lambda^0_{OH^-} \left[OH^-\right] + \Lambda^0_{HCO_3^-} \left[HCO_3^-\right] + \Lambda^0_{CO_3^{2-}} \left[CO_3^{2-}\right] \right) \tag{24}$$

Knowing the partial pressure P_{CO_2}, the concentrations $[CO_2(aq)]$, $[H^+]$, $[OH^-]$, $\left[HCO_3^-\right]$ and $\left[CO_3^{2-}\right]$ can be calculated. The relation between partial pressure of CO_2 and $[CO_2(aq)]$ is given by **Henry's Law**

$$[CO_2(aq)] = K_h \cdot P_{CO_2}(g) \tag{25}$$

with K_h the Henry's constant, describing the solubility of CO_2 in water at different temperatures.

Conductivity increase at 25 °C:

To calculate $P_{CO_2}(g)$ under atmospheric conditions we multiply the total pressure of 1013.25 mbar in the atmosphere with the CO_2 concentration of 390 ppm

$$\underline{P_{CO_2}(g)} = \chi_{CO_2} \cdot P_{total} = \underline{0.4\,\text{mbar}} \tag{26}$$

with K_h=3.4×10^{-2} mol/(l · atm) at 25 °C [25]. And for the CO_2 concentration one gets

$$\underline{[CO_2(aq)]} = K_h \cdot P_{CO_2}(g) = \underline{1.34 \times 10^{-5}\,\text{mol/l}} \tag{27}$$

Now the ion concentrations can be calculated using **charge balance equations**

$$\left[H^+\right] = [HCO_3^-] + [OH^-] + \left[CO_3^{2-}\right] \tag{28}$$

Since to $K_2 << K_1$, the second dissociation step and therefore the contribution of $\left[CO_3^{2-}\right]$ is negligible. Finally we get the ion concentrations

$$\left[H^+\right] = \frac{K_W}{[H^+]} + \frac{K_1\,[CO_2(aq)]}{[H^+]} = \sqrt{K_W + [CO_2(aq)]\,K_1} \tag{29}$$

$$[OH^-] = \frac{K_W}{\left[H^+\right]} \tag{30}$$

$$[HCO_3^-] = \left[H^+\right] - [OH^-] \tag{31}$$

substituting these together with the molar conductivities from Tab. 8 in the reduced (because of $K_2 << K_1$) version of Eq. 24 we get

$$\underline{\kappa} = 10^{-3} \cdot \left(\Lambda^0_{H^+} \left[H^+ \right] + \Lambda^0_{OH^-} \left[OH^- \right] + \Lambda^0_{HCO_3^-} \left[HCO_3^- \right] \right) = \underline{0.96\,\mu\text{S/cm}} \tag{32}$$

This means, according to the upper model, for standard conditions at temperature T=25 °C and pressure P_{total}=1013.15 mbar, the change of conductivity $\Delta\kappa$ of pure water with an initial conductivity of κ_0=0.055 μS/cm at 0 ppm CO_2(g) is about

$$\Delta\kappa = \kappa - \kappa_0 = 0.91\,\mu\text{S/cm} \tag{33}$$

when the CO_2(g) concentration changes to 390 ppm. Conductivities for various CO_2 concentrations can be seen in Table 7. Concentrations from 800 ppm to 1000 ppm are typical indoor values.

Table 7: Conductivities κ for various ambient concentrations of CO_2 at 25°C

Concentration (ppm)	κ (μS/cm)
200	0.68
400	0.97
600	1.19
800	1.37
1000	1.53
1200	1.68
1400	1.81

Table 8: Molar conductivities of ionic species generated by dissolved CO_2 at 25°C and 90°C in pure water [23]

Ion	Λ^0 (Scm^2/mol) @25°C	Λ^0 (Scm^2/mol) @ 90°C
H^+	349,8	610,8
OH^-	198,6	420,0
$HCO3^-$	44,5	102,4

Conductivity increase at 90 °C:

Here one hast to keep in mind that K_h, K_1, K_W and the molar conductivities (see Table 8) are temperature dependent. The partial pressure of CO_2 is decreased because of water vapor pressure of about 0.7 bar, which was neglected for 25 °C. Therefore we get

$$\underline{P_{CO_2}(g)} = \chi_{CO_2} \cdot (P_{total} - 0.7) = \underline{1.17 \times 10^{-4}\,\text{mbar}} \tag{34}$$

Since K_h is temperature dependent, it has to be corrected to 90 °C, which can be done by

$$K_h = K_h^{\Theta} \exp\left(C\left(\frac{1}{T} - \frac{1}{T^{\Theta}}\right)\right) \tag{35}$$

where the constant C is related to the dissolution enthalpy Δ_{sol}H

$$C = \frac{\Delta_{sol}H}{R} = -\frac{dlnK_h}{d(1/T)} \tag{36}$$

with C=2400 [25], we get K_h=8.05 × 10^{-3} mol/(l · atm). In work [23] Henry's constant was found at K_h=5.6 × 10^{-3} mol/(l · atm). For K_1 values between 3 × 10^{-7} and 5 × 10^{-7} were assumed. Therefore continuing the calculation like above and considering the value ranges for K_h and K_1 the conductivity κ for a CO_2 concentration of 390 ppm ranges from 0.68 μS/cm to 0.74 μS/cm.

The intrinsic conductivity of of pure water at 90 °C is κ_0=0.62 μS/cm [23, 26]. Therefore the conductivity increase $\Delta\kappa$ (Eq. 33) for 390 ppm ranges from 0.06 μS/cm to 0.15 μS/cm. If the CO_2 concentration is between 800 ppm and 1000 ppm, the range of $\Delta\kappa$ is between 0.13 μS/cm and 0.36 μS/cm.

Conclusion:
The conductivity of pure water exposed to ambient air at room temperature (25 °C) is very sensitive to the CO_2 content. At higher temperatures (e.g. 90 °C) this sensitivity is much less. This can be expressed by

The **relative increase** of conductivity between 0 ppm and 390 ppm:

- Pure water @ 25 °C (from 0.055 μS/cm to 0.96 μS/cm): **1645 %**
- Pure water @ 90 °C (from 0.62 μS/cm to 0.72 μS/cm): **16 %**

2.5.2 Literature review

A.H. England: On the hydration and hydrolysis of carbon dioxide [27]

Aqueous carbonate species were studied at different pH values by near edge x-ray absorption fine structure spectroscopy (NEXAFS). With this method not only the electronic structure of carbon but also it's local chemical environment can be investigated. This

can be seen by different features in the fine structure. Calculations of the spectra of the corresponding K-edge were done by a combination of molecular dynamics (MD) simulations and a first principles density functional theory (DFT) method.
Spectral differences were identified to distinguish between CO_2(g), CO_2(aq) and carbonic acid, which were related to changes in the C-O bonding strengh, molecular configuration and hydration strength.

The experimental part was done in the liquid phase by a microjet stream within a vacuum chamber. Close to the jet tip an intense x-ray beam (Synchrotron radiation) was positioned, which was tuned over the region of the K-edge of carbon which is between 280 eV and 320 eV. The different pH-values were achieved by preparing a 1 M sodium carbonate Na_2CO_3 solution with 18 MΩcm water. The initial pH of 12 was then reduced by adding appropriate amounts of 1 M HCl. The solution composition at three different pH values was as follows: at pH 12 (98 % CO_3^{2-} and 2 % HCO_3^-), at pH 8.5 (98 % HCO_3^- and 2 % carbonic acid/CO_2) and at pH 3 (100 % carbonic acid/CO_2).

There was a high uncertainty factor for the pH 3 region, where it was not possible to say which carbonate species was present: carbonic acid, CO_2(aq) or CO_2(g). The spectrum showed a sharp feature at 290.7 eV which corresponds to the excitation of the carbon 1s electron (see Figure 11). Within the jet stream the spectrum was identical to the case where the jet was positioned slightly above or below the x-ray beam, showing a small feature just above the K-edge, see Figure 11 (B). This feature indicates gaseous CO_2, in accordance to literature, see Figure 11 (A). The calculated spectrum of carbonic acid shows a feature in the range from 294 eV to 305 eV, this was not seen in experiment. The broader resonance at 310 eV of dissolved CO_2 showed good agreement between experiment and calculation.

In the basic and the mid range pH, the species carbonate and bicarbonate are dominant what can be seen from Eq. 17 to Eq. 19. The MD simulation of the carbonate did not match experiment, therefore a Quantum Mechanic / Molecular Mechanics (QM/MM) approach was applied which agreed well with experiment, see Figure 12 (A). This mismatch was found to be connected to the hydration of the carbonate and the change in planarity of the molecule. For the bicarbonate, both the classical MD and the QM/MM approach agreed with the experiment, see Figure 12 (B).

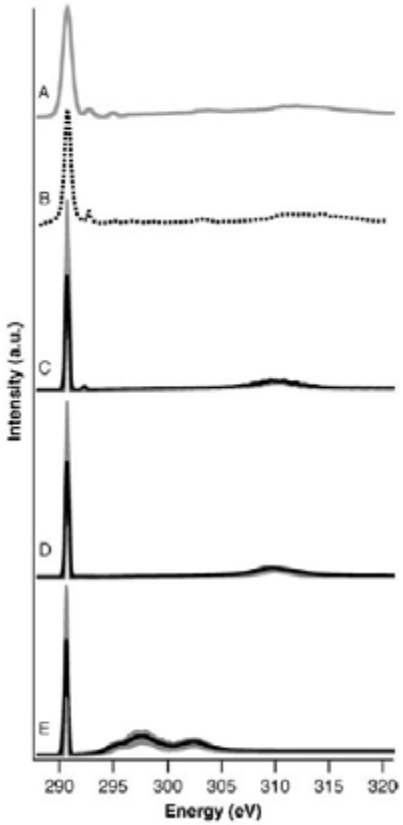

Figure 11: Measured NEXAFS spectra of the carbon K-edge at acidic pH: (A) (literature based) ISEELS spectrum of CO_2(g); (B) measured spectrum; DFT calculated spectra of: (C) gaseous CO_2(g); (D) dissolved CO_2(aq); (E) carbonic acid

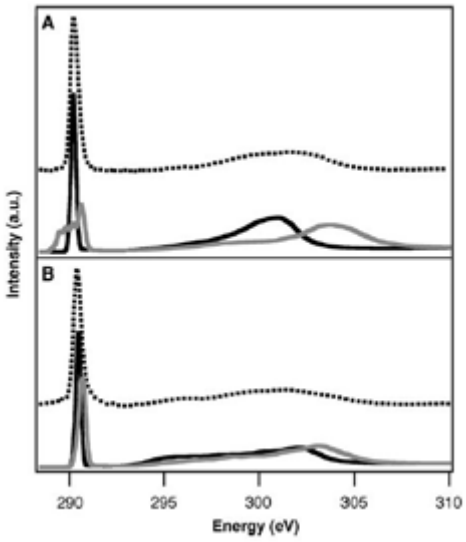

Figure 12: NEXAFS spectra of the carbon K-edge at: (A) basic pH; (B) mid range pH; Measured spectra are shown as dotted lines, calculated spectra as solid lines: QM/MM = black; MD = gray

V.R. Gajevskiy: Electric conductivity of CO_2 aqueous solutions [24]

Investigations of the CO_2+H_2O-system were made for CO_2 concentrations varying between ambient and saturation conditions. Contributions of the CO_2 delivered ionic species to conductivity are found to be additive, in accordance to the law of Kohlrausch. The individual ionic components do not influence each others mobilities significantly. Measured and calculated conductivities were in good agreement.

Carbon dioxide was blown through deionized water at 25 °C until saturation was reached. Then the solution was degassed by stirring. Solution conductivity an pH were measured at the same time.

The hydrogen carbonate (=bicarbonate) was found to be the main contributor to conductivity. The contribution of carbonate and hydroxide is only about 0.1 %. Simultaneous measurement with potentiometric and conductometric sensors which are galvanically coupled did not show substantial interference. A procedure was developed for the calibration of a conductometric sensor with the help of a reference solution with varying pH and an auxiliary pH measurement.

M. Falk: Infrared spectrum of carbon dioxide in aqueous solution [28]

Infrared spectra of $^{12}CO_2$, the isotope $^{13}CO_2$, bicarbonate and carbonate were recorded. A saturated CO_2 solution was prepared by bubbling CO_2 through deionized water. Outgoing from a saturated solution with an assumed concentration of 38.4 mM, different concentrations were achieved by dilution. Carbonate and bicarbonate solutions were prepared by adding K_2CO_3 and $KHCO_3$ in appropriate amounts.

Spectra were recorded via transmission through a 52 μm calcium fluoride cell. The spectrum was corrected by that of pure water, which shows a spectroscopic window between 1800 cm^{-1} and 3000 cm^{-1}. This window is ranging from the symmetric and asymmetric stretching fundamentals at 3280 cm^{-1} and 3490 cm^{-1} to the bending vibration at 1644 cm^{-1} of H_2O(aq).

The antisymmetric stretching fundamental ν_3 was found at 2342 cm^{-1} for $^{12}CO_2$ and at 2277 cm^{-1} for $^{13}CO_2$ and is within this window. The bending vibration ν_2 of CO_2(aq) at 667 cm^{-1} was not covered spectroscopically. No absorption was observed which could be connected to H_2CO_3(aq). The shift between gaseous and dissolved CO_2 is only 6 cm^{-1},

which indicates that the interaction force with the water molecules is very weak. Other work showed, that the CO_2 molecule is connected to oxygen and not (like in other oxygen containing solutes) to the hydrogen of the surrounding water molecules. The CO_2(aq) ν_3 band is within $1\,cm^{-1}$ of the absorption of of solid CO_2.

The simultaneous detection of CO_3^{2-} at $1385\,cm^{-1}$ and HCO_3^- at $1360\,cm^{-1}$ is feasible but not very promising because of strong water absorption between $1300\,cm^{-1}$ and $1400\,cm^{-1}$. Both species do not coincide, but their bands overlap. Aqueous CO_2 is much easier to detect because only a few other molecules absorb in this region. The detection limit was found to be at 0.4 mM.

3 Test system for the cooling circuit

To ensure safe operation of an automotive low temperature PEM fuel cell system the conductivity of the coolant needs to be maintained low (see Section 2.3.2). Therefore testing solutions for evaluating the ability of materials or components within the coolant loop to emit ionic species are desired. In this section such a test system and the evaluation of this system is described which was designed for this purpose.

3.1 System description

The Material Compatibility Testbed (shortly called Testbed) was designed similar to a LT-PEM fuel cell coolant circuit, just without a fuel cell stack for cooling and with special consideration on the material mix of the selected components. This design provides the following advantages compared to the simpler situation of a material test within a bottle (see Section 4):

- Proximity to the "real live" cooling situation
- Accelerated testing conditions (because of moving coolant)
- Facilitation of material- and component testing

A component may be made of combinations of materials and/or may have different surface qualities between the wetted (in contact with coolant) and the non-wetted parts, for example valves, lined hoses, or heat exchanger. In this case a testing procedure with the component immersed in the coolant within some vessel doesn´t make sense. In Figure 13 the flow diagram of the Testbed can be seen. It consists of a closed loop made of PFA hoses, 1.4404 stainless steel piping, heat exchanger, expansion tank, electric heater, circulation pump, ion exchanger, 3-way and 2-way valves and a test chamber. It also contains the following measurement equipment: conductivity (no temperature compensation), temperature, pressure, volume flow. To refill and drain of the system additional valves, a membrane pump and barrels were added. Technical data of the Testbed are:

- System volume: 3-5 liter
- Heating power: 4.5 kW
- Cooling power: 7 kW
- Maxiumum temperature: 95 °C
- Maximum system pressure: 2 bar
- Volume flow: 16-30 l/min

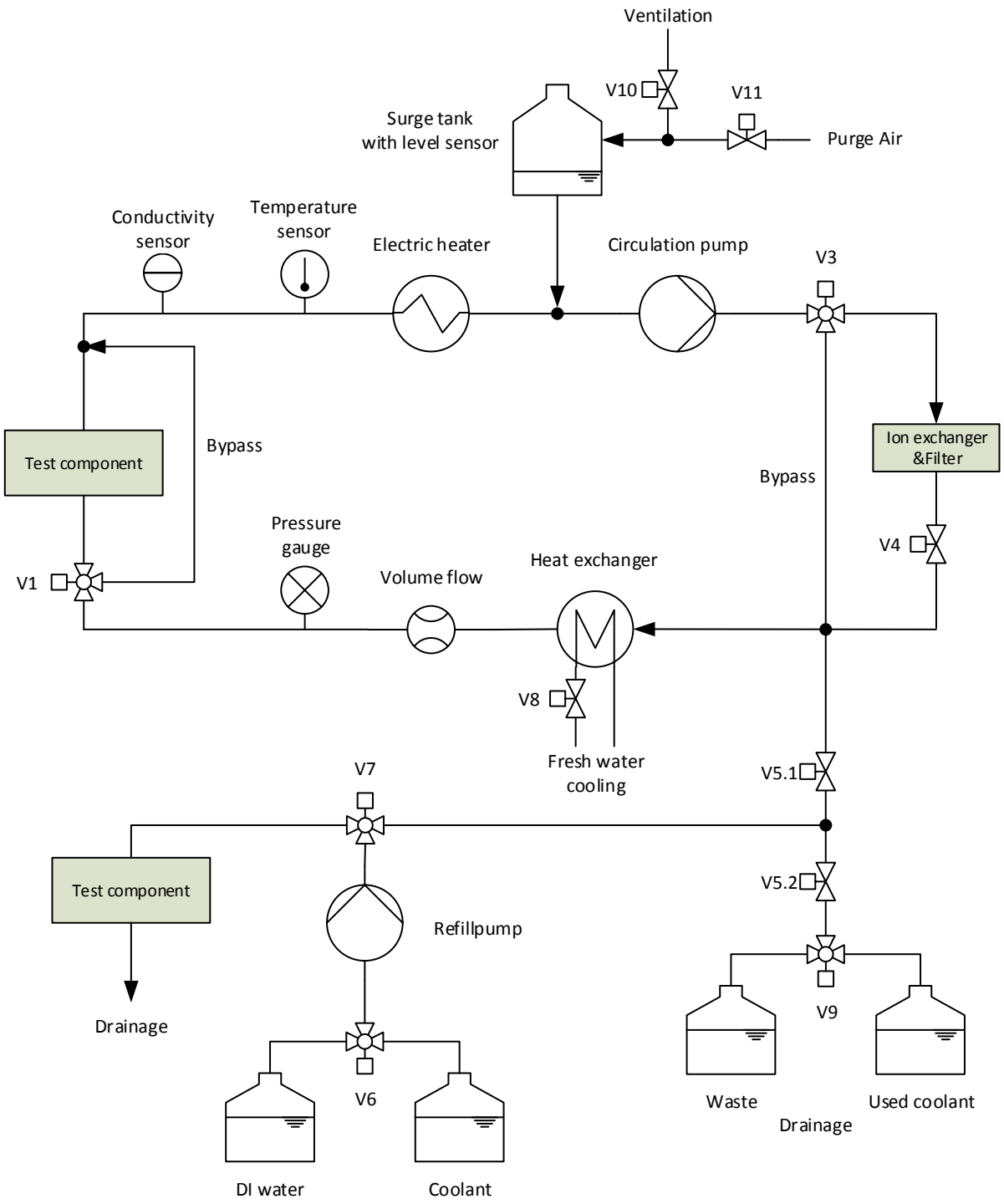

Figure 13: Flow diagram of the Material Compatibility Testbed

3.2 Measurement procedure

In the overview in Figure 14 the procedure can be seen. First the Testbed is drained of and the (previously cleaned) test object is installed, for reference measurement no test object is installed. The automated testing procedure starts with the decision of *Duration* of the test (one Day/seven Days)[7] and if DI water or fuel cell coolant should be used. For possible analytic investigations of the leachant solution *Sample extraction* can be chosen. The wetted surface area of the test object is needed for correction to standard surface area to volume of water ratio. The actual testing procedure starts with a *leak check*, then the system is filled up. In the *Conditioning* phase the liquid is heated up and CO_2 degassing (see below) is performed if necessary. Then the test component or material is flushed and *Testrun* is started with the following conditions:

- Temperature: $(90.0 \pm 0.1)\,°C$
- Pressure: $(0.5 \pm 0.2)\,bar$
- Volume flow: $(20 \pm 1)\,l/min$

The Testrun is interrupted if the upper conductivity limit is reached, which may be caused by unexpected impurities (e.g. dust within a component) or strongly contaminating materials. After the Testrun the system is cooled down to 25 °C which is the standard temperature for most conductivity measurements and therefore useful for comparison to other tests (e.g. leaching tests). After the *Cooling* procedure a sample may be extracted for analysis, if not *Deionisation* of the leachant solution is performed. Then the system is *drained* of and the weight of the leachant solution is measured. After removal of the test object the test is finished.

[7] The duration of seven days in combination with a temperature of 90 °C, which is the upper limit of the standard automotive LT-PEM fuel cell temperature range, is assumed to be sufficient for material and component evaluation and will be discussed in Section 3.5

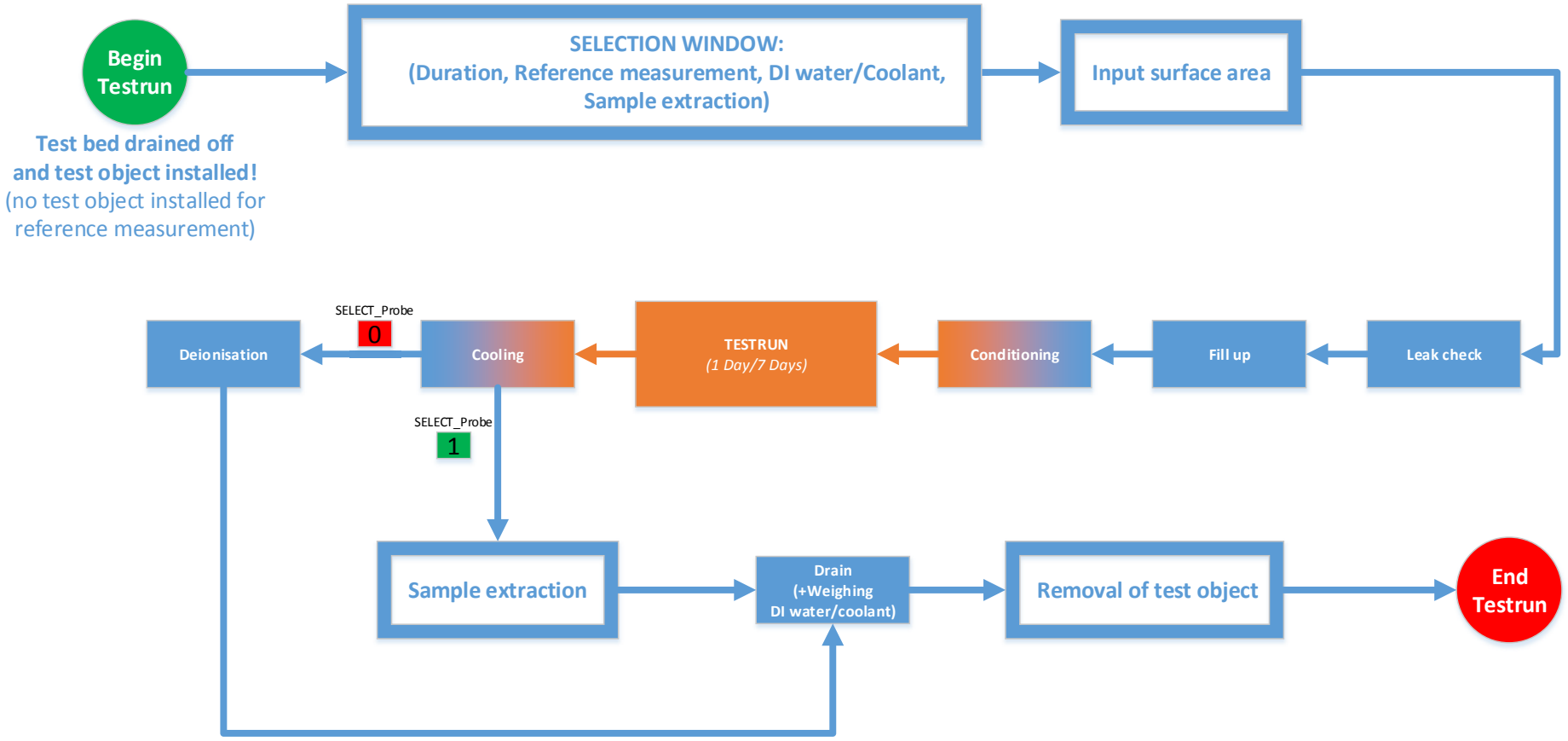

Figure 14: Measurement procedure of the Material Compatibility Testbed

3.3 Evaluation method

The outcome of the measurement is a curve of conductivity versus time. For comparable results this conductivity curve has to be corrected to the same surface area to volume of water ratio $\frac{A_{Sample}}{V_{Water}}$, if the test objects differ in wetted surface area and/or in volume. Therefore weight of the leachant solution and wetted surface area are evaluated. Two standard values for $\frac{A_{Sample}}{V_{Water}}$ occurred as possible basis for this normalization. From the viewpoint of the Testbed this value can be obtained by the surface area of a test material with dimensions of (69.0 ± 0.1) mm x (100.0 ± 0.1) mm x (2.0 ± 0.1) mm which fits into the measuring chamber (see Figure 15) and the volume of Testbed plus measuring chamber. Thereafter this ratio is $(6.9 \pm 0.3)\,\mathrm{mm}^2/\mathrm{ml}$. Another ratio can be obtained from literature based leaching tests where this ratio is $150\,\mathrm{mm}^2/\mathrm{ml}$ [13, 29]. For comparing the Testbed results to each other the former is sufficient, for comparing them to literature the latter ratio makes more sense. Therefore in the evaluation there was a parameter added for comparison to literature. Due to different densities between BASF coolant and DI water and the fact of weighing the liquid to evaluate volume a density correction has to be applied.

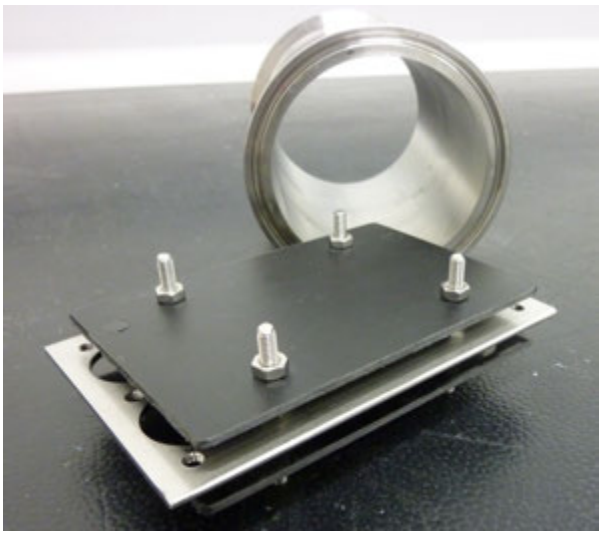

Figure 15: Measuring chamber and sample holder with test sample of the Material Compatibility Testbed

In Figure 16 an evaluation example of a measured silicone hose is shown. In this case the measurement chamber shown in Figure 15 was removed and the hose was installed. All relevant parameters of the whole testing procedure (including also operation modes like conditioning, cooling,...) are shown. This summary is the basis for the measurement

report. The main diagram shows the effect corrections by reference measurements and the normalization to standard $\frac{A_{Sample}}{V_{Water}}$ value of $(6.9 \pm 0.3)\,\mathrm{mm^2/ml}$. The green curve in Figure 16 is the uncorrected measurement, the magenta curve shows the subtraction of averaged[8] reference measurements, the gray curve shows normalization without reference correction and the black curve is the fully corrected curve. Here the correction has big influence because of the high $\frac{A_{Sample}}{V_{Water}}$ value of of the hose. In this case DI water was used for testing therefore the density correction is negligible, for BASF coolant there is a significant influence due to its density of $1.065\,\mathrm{g/cm^3}$.

There are two linear fits in the diagram showing the *conductivity increase rate* in the start phase (the first 20 %) and in the main phase (the last 80 %) of the total test duration which divide the measurement in two parts. The slope of the main phase is used as characterization parameter for reference measurements (see also Figure 21) but it is also used for characterization of test objects. Beside this conductivity increase rate the maximum conductivity ("CondCorrected") at the end of the test is necessary because it can be used for comparison with literature (*solution conductivity*). This value is proportional to the total amount of ions in the system at the end of the test which is important to know.

The *solution conductivity* parameters "NREL_SolCond" and "NREL_SolCond_Corr" are calculated by applying linear temperature correction (25 °C) to the max value and normalizing it to $150\,\mathrm{mm^2/ml}$. The reason for this two parameters was to take into account the issue of dead spaces/volumes (see Section 3.5), therefore the parameter "NREL_SolCond" was added which corresponds to the maximum of the gray curve. The coefficient for temperature correction can be found in the upper right of Figure 16 which is evaluated for each measurement and varies between 1.7 %/°C and 2.5 %/°C. It can be calculated by the following formula [21]

$$\alpha = \frac{(\kappa_{T2} - \kappa_{T1}) \cdot 100\%}{(T2 - T1) \cdot \kappa_{T1}} \tag{37}$$

whereas κ_{T1} is measured at 25 °C. To calculate the conductivity at 25 °C the following formula is used [21]

$$\kappa_{T_{ref}} = \frac{\kappa_T}{1 + \frac{\alpha}{100\%} \cdot (T - T_{ref})} \tag{38}$$

[8]The reference measurement for correction is achieved by the average of the last 3-5 available reference measurements which were performed before the actual measurement of the test object

with T_{ref}=25 °C and T=90 °C. For comparison to "NREL_SolCond" which is calculated from 90 °C the value "NREL_Control" can be taken which is derived from the cooling phase. It turns out that these values match within an error smaller than 5 % and the "NREL_Control" value tends to be smaller. The reason for taking the correction from 90 °C is to avoid possible decrease of conductivity due to adsorption effects. The minimum value of conductivity in the conditioning phase is taken as start value of conductivity.

Also in the upper right the "BASF Coolant Flag" and the "Correction factor" can be found. The latter is the multiplication factor for normalization and the former is the status flag for density correction which is 1 when BASF coolant is used. Other parameters are self-describing. Finally, the following parameters are used for characterization of a test object:

1. *Conductivity increase rate [µS/cm/day]*
2. *(NREL) Solution conductivity [µS/cm]*
3. *Minimum (start value) of conductivity [µS/cm]*

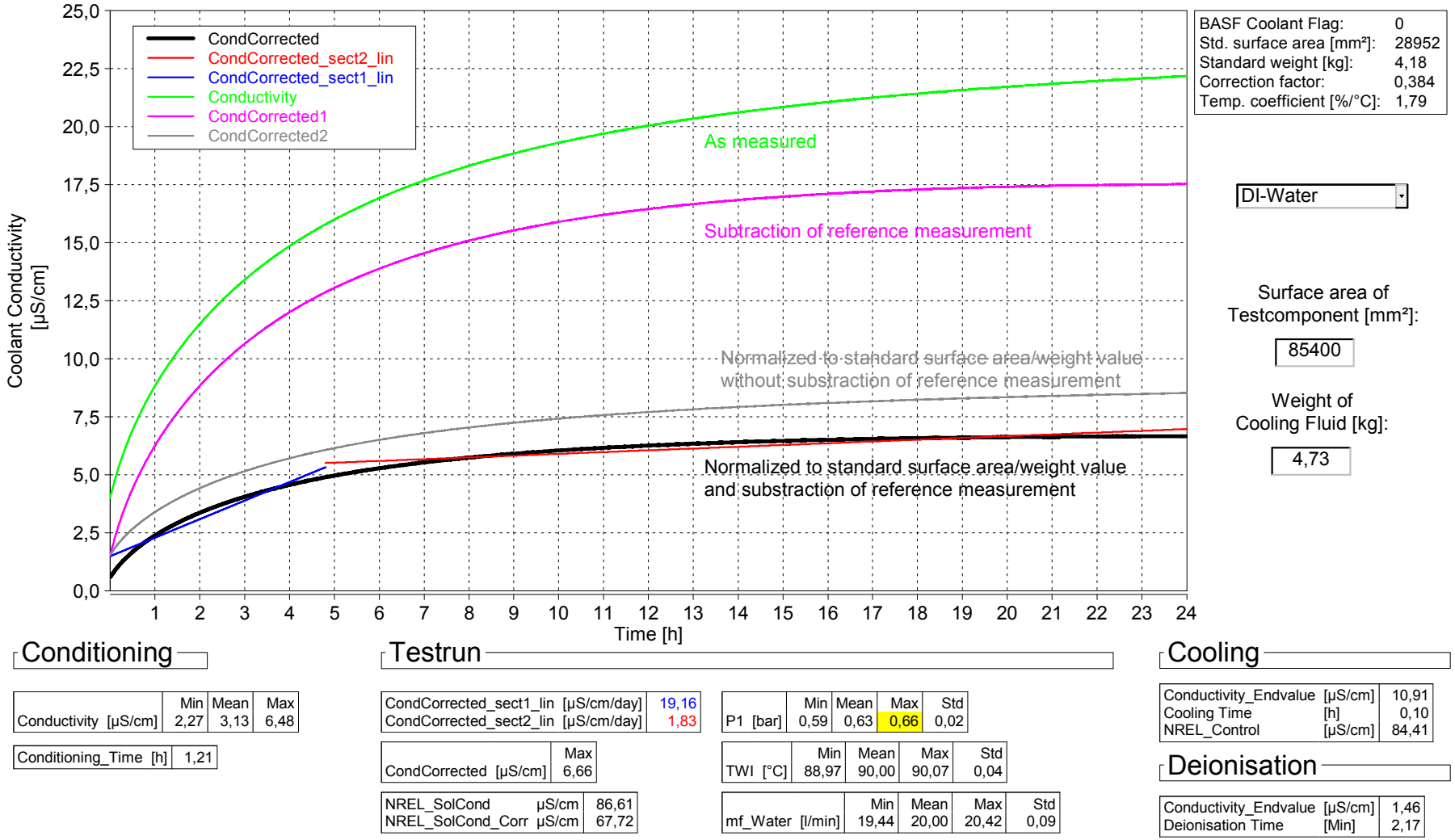

Figure 16: Example evaluation of measurement of a silicone hose including all parameters for measurement report (corresponding to the black curve); The correction effect to normalized conditions the substraction of reference measurements are shown in the main diagram

3.4 Reference measurements

For correct measurement of the contribution of a certain test object to conductivity the contribution of the system itself needs to be considered. This "background" has to be subtracted from the measurement whereas the latter is assumed[9] to be the sum of background and test object. This means reproducible background or reference measurements need to be achieved. After the build up phase of the testbed, the reference measurements showed a relatively large variation in the conductivity increase rate which will be discussed below. Additionally the curvature of the conductivity was upward bended in some cases (see Section 3.4.2) indicating a possible sink of ions. Thus, the reproducibility of the reference measurements needed to be improved, search and removal of possible ion sources and sinks was the next step.

3.4.1 Search for ion sources and sinks: Stainless steel surfaces and dead spaces/volumes

The system consists of stainless steel components (e.g. expansion tank, pipes, electric heater) where some parts contained welds which were created under inert gas conditions to inhibit oxidation. However, stainless steel welds being subject to changing conditions (periodically wetted by deionized water, high temperature changes) may still remain critical parts of the system in terms of corrosion and may further act as source of ions. As thread sealant for cylindrical threads PTFE tape was used. Threaded fittings may contain more dead spaces/volumes than clamp connections (e.g. Tri-Clamp fittings). The design of the system was not in accordance to pharma-standard or food-standards (where avoidance of dead spaces/volumes is mandatory), therefore possible dead spaces/volumes may be present which can act as source or sink for ions. The following points were addressed as possible factors for influencing the ion content

1. Corrosion of stainless steel parts in the system, especially in proximity of welds
2. Corrosion of stainless steel on untreated areas
3. Roughness of stainless steel surfaces
4. Dead spaces/volumes within the system

[9] In case of dead spaces/volumes being the main additional source of ions beside the test object this subtraction may not always be correct. Here a sponge-like behavior might be a valid description.

Optical inspection

Regarding 1. and 2. the system was inspected with an endoscope for visible spots of corrosion. Rusty areas were found at welds or parts in proximity of welds which were subjected to heat during welding, see Figure 17. This (partly heavy) rust formation was probably initiated by the change in surface quality caused by heat treatment during welding. Also the changing conditions within the system may have a supportive effect. In the pictures can be seen that the inert gas conditions were not sufficient to inhibit oxidation (tempering colors). Nearly all welds showed similar conditions.

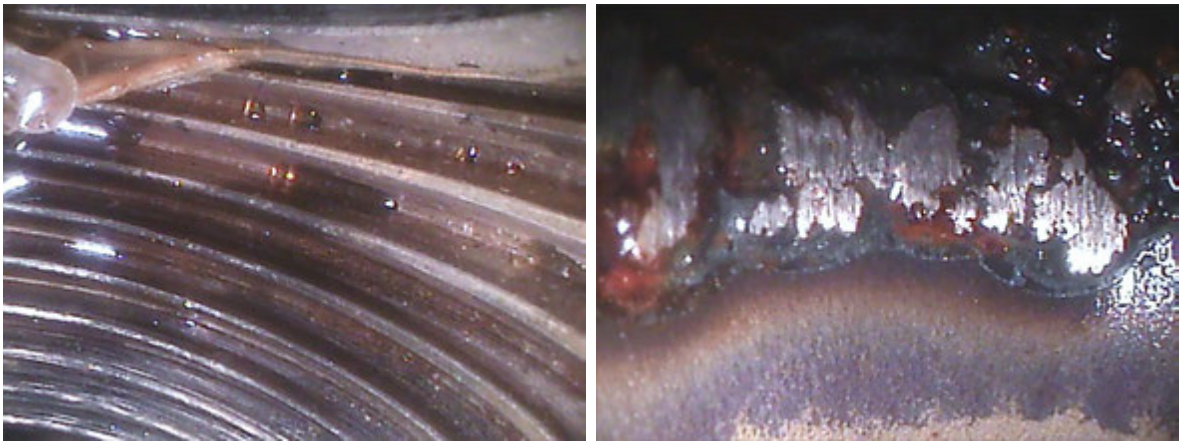

(a) Thread near weld (b) Welded pipe

Figure 17: Rust on stainless steel surfaces in proximity of welds, located at the inner side of pipes

Some rusty spots were also found on "plain" surfaces (not in proximity of welds) which are shown in Figure 18, whereby the right picture shows a pickled and passivated surface within the electric heater. Regarding 3. and 4. no special optical inspection was done, this issues are further discussed below (Conclusion).

Aftertreatment

To get rid of these ion sources all welds were removed by exchanging parts (welded pipes and fittings) as far as possible and if not the parts were treated by pickling and passivating. A stainless steel weld within the expansion tank before and after pickling and passivating can be seen in Figure 19.
These pictures show that the tempering colors vanished but the surface still doesn´t look like a smooth stainless steel surface. Usually welds are sanded or polished before pickling and passivating which was not possible in this case. However, also well treated stainless

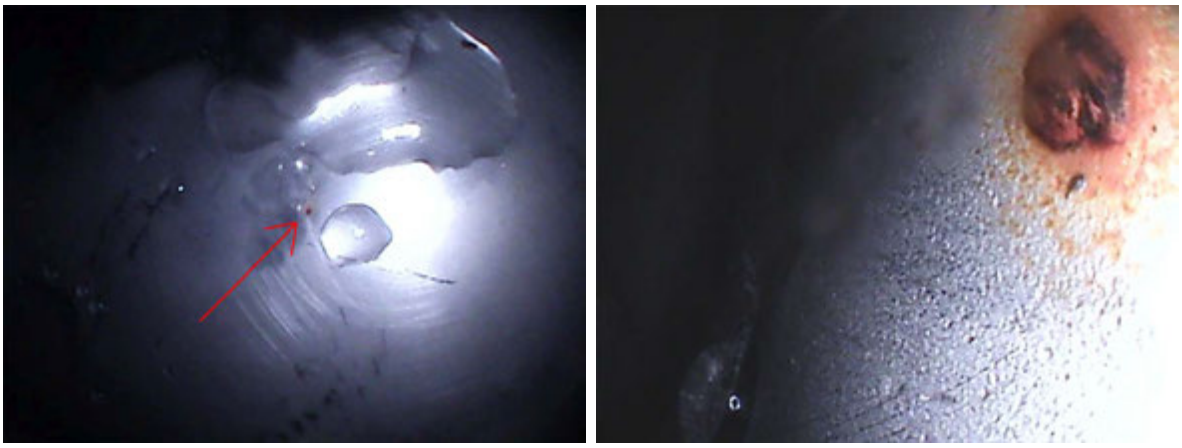

(a) Expansion tank (b) Electric heater

Figure 18: Stainless steel corrosion on untreated areas

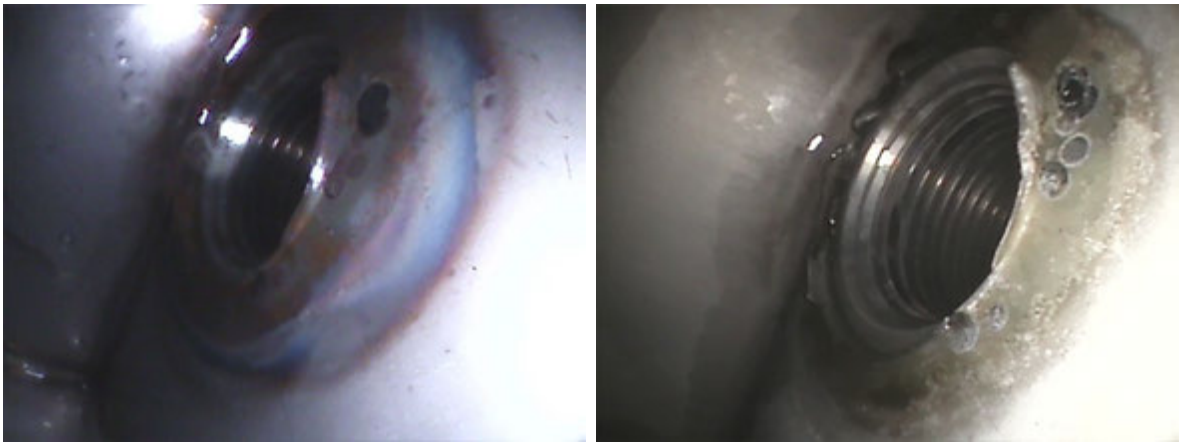

(a) Before treatment (b) After treatment and 6 hours operation

Figure 19: Stainless steel welds inside expansion tank before and after pickling and passivating

steel welds showed new corrosion spots after a short operation time after pickling and passivating. The pictures of the electric heater which are shown in Figure 20 were made after an operation time of 6 hours and again after 2 weeks. Although the rusty spots could be removed by pickling and passivating new locations appeared which can be seen in the pictures.

Conclusion

The results from above suggest, that stainless steel surfaces which are in contact with DI water at changing conditions are very susceptible to corrosion especially in proximity of welds. Surface roughness may be an important parameter as indicated by corrosion

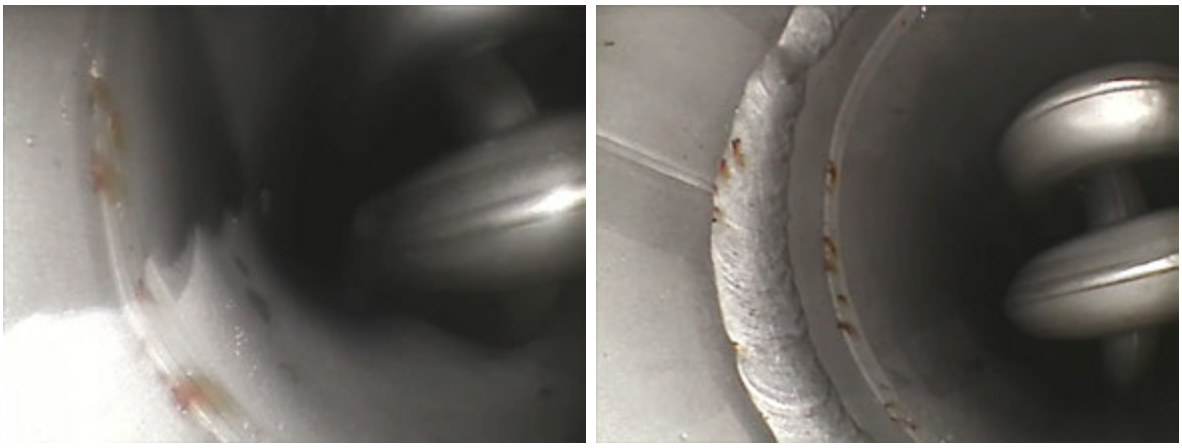

(a) After treatment and 6 hours operation (b) After treatment and 2 weeks operation

Figure 20: Stainless steel surface inside of electric heater, both pictures after pickling and passivating

tests in Section 4.3. Usually the roughness of a pickled and passivated stainless steel surface is about Ra $\approx 2.5\,\mu$m [30]. For higher corrosion resistance and minimizing of surface depositions a roughness Ra $\leq 0.8\,\mu$m is recommended [31, 30]. Reduction of surface roughness of components was not done within this work but may be considered for possible future modifications.

The conductivity increase rate of reference measurements is shown in Figure 21, whereby the reference measurements No. 1 to 14 reflect the condition of the testbed as it was built up (without any treated/exchanged parts). After removal of most of the welded parts and pickling and passivating the variation in the conductivity increase rate seem to be much lower. Higher values can be seen after pickling and passivating which may be related to residual amounts of chemicals. Also just to open the system bears the risk of contamination. What clearly can be seen is the effect of using BASF coolant. When the system is subsequently operated with DI water the increase rate is high. This is an interesting effect which may be related to hindered CO_2 degassing when residual amounts of BASF coolant are present (see Section 3.4.2).

A slightly decreasing trend can be seen in the average value of conductivity increase rate which is shown by the linear fit in Figure 21. This is an indication that the cleanliness of the testbed gets better and better and can be seen as indication that dead spaces/volumes are present in the system. Another indication is the effect of a higher contaminating test object also changing the cleanliness state of the system. Therefore an additional check of the cleanliness of the system and cleaning procedure should be included to ensure a comparable state before each test.

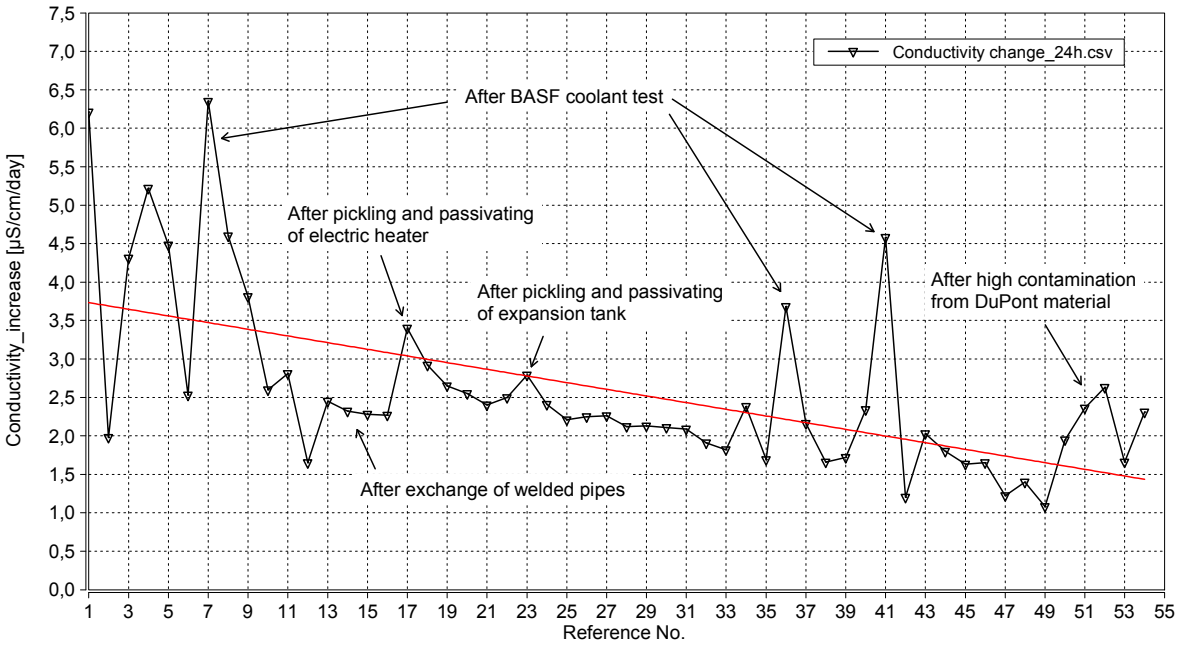

Figure 21: Change of conductivity increase of reference measurements over time; Reference measurements after modifications are marked

3.4.2 Search for ion sources and sinks: CO_2 degassing effect

In Figure 22, a typical reference measurement of fresh DI water at constant temperature where the effect of CO_2 degassing can be seen. This effect depends on the cleanliness of the testbed which will be discussed below. It can be seen in the conductivity curve within the first 10-15 hours where the curvature is upward bended. The conditioning phase was about 30 min and is shown in Figure 23. What can be seen in the conditioning phase is a nonlinear relation of conductivity and temperature (which was found to be linear after CO_2 degassing, see Figure 28) during the heat up phase. Also a slightly decrease at constant temperature after 18 min can be seen.

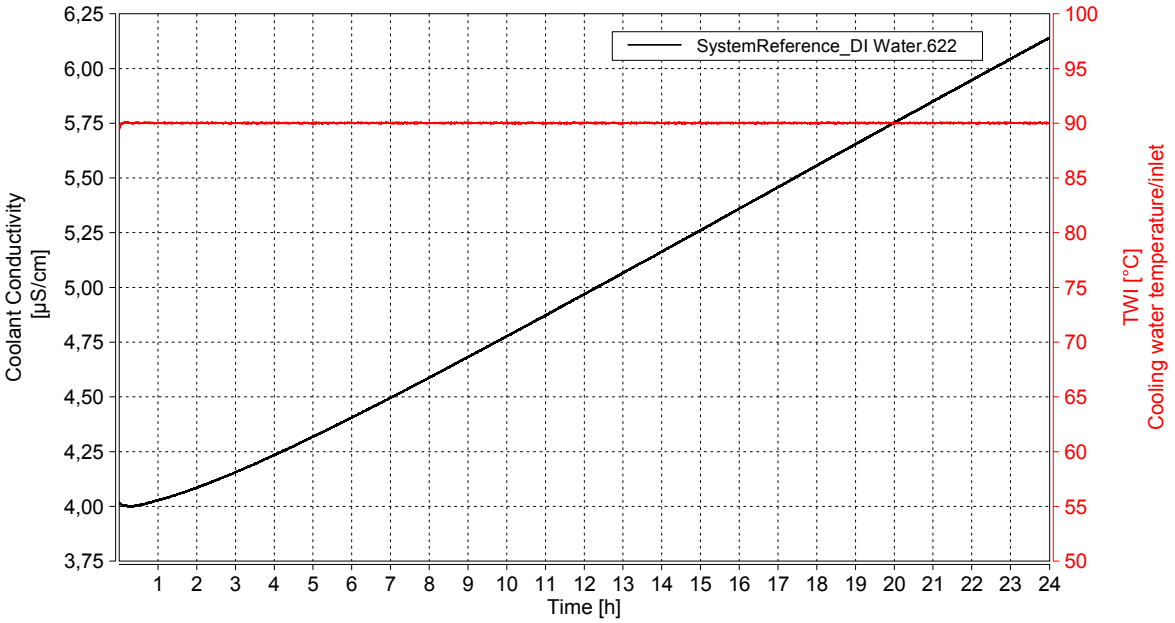

Figure 22: 24 h reference measurement of conductivity showing CO_2 degassing effect by upward bended curve

Modification of conditioning phase

Therefore a procedure was included to the conditioning phase to achieve faster degassing. It is well known that solubility of gases in liquids usually decreases with increasing temperature[10]. Hence, the system was heated up to higher temperature (95 °C instead of 90 °C) during conditioning in a first step. Here the conductivity changes by $-0.8\,\mu$S/cm in a bit more than an hour. This is measured at 90 °C where the cursors are positioned in Figure 24. In a second step the system was periodically pressurized. The reason for this is owed to an accidental observation. To get rid of excess CO_2 in the gas phase while degassing the system was periodic pressurized which can be seen in Figure 25. When the pressure pulses are applied, the conductivity decreases faster. Somehow this disturbance "helps" the gas to get out of the liquid. This leads to a change in conductivity of $-1.4\,\mu$S/cm within a comparable time frame to above (Figure 26). After this enhanced conditioning the CO_2 effect has no notable influence on the reference measurement, see Figure 27.

[10]Le Chatelier's principle: Dissolving gases in liquids usually is an exothermic reaction (energy increases, heat is created), therefore if the liquid is heated up stress is created at the product side of the reaction. This causes a shift in the equilibrium towards the reactants side (the gas phase), the solubility decreases [32].

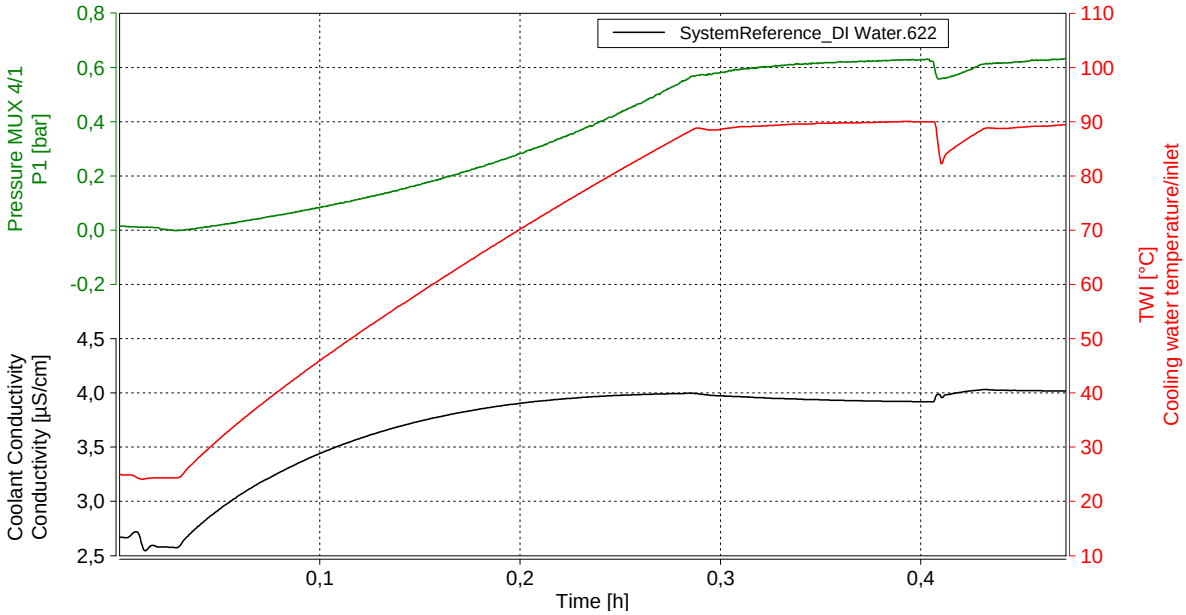

Figure 23: Simple conditioning with heat up phase only

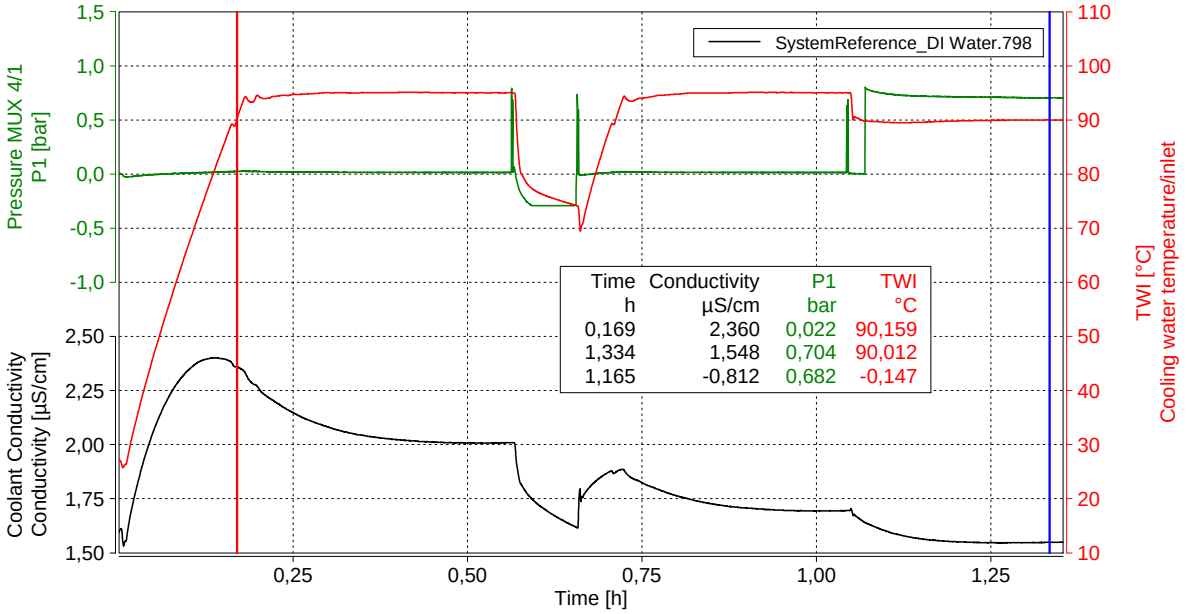

Figure 24: Conditioning with increased duration and temperature

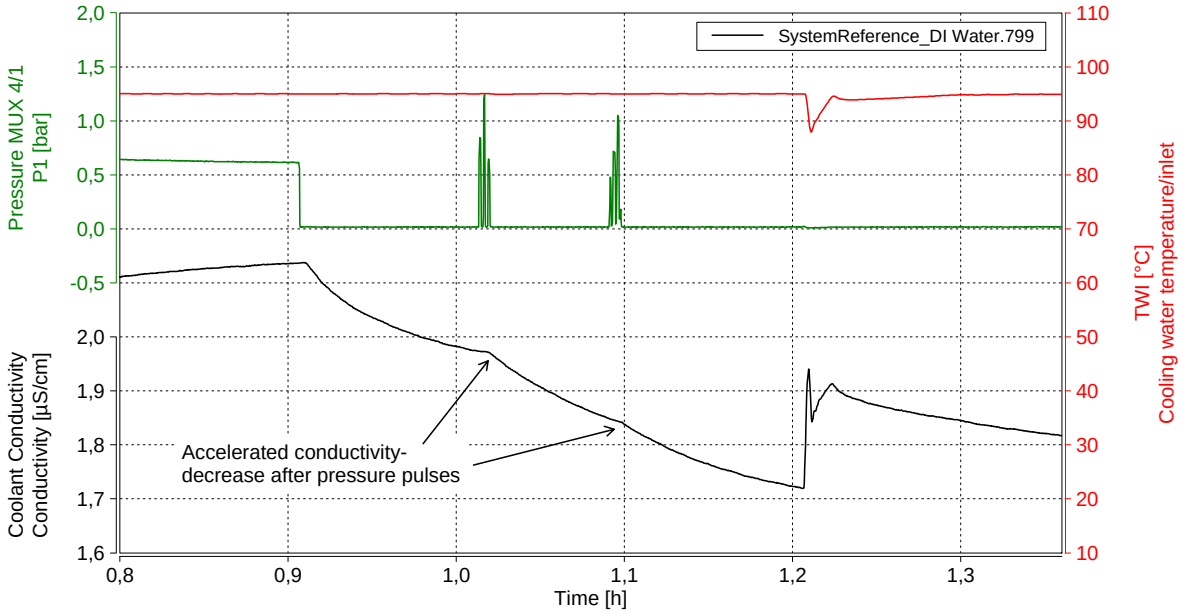

Figure 25: Effect of applying periodic pressure pulses

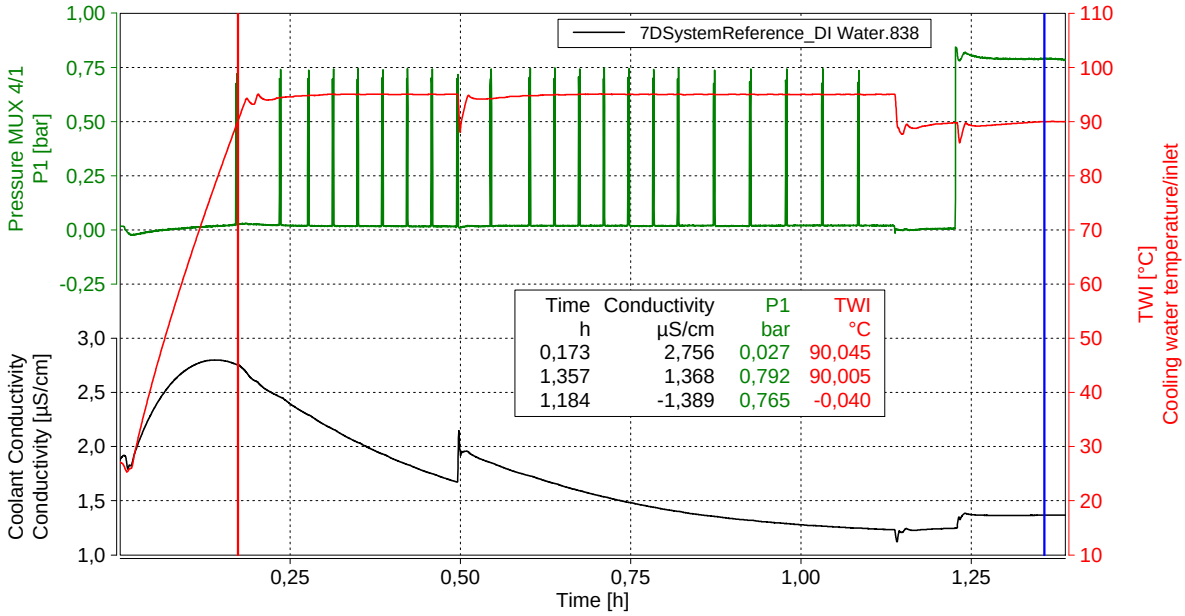

Figure 26: Enhanced conditioning with additional pressure pulses

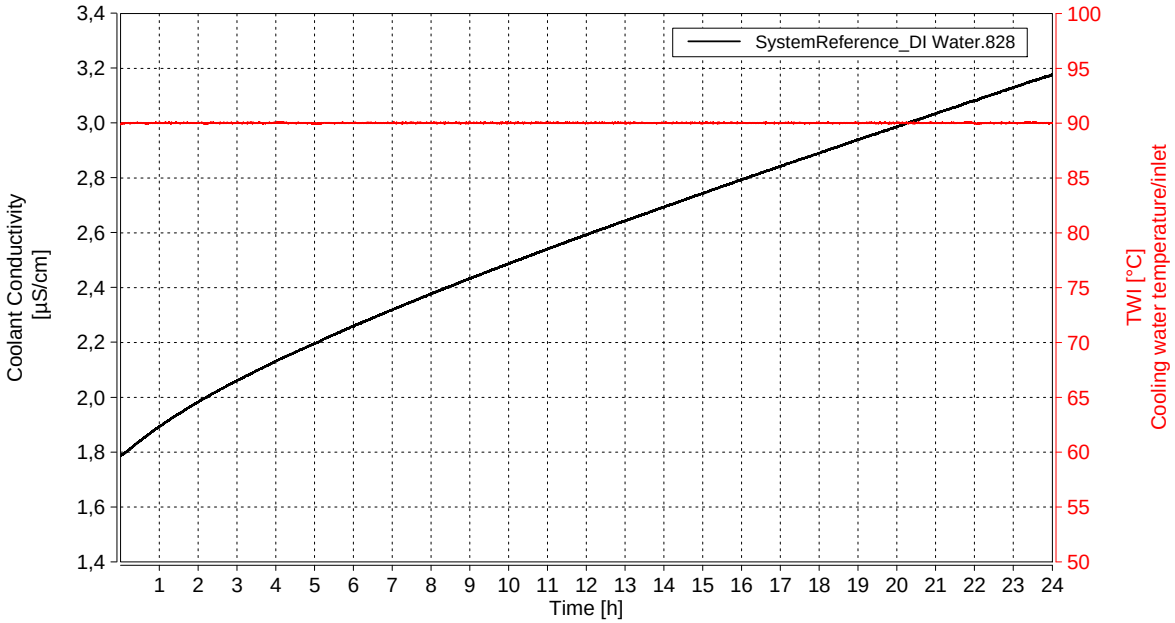

Figure 27: 24 h reference measurement of conductivity after CO_2 degassing by applying elevated temperature and periodic pressure pulses

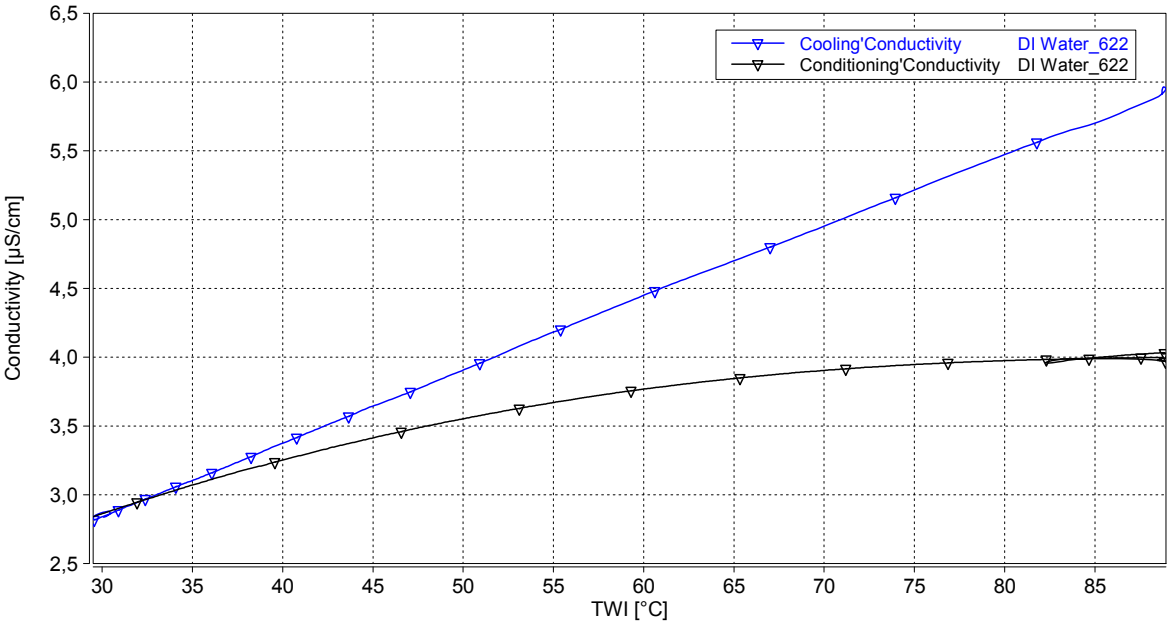

Figure 28: Relation between conductivity and temperature of DI water before (black curve) and after (blue curve) CO_2 degassing

Ethylene glycol hindered CO_2 degassing

Figure 29 shows a conditioning phase of DI water with residual amounts of BASF coolant. No decrease of conductivity can be seen at constant temperature (compare to Figure 24 and 26), on the contrary, the conductivity increases. This effect is assumed to be a further consequence of reduced CO_2 degassing. As shown by measurements in Section 4.2 and by Equations 17-19, the pH value of DI water is lower with dissolved CO_2 therefore making the DI water more corrosive. This conditioning phase corresponds to reference No. 41 in Figure 21 which shows a high increase rate.

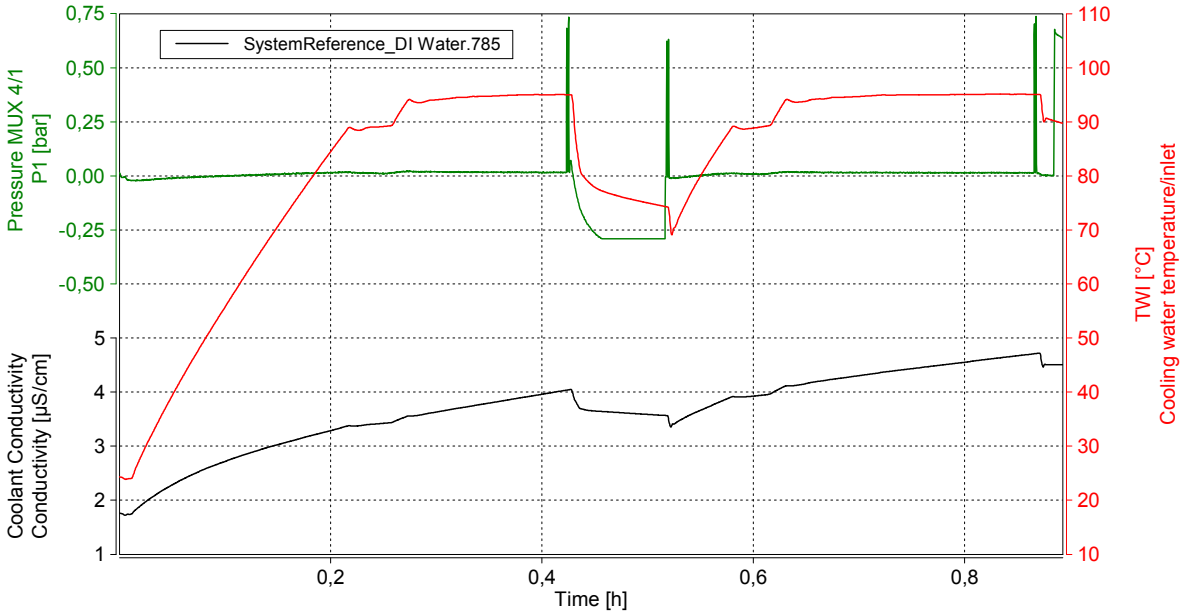

Figure 29: Conditioning phase of DI water with residual amount of BASF coolant, showing no CO_2 degassing effect

BASF coolant reference

If the system is operated with BASF coolant the conductivity curve also shows an upward bend, see Figure 30. The duration of this measurement is one week, compared to DI water this effect shows a much larger time scale. The upward bend can be seen within the first 20 hours, another upward bend region begins after 90 hours. As indicated by BASF degassing tests at room temperature (Section 4.2, Figure 40), the CO_2 is much stronger captured in the ethylene glycol containing coolant than in DI water which was found by a much larger time scale for degassing. The solubility of CO_2 in DI water/etlylene glycol mixtures increases as the amount of ethylene glycol increases [33], which fits this assumptions. The conditioning procedure from above does not work for the BASF

coolant, there was no decreasing conductivity found by applying periodic pressure or elevated temperature (within a timescale of 1-2 hours).
Due to the fact, that even residual amounts of BASF coolant in DI water didn´t show any upward bend in the conductivity curve the upward bend of the pure coolant may also have other reasons. Oxidation of Ethylene glycol in mixtures with DI water is a well known phenomenon of coolant degradation, leading to increased conductivity [1]. This thermal oxidation decreases pH value and increases corrosion of metallic components [2, 34]. In some coolant types antioxidants are added as corrosion inhibitors, which may be the case of the used BASF coolant but there was no detailed information available ("selected non-ionic inhibitors") about this additives. A special conditioning phase may be employed by heating to even higher temperatures and for longer periods of time to find out if CO_2 degassing plays a role. In this case the upward bend should vanish. If the upward bend doesn´t vanish a degradation effect would be more likely. However, the upward bend region after 90 hours and work [34] suggest, that degradation of ethylene glycol is the case. This investigative step would be important for future testing with ethylene glycol based fuel cell coolants.

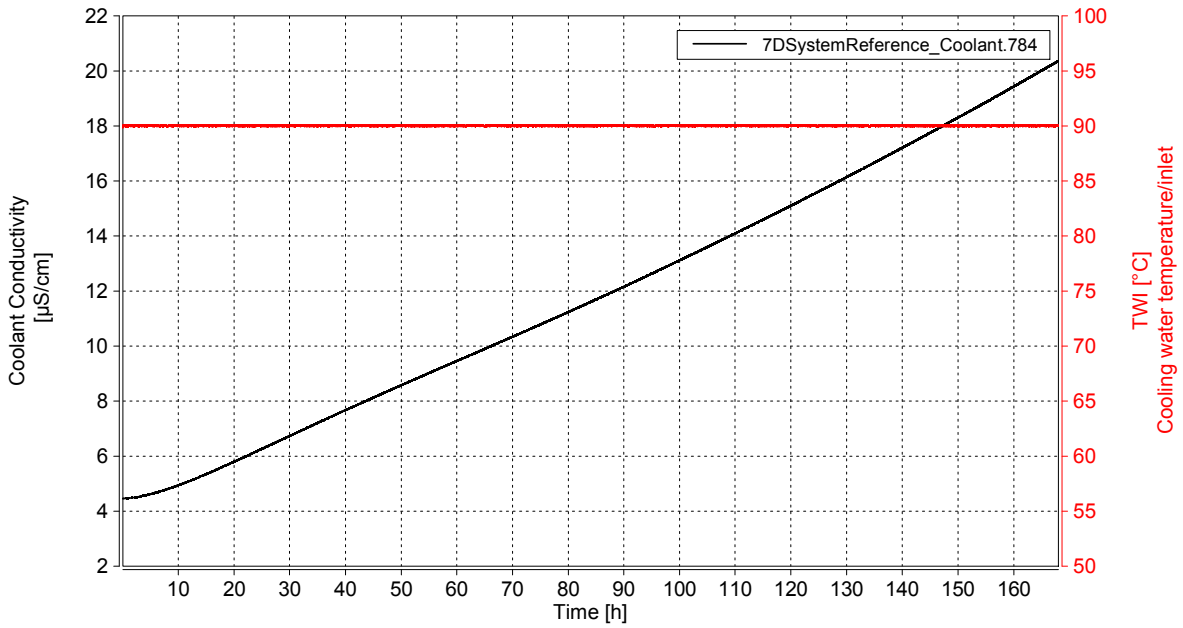

Figure 30: One week reference measurement with BASF coolant

3.5 Evaluation by reference materials

To get an orientation of how much the conductivity increase of the testbed over time could be acceptable or not for a certain test object, other work was taken as basis. There have been carried out system derived contaminant studies by the National Renewable Energy Laboratory (NREL), General Motors and the University of South Carolina [13, 29, 35, 36, 12]. This was a collaborative work between the years 2009 and 2014 and the received data was published online [13], with Huyen N. Dinh as lead autor. The selection of these materials was based on physical properties (e.g. operating conditions in an automotive fuel cell system, processability), comercial availability, cost and by input from OEMs and fuel cell system manufacturers [35]. Some of these material were chosen for the evaluation of the testbed, see Table 9. The tests published by NREL were carried out in bottles, therefore additional bottle tests were performed in parallel to reproduce these tests (see Section 4.1).

Table 9: Polymeric materials used in the evaluation of the Material Compatibility Testbed

Material	Manufacturer	Trade name	Grade	No.
PA66	DuPont	Zytel	PLS90G30DR BK099[1]	P1
PA[4]	DuPont	Zytel	PLS95G35DH1 BK549[2]	P2
PA66	DuPont	Zytel	70G30HSLR BK099[3]	P3
PBT	DuPont	Crastin	HR5330HF BK503	S1
PPA	DuPont	Zytel	HTN51G35HSLR BK420	S2
PBT	DuPont	Crastin	6130 NC010	S3
PPS	Chevron Phillips	Ryton	R4-200 BL	S4
PPS	Chevron Phillips	Ryton	R7-120 BL	S5

3.5.1 Experimental

The samples were cut to two plates with dimensions of (69.0 ± 0.1) mm x (100.0 ± 0.1) mm x (2.0 ± 0.1) mm. When samples were thicker dimensions were reduced to achieve $(6.9 \pm 0.3)\,\mathrm{mm}^2/\mathrm{ml}$. Holes were drilled for mounting on the sample holder (see Figure 15). Each sample was cleaned with IPA and subsequently with DI water, then the samples were weighed. Each polymer sample was tested for one week in the Testbed. Between each test the Testbed was filled with fresh DI water and a reference measurement was performed to minimize influence of dead spaces/volumes. To evaluate the mass loss

[1] No color information was available from online data, BK099 was purchased
[2] No color information was available from online data, BK549 was purchased
[3] No color information was available from online data, BK099 was purchased
[4] Nylon unspecified

of the samples water uptake needed to be considered. The mass of the samples after the test was higher than before. Therefore the material was cleaned with IPA and DI water and subsequently put into an oven at 80 °C for 3 days together with an untreated sample of the same material. This reference takes into account the residual humidity in the new samples. Then the corrected mass loss was calculated (see below).

Corrected mass loss calculation:

First the relative mass loss of the sample Δm^{rel}_{Sample} and the reference Δm^{rel}_{Ref} are calculated

$$\Delta m^{rel}_{Sample} = \frac{m_{Sample,new}}{m_{Sample,dry}} \tag{39}$$

$$\Delta m^{rel}_{Ref} = \frac{m_{Ref,new}}{m_{Ref,dry}} \tag{40}$$

whereby the relative mass loss of the sample should be higher. The theoretical (if it would not have been boiled) mass of the dried sample $m^{theoretical}_{Sample,dry}$ can therefore calculated by

$$m^{theoretical}_{Sample,dry} = \frac{m_{Sample,new}}{\Delta m^{rel}_{Ref}} \tag{41}$$

Now the corrected mass loss Δm_{Corr} can be calculated by subtracting the real mass $m^{real}_{Sample,dry}$ of the dried sample.

$$\Delta m_{Corr} = m^{theoretical}_{Sample,dry} - m^{real}_{Sample,dry} \tag{42}$$

3.5.2 Results and discussion

In the appendix in Section 10.2 the measurement protocols for all measurements can be found (Figure 54 to 62). The measurement of P2 and S5 show a jump of the conductivity value at about 100 μS/cm caused by a malfunction of the measurement electronic of the conductivity sensor, see Figure 55 and 62. The end value of conductivity NREL_SolCond can be compared to the value NREL_Control of the cooling phase where the conductivity is measured at lower temperatures and where the effect of this jump vanished. Both values matched within an error smaller than 3 % comparable to the other results, meaning that the influence of this malfunction is negligible.
In Table 10 the conductivities at the begin κ_{start} and after the test κ^{nrel}_{end} and $\kappa^{nrel-corr}_{end}$ are shown and compared to the values $\kappa^{nrel-lit}_{end}$ found in the NREL publication. The values $\kappa^{nrel-corr}_{end}$ of samples P1 and P3 are smaller than the literature values by a factor of about 3-4, S1 by a factor of 11 and S2 by a factor of 5. The values κ^{nrel}_{end} of samples

P1, P3, S1 and S2 by a factor of abut 2. Both values of sample P2 exceed the literature value by a factor of about 3 for sample S5 by a factor of 11. The high conductivity value of S5 is assumed to be caused by a crack of the sample which increased its surface area significantly. This can be concluded as a poor match. For sample S3 the values fit better, especially $\kappa_{end}^{nrel-corr}$. The literature value of S4 also shows a better fit. Also the conductivity increase rates $\Delta\kappa/day$ can be seen which may be more relevant for characterization of reference measurements, therefore is not further discussed in this section.

Table 10: Measured and normalized (to 150 mm^2/ml) conductivities (T25-lin) before and after the *one week test in the Testbed* of DuPont samples compared to results of H.N. Dinh (NREL)

Sample	κ_{start} [μS/cm]	$\Delta\kappa/day$ [μS/cm/day]	κ_{end}^{nrel} [μS/cm]	$\kappa_{end}^{nrel-corr}$ [μS/cm]	$\kappa_{end}^{nrel-lit}$ [μS/cm]
P1	1.7±0.1	1.2±0.3	218±11	96±5	435.0
P2	1.6±0.1	5.2±0.3	1154±58	1028±52	347.0
P3	1.7±0.1	2.1±0.3	566±28	438±22	1441.0
S1	1.8±0.1	0.5±0.1	131±7	33±2	378.0
S2	1.7±0.1	0.9±0.1	181±9	82±4	398.0
S3	1.7±0.1	0.2±0.1	107±5	47±2	58.5
S4	1.7±0.1	0.7±0.1	130±7	35±2	64.2
S5	1.9±0.1	7.4±0.3	1157±58	1075±54	94.4
Reference	1.8±0.1	(1.3±0.3)[1]	3.8	-	1.9

Assignment of variables between tables and measurement protocols in appendix:
κ_{start}.....*Conductivity Min (Conditioning)*
$\Delta\kappa/day$.....*CondCorrected_sect2_lin*
κ_{end}^{nrel}.....*NREL_SolCond*
$\kappa_{end}^{nrel-corr}$...*NREL_SolCond_Corr*
$\kappa_{end}^{nrel-lit}$.....*Solution conductivity from literature (NREL) [13]*

Compared to the normalized (to 150 mm^2/ml) solution conductivity values of the six weeks test (see Section 4.1.3) a better match can be found, see Table 11. The relative mass loss of the six weeks leaching test exceeds the relative mass loss of the test in the Testbed by (34 ± 11) % (see below). Therefore the testbed results of conductivity should show a tendency to smaller values which is the case.

[1]The $\Delta\kappa$ values of the measurements can be smaller than from the reference value (left column) because the reference measurement is already subtracted

Table 11: Comparison of one week Testbed result, six weeks bottle tests and literature values

Sample	$\kappa_{end}^{nrel-corr}$ [μS/cm]	$\kappa_{end}^{6w-norm}$ [μS/cm]	$\kappa_{end}^{nrel-lit}$ [μS/cm]
PLS90G30DR BK099 (P1)	96±5	240±20	435.0
PLS95G35DH1 BK549 (P2)	1028±52	1108±20	347.0
70G30HSLR BK099 (P3)	438±22	591±20	1441.0
HR5330HF BK503 (S1)	33±2	36.1±2	378.0
HTN51G35HSLR BK420 (S2)	82±4	242±20	398.0
6130 NC010 (S3)	47±2	143.3±7	58.5
R4-200 BL (S4)	35±2	54.8±3	64.2
R7-120 BL (S5)	1075±54	77.9±4	94.4

In Table 12 and 13 the mass loss of the samples is shown. As mentioned above the relative mass loss is lower compared to the six weeks leaching test in Section 4.1.3. This mass loss can be compared to the TDS values by calculation via Equation 16 (Section 2.4.4) and is shown for P1-P3. Compared to the real mass losses the calculated TDS values are much lower. One reason for this difference may be related to the cleaning procedure after the test where deposits on the surface were removed (see discussion in Section 4.1.4). However, the difference between the mass loss and the calculated TDS values are an indication that there is a significant amount of non ionic impurities in the leachant solutions. It also suggests that this formula is not applicable for estimation of the mass loss. In Table 13 the mass of sample S3 was higher after 4 days drying at 80 °C, in this case there may be still significant amounts of water in the sample. Sample S3 also showed a slightly increase in mass. This is assumed to be caused by insufficient drying conditions. In this case more samples were dried at the same time compared to P1-P3 and the thickness of the samples was higher (see also Section 4.1.3).

Table 12: Mass loss of polymer samples P1-P3 after *one week in testbed*

	P1	P2	P3
$m_{Ref,new}$ (g)	27.6154	29.2933	28.0107
$m_{Ref,dry}$ (g)	27.4032	29.0804	27.8005
Δm_{Ref}^{rel}	1.0077	1.0073	1.0076
$m_{Sample,new}$ (g)	37.4790	39.6171	37.8790
$m_{Sample,dry}$ (g)	37.0149	38.6607	37.3846
Δm_{Sample}^{rel}	1.0125	1.0247	1.0132
$m_{Sample,dry}^{theoretical}$ (g)	37.1910	39.3292	37.5947
$\boldsymbol{\Delta m_{Corr}}$**(mg)**	**176.1±0.8**	**668.5±0.8**	**210.1±0.8**
$\boldsymbol{TDS}$**(mg)**	**18.2±5.5**	**195.3±58.6**	**83.2±25.0**
$\boldsymbol{\Delta m_{Corr}^{rel}}$ **(%)**	**0.474±0.002**	**1.700±0.002**	**0.559±0.002**

Table 13: Mass loss of polymer samples S1-S5 after *one week in testbed*

	S1	S2	S3	S5
$m_{Ref,new}$ (g)	48.3482	34.2695	38.5721	14.7676
$m_{Ref,dry}$ (g)	48.2840	34.1924	38.5199	14.7642
Δm^{rel}_{Ref}	1.0013	1.0023	1.0014	1.0002
$m_{Sample,new}$ (g)	78.4167	63.6666	54.1473	100.6696
$m_{Sample,dry}$ (g)	78.2270	64.3964	54.0984	100.5400
Δm^{rel}_{Sample}	1.0024	0.9887	1.0009	1.0013
$m^{theoretical}_{Sample,dry}$ (g)	78.3126	63.5234	54.0740	100.6464
$\boldsymbol{\Delta m_{Corr}}$**(mg)**	0.0856	-0.8730	-0.0244	0.1064
$\boldsymbol{\Delta m^{rel}_{Corr}}$**(%)**	**0.109±0.001**	**-1.374±0.001**	**-0.045±0.001**	**0.106±0.001**

3.6 Proposals for enhancement of testbed design

Regarding the issues which were addressed in Section 3.4.1 the following suggestions for improvement of the system can be made: (1) To minimize the effect of stainless steel corrosion the quality of the wetted stainless steel surfaces needs to meet sanitary standard. (2) Prevention or minimization of dead spaces/volumes is another important factor to reduce unwanted contamination. (3) Welded stainless steel parts need to be properly treated and also should meet sanitary standard quality. (4) Clamp connections are recommended (e.g. ISO 2852, DIN 32676) which fulfill requirements suggested above. (5) Smooth PTFE hoses or PTFE lined hoses are recommended because of reduced pressure drop and better removal of residual coolant and contaminants compared to corrugated PFA hoses. The PFA bottle tests in Section 4.3.3 and 4.4 show an increase of conductivity which is assumed to be caused by the material of the bottles, this effect also may be less with PTFE.

Degassing of DI water / coolant before filling the system would prevent non-linearity of reference measurements and reduce CO_2 induced acidity of the DI water. This was assumed to influence the conductivity increase of reference measurements.

The one week bottle tests in Section 4.1.4 showed that the BASF coolant led to a significant difference in conductivity increase which was lower by a factor of 3.7 compared to DI water for two polyamide materials. Therefore the question occurs if it does make sense to test with this special type of coolant. The amount of ethylene glycol in the BASF coolant varies (45-55 %) which may influence the test. Another influence can be the case if the coolant of another manufacturer is used. Therefore, to stay on the safe side (more contaminants are leached out), to enhance reproducibility of tests, to safe

money and to keep things more simple, DI water is assumed to be the better choice for testing.

4 Bottle tests

4.1 Leaching tests

4.1.1 Introduction

To get a comparable basis for the results of the testbed, the materials from Table 9 were investigated under the same conditions as found in work [13, 29]. The materials were put into bottles with DI water and subsequently into an oven at 90 °C for 6 weeks. The surface area to volume of water ratio was 150 mm^2/ml for the 6 weeks tests. The resulting leachant solution was analyzed and conductivity was measured. In this work the mass loss of the tested materials was measured as well. Additionally shorter tests were performed as one week tests and a one hour boiling test whereby the surface area to volume of water ratios were changed.

4.1.2 Boiling test of DuPont material

A one hour boiling test was performed, to evaluate a testing procedure under accelerated conditions and to get a first insight into the contamination potential of a material. Another important goal of this test was to determine the mass loss of the sample.

Experimental:

The following material was chosen for this test: 70G30HSLR BK099 from DuPont (see Table 9). The sample was cleaned with IPA first and then with DI water. Subsequently it was dried with compressed air to prevent further water uptake. The Sample with the dimensions of (100.0 ± 0.1) mm × (69.0 ± 0.1) mm × (2.0 ± 0.1) mm was weighed and then immersed into DI water within a glass beaker. At the end of the test (590 ± 2) ml DI water were measured, therefore the $\frac{A_{Sample}}{V_{Water}}$ was (24.5 ± 0.2) mm^2/ml. Teflon coated stir bars were added as condensation nuclei and the beaker was covered by a watch glass. The conductivity[11] of the DI water and the mass of the samples were measured before and after the test at room temperature. The sample was boiled on a combined hot-plate magnetic-stirrer device for one hour.

[11] All conductivities were measured with linear temperature compensation of 2 % per degree, with 25 °C as reference temperature (T25-lin)

Results and discussion:

The conductivity of the DI water before the test was $(1.79 \pm 0.04)\,\mu$S/cm. The conductivity after the test was $(15.72 \pm 0.30)\,\mu$S/cm and the amount of the solution was 590 ml. Due to water uptake, the mass of the samples after the leaching test was higher than before. Therefore the material was put into an oven at 80 °C for 3 days together with an untreated sample of the same material as reference to take into account the residual humidity in the new samples. The corrected mass loss calculation was done as described in Section 3.5. In Table 14 the weight of the sample, reference and the corrected mass loss Δm_{Corr} are shown. This real[12] mass loss of (3.5 ± 0.8) mg can be compared to the TDS calculation via Equation 16 which was described in Section 2.4.4 and is also shown in Table 16. Although being a rough estimation the order of magnitude is on a comparable level.

Table 14: Mass loss of polymer sample after 1 h boiling test

	70G30HSLR BK099
$m_{Ref,new}$ (g)	19.4632
$m_{Ref,dry}$ (g)	19.2988
Δm^{rel}_{Ref}	1.0085
$m_{Sample,new}$ (g)	19.5429
$m_{Sample,dry}$ (g)	19.3743
Δm^{rel}_{Sample}	1.0087
$m^{theoretical}_{Sample,dry}$ (g)	19.3778
$\boldsymbol{\Delta m_{Corr}}$**(mg)**	**3.5±0.8**
$\boldsymbol{TDS}$**(mg)**	**6.0±1.8**
$\boldsymbol{\Delta m^{rel}_{Corr}}$ **(%)**	**0.018±0.004**

4.1.3 Six weeks leaching test

For this test the samples which are shown in Table 9 were used. An important fact is that for the samples P1-P3 no color information was available from the literature, therefore the most used color in the automotive industry was purchased (black), which was already mentioned in Table 9. For this reason additional samples were purchased (S1-S5) where color information was available.

[12] There may be an (unknown) additional error present for the mass loss correction due to possible remaining humidity within the sample after the drying process

Experimental:

Each sample was cut to 4 plates with dimensions of (49.0 ± 0.1) mm x (42.8 ± 0.1) mm x (2.0 ± 0.1) mm, cleaned with IPA first and then with DI water. Subsequently they were dried with compressed air to prevent further water uptake and each sample was weighed (4 plates together). Then they were put into DI water filled PP bottles with surface area to volume of water ratio $\frac{A_{Sample}}{V_{Water}}$ of $(152 \pm 2)\,\mathrm{mm}^2/\mathrm{ml}$. The uncertainty of the dimensions is included into the error of the $\frac{A_{Sample}}{V_{Water}}$ ratio. Another bottle filled with DI water only was added as reference. The bottles were then put into an oven for six weeks at 90 °C. The conductivity[13] of all samples was measured before and after the test at room temperature. After the test materials were removed from the leachant solution to prevent further leaching or re-adsorption and conductivity was measured. The samples were cleaned with IPA and DI water, then they were put into an oven at 80 °C for 4 days together with a reference material. Then the mass loss calculation was done as described in Section 4.1.2.

Results and discussion:

The conductivities of the solutions are shown in Table 15. Tested under the same conditions as described in work [13, 29], the conductivities do not match. The order of the conductivities from low to high is P1 < P3 < P2 and didn´t match the order of NREL, which is P2 < P1 < P3. The conductivity of Sample P2 showed the highest value of $(1241 \pm 20)\,\mu$S/cm whereas it was the lowest with $(347 \pm 20)\,\mu$S/cm in the work of Dinh. The conductivity of sample S1 was lower by a factor of 10 than literature, the samples S4 and S5 show a good match.
The first test was started with 120 ml DI water, during the test some of the water escaped reducing the amount to (104.0 ± 0.3) ml (P1), (108.0 ± 0.3) ml (P2) and (107.0 ± 0.3) ml (P3) until the end of the test, this means the $\frac{A_{Sample}}{V_{Water}}$ value exceeds $(152 \pm 2)\,\mathrm{mm}^2/\mathrm{ml}$. For that reason in column 3 of Table 15 a normalized (to $150\,\mathrm{mm}^2/\mathrm{ml}$) value was added. Also water uptake of the samples has to be considered which was found to be 6 % for P1 and P3. Therefore an additional amount of (1.0 ± 0.1) ml water was trapped in these samples. No information of water uptake was available for P2. The second test startet with 110 ml DI water, the residual amounts after the test were (94.9 ± 0.3) ml (S1), (95.6 ± 0.3) ml (S2), (92.9 ± 0.3) ml (S3), (96.2 ± 0.3) ml (S4) and (96.1 ± 0.3) ml (S1). In Table 16 and 17 the mass loss of the samples is shown. Compared to the 1 h boiling

[13] All conductivities were measured with linear temperature compensation of 2 % per degree, with 25 °C as reference temperature (T25-lin)

Table 15: Conductivities (T25-lin) before and after the *six weeks leaching test* of DuPont samples compared to NREL results

Sample	κ_{start} [μS/cm]	κ_{end}^{6w} [μS/cm]	$\kappa_{end}^{6w-norm}$ [μS/cm]	$\kappa_{end}^{nrel-lit}$
PLS90G30DR BK099 (P1)	2.50±0.05	281±20	240±20	435.0
PLS95G35DH1 BK549 (P2)	3.16±0.06	1241±20	1108±20	347.0
70G30HSLR BK099 (P3)	2.99±0.06	670±20	591±20	1441.0
HR5330HF BK503 (S1)	3.40±0.06	41.6±2	36.1±2	378.0
HTN51G35HSLR BK420 (S2)	3.40±0.06	279±20	242±20	398.0
6130 NC010 (S3)	3.40±0.06	169.7±9	143.3±7	58.5
R4-200 BL (S4)	3.40±0.06	62.7±3	54.8±3	64.2
R7-120 BL (S5)	3.40±0.06	89.2±5	77.9±4	94.4
Reference 1	2.44±0.05	2.48±0.2	-	1.9
Reference 2	2.45±0.05	2.50±0.2	-	-

test for P3 the relative mass loss of the six weeks leaching test is 39 times higher. This mass loss can be compared to the TDS calculation via Equation 16 and can be found in Table 16. Compared to the real mass losses the calculated TDS values are much lower. One reason for this difference may be related to the cleaning procedure after the test where deposits on the surface were removed. This may be relevant for P1 and P3. Sample P1 showed visible deposition effects on its surface, similar to Figure 32(b). These were red colored and could be removed with IPA and DI water. Sample P3 didn´t show visible deposits but cleaning showed brown colored deposits. P2 showed a mat (leached out) surface and didn´t show visible or removable deposits, it lost nearly 2.5 % of its mass which is a lot. The difference between the mass loss and the calculated TDS values are an indication that there is a significant amount of non ionic impurities in the leachant solutions. To get the correct TDS value from Equation 16 the conductivities needed to be higher by a factor of about 7 for sample P1 and P2 and by a factor of 3 for sample P3. The mass loss of the samples S1-S5 was negative for S2, S3 and S5 which is assumed to be caused by insufficient drying conditions. In this case more samples were dried at the same time compared to P1-P3 and the thickness of the samples was higher. The solutions were colored after test as shown in Figure 31(a). Floating deposits were found on the solutions of P3 and P1, none could be found for P2 (see Figure 31). Even after some weeks, no sedimentation was observed at all solutions.

Table 16: Mass loss of polymer samples after *six weeks leaching test*

	PLS90G30DR BK099	PLS95G35DH1 BK549	70G30HSLR BK099
$m_{Ref,new}$ (g)	27.6154	29.2933	28.0107
$m_{Ref,dry}$ (g)	27.4032	29.0804	27.8005
Δm^{rel}_{Ref}	1.0077	1.0073	1.0076
$m_{Sample,new}$ (g)	23.0423	24.6059	23.2486
$m_{Sample,dry}$ (g)	22.7220	23.8263	22.9115
Δm^{rel}_{Sample}	1.0141	1.0327	1.0147
$m^{theoretical}_{Sample,dry}$ (g)	22.8652	24.4271	23.0741
$\boldsymbol{\Delta m_{Corr}}$**(mg)**	**143.2±0.8**	**600.8±0.8**	**162.6±0.8**
$\boldsymbol{TDS}$**(mg)**	**19±6**	**87±26**	**47±14**
$\boldsymbol{\Delta m^{rel}_{Corr}}$ **(%)**	**0.626±0.004**	**2.459±0.003**	**0.705±0.004**

Table 17: Mass loss of polymer samples S1-S5 after *six weeks leaching test*

	S1	S2	S3	S5
$m_{Ref,new}$ (g)	48.3482	34.2695	38.5721	14.7676
$m_{Ref,dry}$ (g)	48.2840	34.1924	38.5199	14.7642
Δm^{rel}_{Ref}	1.0013	1.0023	1.0014	1.0002
$m_{Sample,new}$ (g)	37,5296	31,1139	25,8152	48,2297
$m_{Sample,dry}$ (g)	37,4471	31,6352	25,8635	48,3610
Δm^{rel}_{Sample}	1,0022	0,9835	0,9981	0,9973
$m^{theoretical}_{Sample,dry}$ (g)	37,4798	31,0439	25,7803	48,2186
$\boldsymbol{\Delta m_{Corr}}$**(mg)**	**0,0327**	**-0,5913**	**-0,0832**	**-0,1424**
$\boldsymbol{\Delta m^{rel}_{Corr}}$**%**	**0,087±0.002**	**-1,905±0.002**	**-0,323±0.002**	**-0,295±0.002**

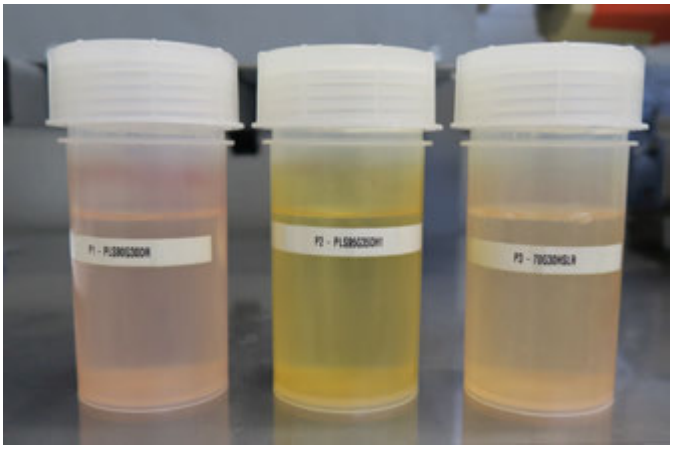

(a) PP bottles after six weeks leaching test

(b) Leachant solution of P1

(c) Leachant solution of P2

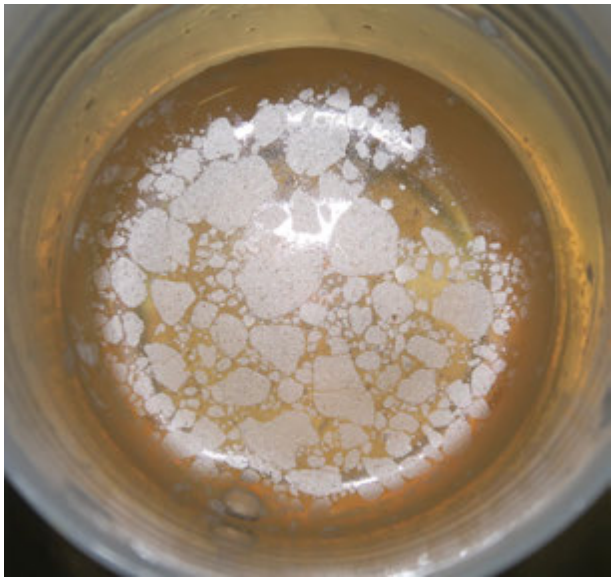

(d) Leachant solution of P3

Figure 31: Leachant solutions after six weeks leaching test of PLS90G30DR BK099 (P1), PLS95G35DH1 BK549 (P2) and 70G30HSLR BK099 (P3)

4.1.4 One week leaching tests

Accompanying to the six weeks leaching test, some weekly leaching tests were performed. One goal was to reproduce the relation between the conductivities of the samples of the six weeks test (Test 1) and to see if there is an effect between different batches (Test 2). Another goal was to confirm the assumption that there is a linear relation between the change in surface area to volume ratio and the conductivity increase, in other words to see the scaling effect (Test 3). Test 4 was added to check the influence of BASF fuel cell coolant. Because of the missing color information on the NREL website non-colored versions of DuPont Materials PLS95G35DH1 NC010 (P2/NC) and 70G30HSLR BK099 (P3/NC) were purchased and tested (Test 5). Evaluation of the mass loss caused by cleaning the samples after the test was performed as well (Test 6). For one of the reference bottles a used bottle of a previous six weeks test was taken which showed a non-removable colored appearance. This was for checking the influence of used bottles.

Experimental Test 1:

The samples P1, P2, P3, S1, S2, S3, S4 and S5 (see Table 9) were cut to 4 plates, cleaned with IPA first and then with DI water. Then they were put into DI water filled PP bottles with surface area to volume of water ratio $\frac{A_{Sample}}{V_{Water}}$ of $(102 \pm 3)\,\mathrm{mm^2/ml}$. The uncertainty of the dimensions is included into the error of the $\frac{A_{Sample}}{V_{Water}}$ ratio. Another bottle filled with DI water only was added as reference. The bottles were then put into an oven for one week at 90 °C. The test was started with 120 ml DI water, during the test some of the water escaped reducing the amount to $(118 \pm 1)\,\mathrm{ml}$ at the end of the test. The conductivity[14] of all samples was measured before and after the test at room temperature. After the test materials were removed from the leachant solution to prevent further leaching or re-adsorption and conductivity and mass loss was measured.

Experimental Test 2, 4 and 5:

The second batch of the samples PLS90G30DR BK099 (P1/2), PLS95G35DH1 BK549 (P2/2) and 70G30HSLR BK099 (P3/2) from DuPont (see Table 9) were cleaned as described in Test 1. Then they were put into DI water filled PP bottles with surface area to volume of water ratio $\frac{A_{Sample}}{V_{Water}}$ of $(98 \pm 3)\,\mathrm{mm^2/ml}$. The dimensions of the 4 plates were 47.5 mm x 26 mm, where the thickness of P1 was 2 mm and of P3 4 mm. Sample P2, P2/NC and P3/NC were prepared with $(150 \pm 5)\,\mathrm{mm^2/ml}$ and dimensions of 55 mm

[14] All conductivities were measured with linear temperature compensation of 2 % per degree, with 25 °C as reference temperature (T25-lin)

x 30 mm x 2 mm. Two additional bottles filled with BASF coolant were prepared under the same conditions with samples P1 and P3.

Experimental Test 3:

Samples of the polymer 70G30HSLR BK099 from DuPont (see Table 9) were cleaned as described in Test 1. Then they were put into DI water filled PP bottles with different surface area to volume of water ratios of $\frac{A_{Sample}}{V_{Water}}$ of $(98.6 \pm 3.0)\,\mathrm{mm}^2/\mathrm{ml}$ (4 plates), $(49.3 \pm 2.0)\,\mathrm{mm}^2/\mathrm{ml}$ (2 plates) and $(24.6 \pm 1.0)\,\mathrm{mm}^2/\mathrm{ml}$ (one plate). The dimensions of the plates were 47.5 mm x 26 mm x 4 mm.

Experimental Test 6:

To evaluate the mass loss caused by cleaning, the samples (received from Test 1) P1, P2 and P3 with deposits on the surface were put into an oven for 4 days at 80 °C. Then they were weighed, cleaned with IPA and DI water and again put into the oven for one day to remove residual cleaning liquid. Then the weight was measured again.

Results and discussion:

The conductivities of *Test 1* can be seen in Table 18 with comparison to the six weeks test, also the data from NREL website [13] is shown. Compared to this work, the surface to volume ratio was smaller ($(102 \pm 2)\,\mathrm{mm}^2/\mathrm{ml}$ instead of $150\,\mathrm{mm}^2/\mathrm{ml}$) and the leaching time was reduced (one instead of six weeks), therefore smaller quantities of the conductivities were expected compared to the six weeks test which was confirmed. The order of the conductivities from low to high is P1 $<$ P3 $<$ P2 and matches with the six weeks leaching test. Again no match was found the order of NREL, which is P2 $<$ P1 $<$ P3. The relation between the conductivities P1 : P2 : P3 is 1 : 4.4 : 2.4 for the six weeks and 1 : 8.4 : 4 for the one week test, indicating that P2 and P3 have higher initial contamination potential compared to P1. This fits with information in the data sheet from DuPont that P1 has a "superior resistance to hot engine coolant". The solutions were colored after the test where P2 showed the highest color intensity, see Figure 32(a). Sample P1 showed visible (see Figure 32(b)) deposition effects on its surface which were red colored and could be removed with IPA and DI water. Sample P2 showed a mat (leached out) surface without notable deposits. Sample P3 didn´t show visible deposits but cleaning with IPA and DI water showed brown colored deposits.

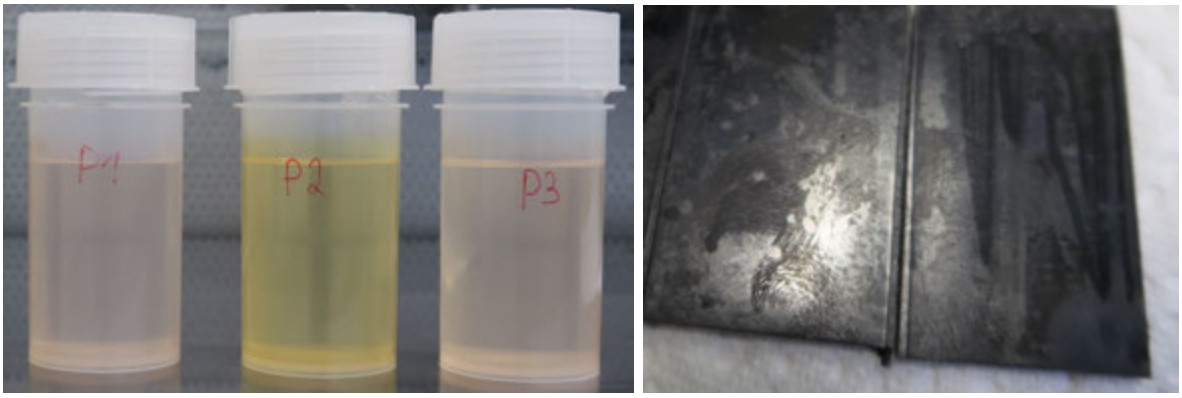

(a) PP bottles after one week leaching test (b) Sample P1 with removable deposits

Figure 32: One week leaching test of PLS90G30DR BK099 (P1), PLS95G35DH1 BK549 (P2) and 70G30HSLR BK099 (P3)

Table 18: Conductivities (T25-lin) before and after the *one week leaching test* of DuPont samples compared to NREL results

Sample	κ_{start} [μS/cm]	κ_{end}^{1w} [μS/cm]	κ_{end}^{6w} [μS/cm]	$\kappa_{end}^{nrel-lit}$
P1	1.4±0.1	82±4.0	281±20	435.0
P2	1.4±0.1	698±20	1241±20	347.0
P3	1.4±0.1	333±20	670±20	1441.0
S1	2.5±0.1	8.1±0.5	41.6±2.0	378.0
S2	2.5±0.1	110.8±5.5	279±20	398.0
S3	2.5±0.1	36.0±1.8	169.7±8.5	58.5
S4	1.4±0.1	47.8±2.4	62.7±3.2	64.2
S5	1.9±0.1	72.7±3.6	89.2±4.5	94.4

The samples S1 and S2 show a very strong mismatch especially S1 which seems to be the absolute minimum contaminating material in these tests. S3, S4 and S5 show a good match with lower values which again fits with the fact of shorter time and smaller surface area to volume ratio.

The outcome of the *Tests 2, 3, 4 and 5* can be seen in Table 19. The effect of using another batch shows a significant difference for P3/2 where the conductivity is nearly two times higher than the first batch (Table 18). This may be an effect of using another batch. Another possible reason is related to the thickness of the plates because the first batch had 2 mm thickness and the second batch 4 mm. The volume (and therefore the mass) increases by a factor of 1.8 if the thickness changes from 2 to 4 mm (other dimensions: 47.5 mm x 26 mm) and the surface area is held constant. Therefore "more"

material was tested which can be the explanation if also substances from deeper under the surface contribute to conductivity. P1/2 and P2/2 show a good match, the thickness was equal to the first batch. The scaling effect between 4, 2 and 1 plates shows a linear relation with an error smaller than the measurement error (see Figure 33). This is an important result which means that correction to other values of $\frac{A_{Sample}}{V_{Water}}$ should be applicable, within certain boundaries. The conductivities of the BASF samples are lower by a factor of 3.7 (P3/2) and 3.8 (P1/2) which means testing with BASF coolant may comparable to DI water if this factor doesn´t change significantly. This would be interesting point for further investigations.

The non-colored samples P2/NC and P3/NC show another interesting result. The conductivity of P2/NC is lower by a factor of 3.5 compared to P3/NC which is similar to the relation of NREL results where this factor is 4.1. But on the other hand, the overall magnitude seems to small. However, to see if the conductivity of the non-colored material reaches the literature values another six weeks test needed to be performed which was not carried out within this work.

Table 19: Conductivities (T25-lin) before and after the *one week leaching test* of DuPont samples compared to NREL results

Sample	κ_{start} [μS/cm]	κ_{end} [μS/cm]
P1/2	2.4±0.1	92±4.6
P2/2	2.0±0.1	690±20[1]
P3/2	3.0±0.1	622±20
P3/2 (2x)	3.0±0.1	325±20
P3/2 (1x)	2.9±0.1	156±7.8
P1/2 (BASF)	1.2±0.1	24±1.2
P3/2 (BASF)	1.4±0.1	166±8.3
P2/NC	1.5±0.1	72±3.6[1]
P3/NC	2.3±0.1	251±20[1]

The evaluation of the mass loss (*Test 6*) caused by cleaning the samples can be found in Table 20. Compared to the relative mass loss of the six weeks leaching tests (Table 16) this contribution is 13 % of the total relative mass loss of sample P1, 2 % for sample P2 and 10 % of sample P3´s relative mass loss. This is a significant amount which can be estimated for the six weeks samples by comparing the normalized (to 150 mm^2/ml) conductivities of the one and the six weeks leaching tests. Thereafter the mass loss due

[2]Normalized to 100 mm^2/ml

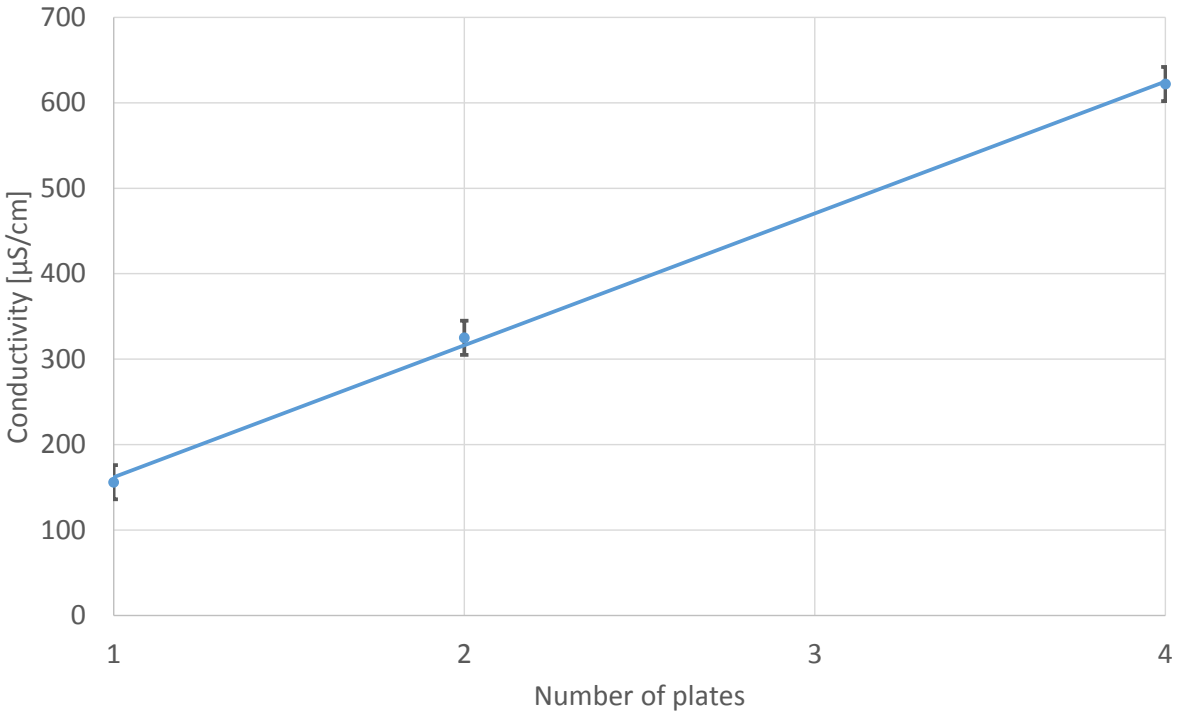

Figure 33: Linearity of scaling for sample P3

to cleaning would be 26 % for P1, 2.1 % (nearly unchanged) for P2 and 12 % for P3. Therefore to evaluate the amount of mass in the leachant cleaning of the samples is not recommended.

The used reference bottle with non-removable colored appearance didn´t show an increase in conductivity compared to the other reference bottles. Therefore it is assumed that the same PP bottle can be used for several tests in series even when its appearance is permanently colored from another test. Of course careful cleaning is mandatory between tests.

Table 20: Mass loss of polyamide samples caused by cleaning after the one week leaching test

Sample	m_{before} [g]	m_{after} [g]	Δm_{abs} [mg]	Δm_{rel} [%]
PLS90G30DR BK099 (P1)	14.8718	14.8605	11.3	0.08
PLS95G35DH1 BK549 (P2)	15.7255	15.7179	7.6	0.05
70G30HSLR BK099 (P3)	15.1634	15.1524	11.0	0.07

4.2 Degassing tests

4.2.1 Introduction

There was an issue with decreasing conductivity at constant temperature when the testbed was operated with fresh DI water (Section 3.4.2) which was found to be related to a CO_2 degassing effect at elevated temperature. This effect could not be observed when BASF coolant (ethylene glycol based) was used. Even residual amounts of BASF coolant in the Testbed showed significant influence on the degassing effect. Beside calculations of the contribution of CO_2 to conductivity of DI water (Section 2.5.1) additional degassing tests were carried out. The aim of these tests was to find out the "real" change in conductivity caused by CO_2 in DI water, to look more closely on the effects caused by traces of BASF coolant and to see what is the time scale for back diffusion of CO_2 into degassed DI water. The method of substitution by inert gas was used for degassing, in other words bubbling it through the solution.

4.2.2 Experimental

Degassing of DI water and subsequent CO_2 diffusion:

For degassing DI water with an amount of 150 ml within a glass beaker was used which was open to atmosphere. Conductivity meter and degassing unit were flushed several times with fresh DI water to maintain low conductivity, then they were put into the DI water. Conductivity and temperature were measured continuously. In the first test series the degassing unit of a HPLC with helium 6.0 was used, the flow rate was much lower than 30 l/h. The pH value was measured before and after degassing. In the second test series an additional flow meter was used to achieve well defined gas flow, here argon 4.8 was used at a flow rate of 30 l/h. As degassing unit for the second series the head from a gas wash bottle was used (Figure 34). These two test series were carried out in two different labs. The degassing was stopped when conductivity reached a steady state.

Degassing of DI water and subsequent CO_2 diffusion with ethylene glycol added:

Deionized water was degassed like described above with helium 6.0 in the first test and with argon 4.8 in the second test. At the lower equilibrium of conductivity degassing was stopped and 1 %vol ethylene glycol was added. Because of using BASF coolant

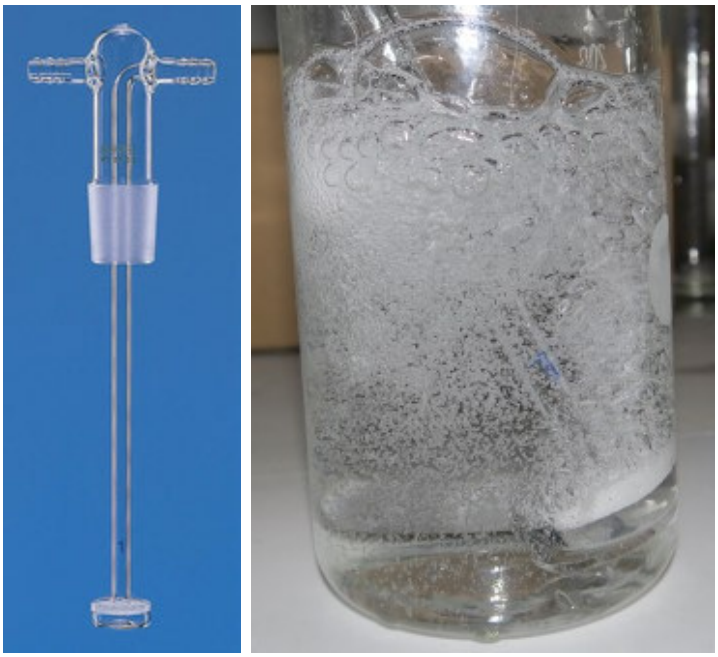

(a) Head of gas wash bottle (b) Degassing of DI water with argon

Figure 34: Degassing equipment of second (argon) test series

which contains 50 %vol ethylene glycol in DI water an absolute amount of 3 ml BASF coolant was added to 147 ml DI water.

Degassing of DI water/ethylene glycol mixture and subsequent CO_2 diffusion:

A mixture of DI water and 1 %vol ethylene glycol (150 ml total amount) was degassed with helium 6.0 in the first test and with argon 4.8 in the second test, conditions like described above. The difference to the test above was that the BASF coolant was added before the degassing procedure started.

Degassing of pure BASF coolant

Pure BASF coolant was degassed with helium 6.0 in the first test and with argon 4.8 in the second test, conditions like described above. The pH value was measured before and after degassing.

4.2.3 Results and discussion

The difference of degassing DI water with different flow rates and gases can be seen in Figure 35. The decrease of conductivity is comparable but the higher flow rate changes

the timescale of degassing which is shown in more detail in Figure 36. The faster degassing is assumed to be owed mainly to the higher flow rate and not to the type of gas. To compare the increase rate of conductivity over time caused by back diffusion two cursors were added in Figure 35 and 37. The increase rate of conductivity between these two cursors is compared. Thus, the increase rate of DI water conductivity is $5.2\,\mu$S/cm/day for helium and $2.5\,\mu$S/cm/day for argon. This difference may be related to different ambient concentrations of CO_2 between the labs. When 1 %vol ethylene glycol is added after degassing this increase is smaller, that is $1.42\,\mu$S/cm/day for helium and $1.27\,\mu$S/cm/day for argon (Figure 37).

It also seems from the first test series (helium) that the decrease in conductivity $\Delta\kappa$ is smaller with ethylene glycol added (black curve in Figure 37). This was found to be related to the "weaker" degassing conditions at lower flow rates.

Pure DI water showed a pH-value[15] of (5.8 ± 0.2) before and pH (7.3 ± 0.2) after CO_2 degassing. Pure BASF coolant showed the same value of pH (6.0 ± 0.2) before and after degassing.

In Figure 38 the difference between the CO_2 back diffusion process between DI water and the mixture of DI water and ethylene glycol is shown, both under degassing conditions with argon at 30 l/h. When the degassing tests of both solutions with argon at 30 l/h are compared (see Figure 39), the mean decrease of conductivity $\Delta\kappa$ is $(1.52 \pm 0.20)\,\mu$S/cm whereas the DI water/glycol mixtures showed a larger $\Delta\kappa$. Within the first three minutes DI water degassing seems to be faster.

The degassing test of pure BASF coolant with helium at lower gas flow didn´t show any effect on conductivity. It stayed at a constant level of $(1.19 \pm 0.02)\,\mu$S/cm. The test with argon at 30 l/h flow rate effected conductivity as shown by Figure 40. Compared to DI water the effect is much lower and for a conductivity decrease of 10 % it takes 50 min which is by a factor 160 longer than for DI water degassing. The solubility of CO_2 in DI water/ethylene glycol mixtures increases as the amount of ethylene glycol increases [33], which is assumed to be the reason for the difference in time scale.

[15]The large error in the pH measurement is owed to the influence of the reference electrode on pH measurement. Measuring in 150 ml BASF coolant the pH value changed from pH 6 to pH 5 within 2 minutes, whereas conductivity increased from $1.2\,\mu$S/cm to $18\,\mu$S/cm.

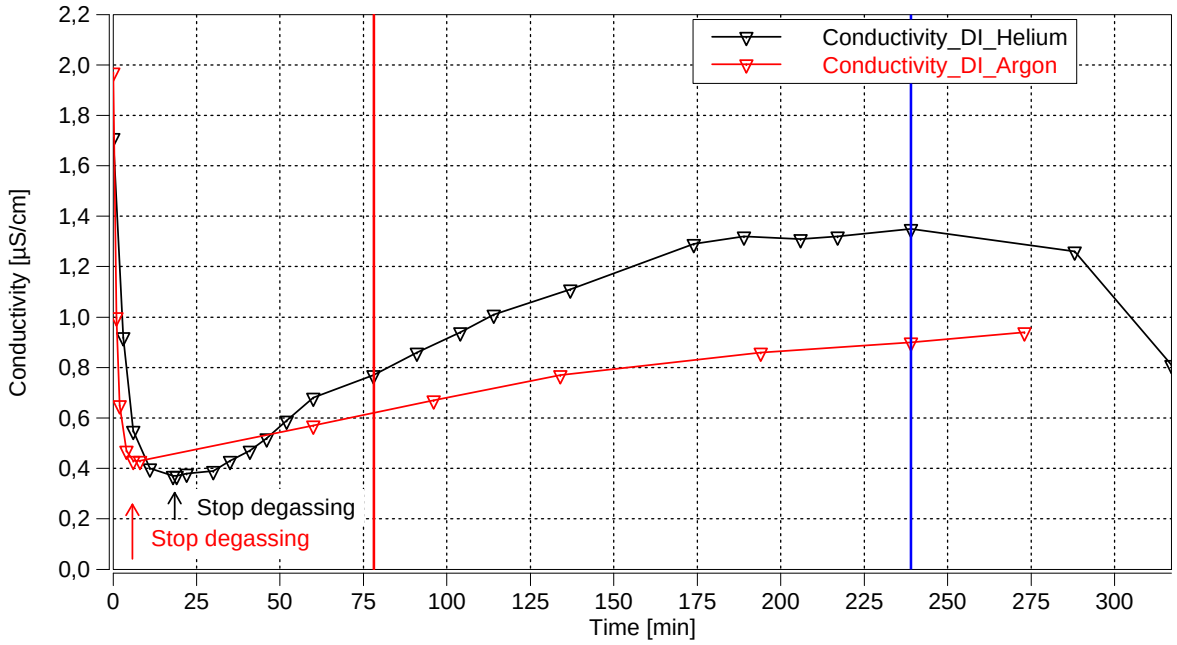

Figure 35: Conductivity (T25-lin) while degassing of DI water with helium and argon at different flow rates and subsequent balancing process under ambient conditions; Cursors for comparison of conductivity increase rate added

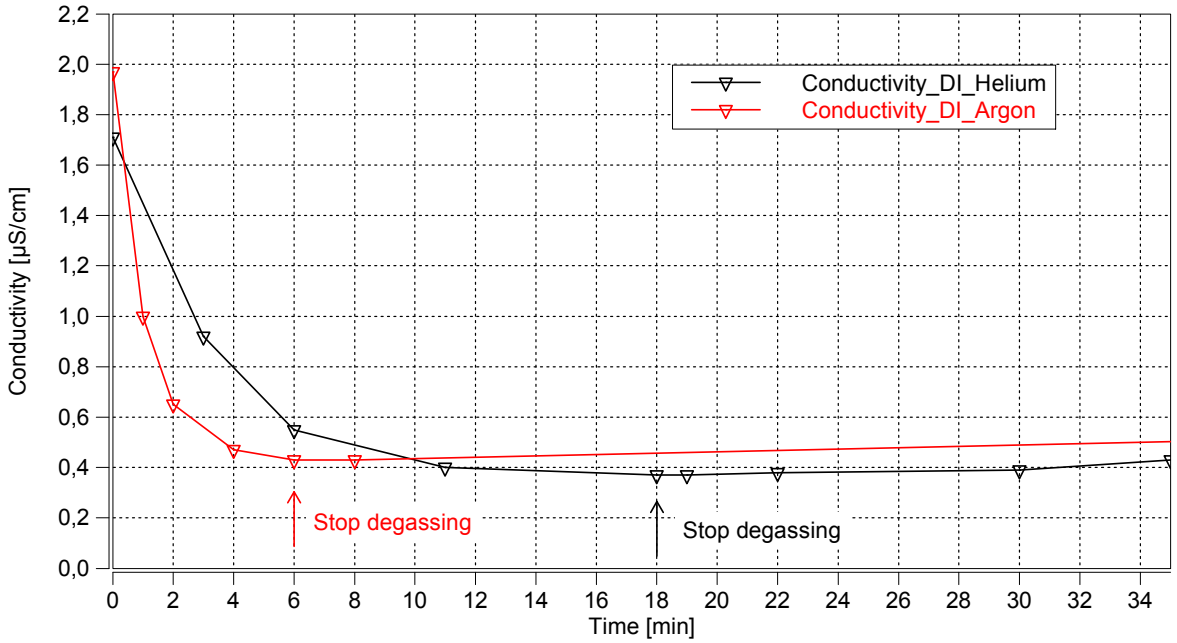

Figure 36: Conductivity (T25-lin) while degassing of DI water with helium and argon at different flow rates

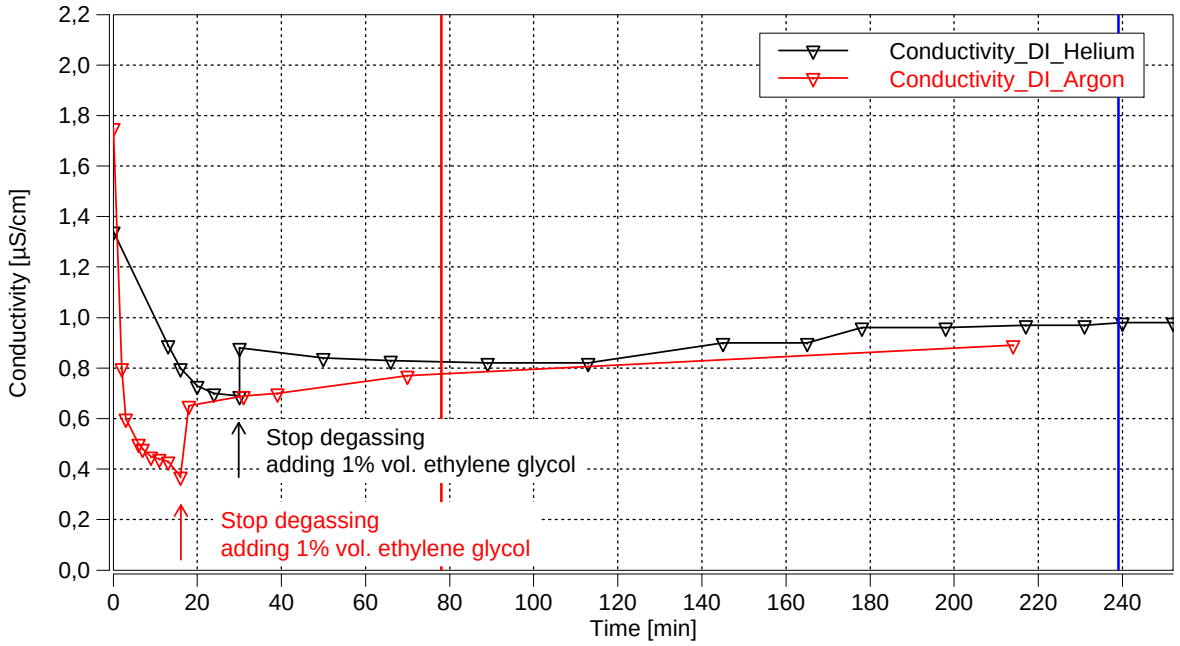

Figure 37: Conductivity (T25-lin) while degassing of DI water with helium and argon at different flow rates, 1 %vol ethylene glycol added after degassing, subsequent balancing process under ambient conditions; Cursors for comparison of conductivity increase rate added

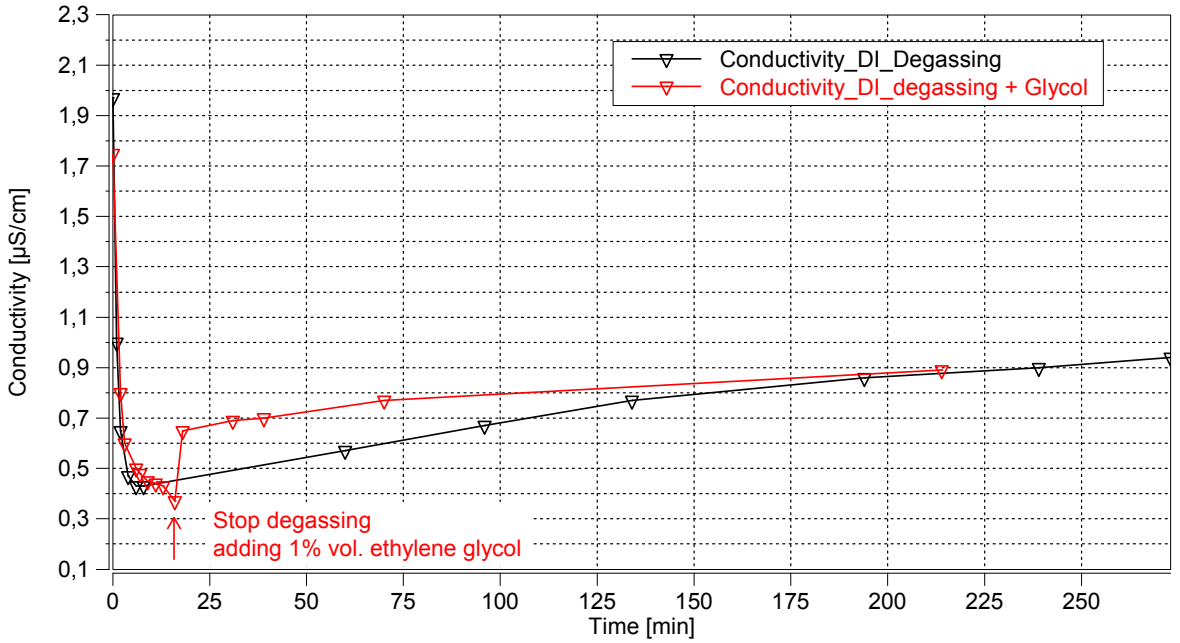

Figure 38: Conductivity (T25-lin) while degassing of DI water with argon and subsequent balancing process under ambient conditions, compared to an equal sample with 1 %vol ethylene glycol added after degassing

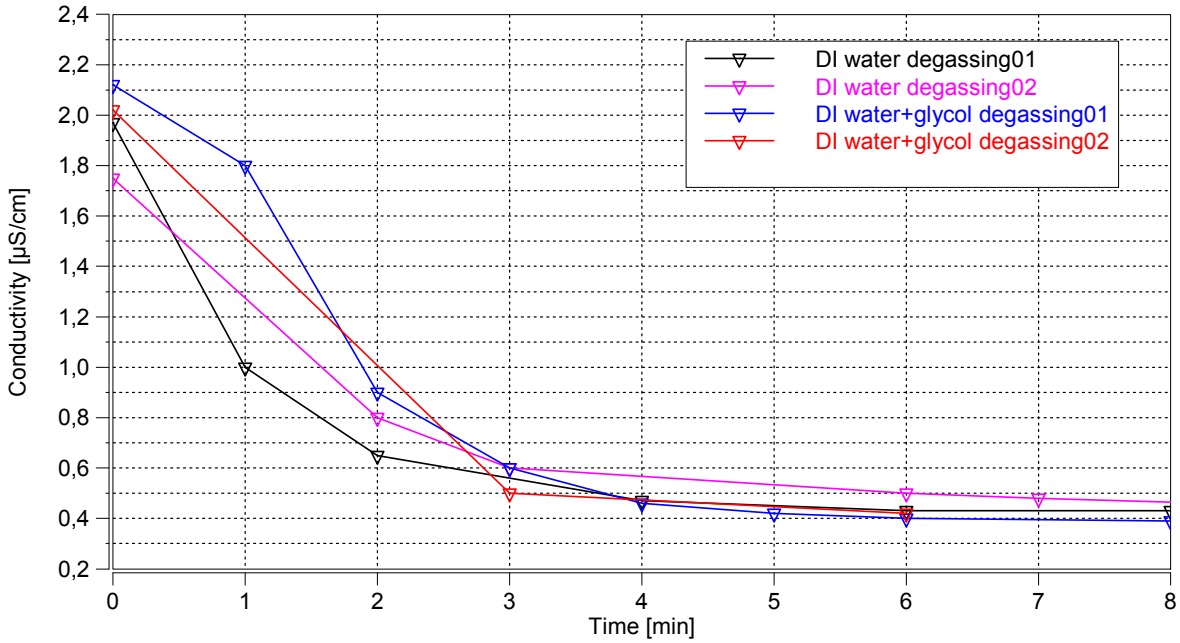

Figure 39: Comparison of conductivities (T25-lin) while degassing process (only with argon) between DI water and a mixture of DI water with 1 %vol ethylene glycol added

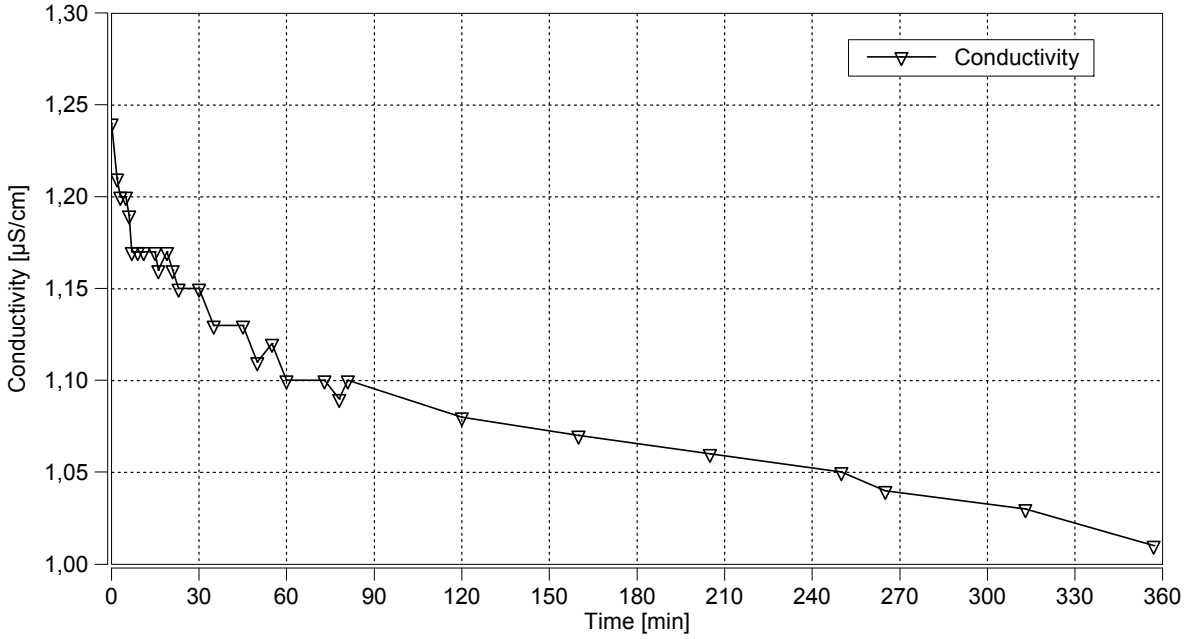

Figure 40: Degassing of BASF coolant (DI water/ethylene glycol=50/50) with argon 4.8

4.3 Stainless steel corrosion test

4.3.1 Introduction

Due to the search for ion sources and the use of different grades of stainless steels within the system, the question occurred if there is an issue with bimetallic corrosion between different grades of stainless steels. The different grades of *austenitic chromium-nickel-molybdenum stainless steels* used in the test system are shown in Table 21.

Table 21: Types of different grades of austenitic corrosion resistant stainless (V4A) steels and their composition [37]

EN-standard	SAE-standard	Composition
1.4401	316	X5CrNiMo17-12-2
1.4404	316L	X2CrNiMo17-12-2
1.4571	316Ti	X6CrNiMoTi17-12-2
1.4408	-	GX5CrNiMo19-11-2

Figure 41: Austenitic stainless steel samples and filled bottles after corrosion test - Overview (Test protocol: DI water, 3 days, 90 °C)

4.3.2 Experimental

All stainless steel samples[16] were cleaned with IPA in the first step and subsequently by ultrasonic bath for 30 minutes at 60 °C in fresh DI water. After that the samples were put into 180 ml PFA bottles and then two times flushed with fresh DI water. The

[16]Type of 1.4571 samples: C-GE 18-LR OMD, C-DKL 18-L M26x1,5 DN16; Thread of 1.4404 sample with hose connector: 1/2"; Swagelok SS-22-MTA-7-8RG (1.4404)

bottles were filled again and the conductivity was measured before and after the test. In Figure 41 the samples and the bottles can be seen. In Table 22 the combinations of the stainless steel samples and conductivities before and after the test can be found. P3 and P4 are bimetallic samples, P1 and P2 are combinations of the same grade. As reference one PFA and one PP bottle filled with DI water were taken. The four samples in the PFA bottles were put into an oven for 3 days at 90 °C, the PP reference was added 24 h after the test started. At the end of the test, the bottles were cooled under room temperature conditions. Subsequently, the stainless steel samples were removed and conductivity was measured.

4.3.3 Results and discussion

The samples P2 and P3 showed the highest conductivities[17], were P2 is mono-metallic and P3 is bimetallic (see Table 22). P1 and P4 show lower conductivities with P4 being even lower as the reference P1. There was no correlation found between the bimetallic samples and conductivity increase. The main difference between the low- and the high conductivity samples was the amount of rough surface area, which was the highest at P2 and P3 (see Figure 41 and 42). The 1.4408 samples were made of casting steel with more or less amount of rough surface area. On sample P3, Figure 42 (c), there were some spots found with the typical brown rust color. One part of P4 was a 1.4404 Swagelok connection with high surface quality, see Figure 42 (d). On the bottom of all samples corrosion products were found were P2 and P3 show the largest amounts, see Figure 43. The references R1 and R2 didn´t show corrosion products at the bottom.

Table 22: Conductivity before and after stainless steel corrosion test (Test protocol: DI water @ 90 °C, 3 days); compensation: T25-lin

Sample	κ_{begin} [μS/cm] @ 23.3 °C	κ_{end} [μS/cm] @ 25.5 °C
R1 (PFA)	3.29±0.07	7.58±0.15
R2 (PP)	2.53±0.06	1.14±0.03
P1 (PFA, 2 x 1.4571)	3.24±0.07	8.50±0.17
P2 (PFA, 2 x 1.4408)	3.22±0.07	11.42±0.23
P3 (PFA, 1.4408 + 1.4571)	3.25±0.07	11.80±0.23
P4 (PFA, 1.4408 + 1.4404)	3.23±0.07	7.41±0.15

Also the PFA bottles seem to increase the conductivity significantly as all the values are higher than 7.4 μS/cm. In comparison, the conductivity of the PP reference R2 is

[17] All conductivities were measured with linear temperature compensation of 2 % per degree, with 25 °C as reference temperature (T25-lin)

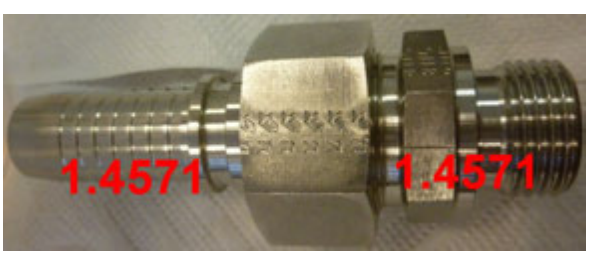

(a) Sample P1

(b) Sample P2

(c) Sample P3

(d) Sample P4

Figure 42: Austenitic stainless steel samples after corrosion test

at 1.14 μS/cm which is even lower than before the test. The reason for this decrease may be related to CO_2 degassing due to the high temperature. Another reason could be owed to adsorption processes at elevated temperatures, but the CO_2 contribution is assumed to be the main effect. It can be concluded, that the contribution of the PFA bottles to the conductivity increase is even more than the contribution of the stainless steel samples and no bimetallic corrosion could be observed.

4.4 Evaluation of PFA and PP bottles for leaching tests

4.4.1 Introduction

PP bottles were chosen for the leaching tests because of other work [29]. The PFA bottles were chosen since its properties are similar to PTFE. For the same reason the test system for the cooling circuit was built up with PFA houses. Nevertheless, the corrosion test in the last section showed an increase in conductivity which may be related to the PFA bottles, therefore two other tests were performed to confirm this result without metallic samples and to compare PP and PFA bottles. Another reason for this tests is the fact, that the PP bottle of the corrosion test in Section 4.3.3 was only for 2 days in the oven because it was added later.

4.4.2 Experimental

For one test, 3 PFA bottles and one PP bottle were filled with DI water and put into an oven for 2 weeks at 90 °C. For a second test 5 PP and 2 PFA bottles were used, the duration of the second test was reduced to 3 days. The 5 PP bottles from the second test were new ones, the 2 PFA bottles were already used for the 3 days corrosion test. Before the test, all bottles were cleaned with IPA and then two times flushed with fresh DI water.

4.4.3 Results and discussion

The results are shown in Table 23 for the first and in Table 24 for the second test. The first test (2 weeks) showed a large difference in the change of conductivities between the PFA bottles and the PP bottle. Again the conductivity of the PP bottle is lower than at the beginning, which was already discussed in Section 4.3.3. In contrast, the conductivity of the PFA bottles R1 and R2 after the test increased by a factor of 3.8 which is even higher, when the CO_2 degassing effect is taken into account.
The duration of the second test was only 3 days, therefore the change in conductivity was smaller in case of the PFA bottles (R6 and R7 in Table 24). Another reason for the lower increase may be the fact, that the PFA bottles were already used, as mentioned above. The new PP bottles didn´t show a significant increase in conductivity. The "worse performance" is very surprising because PFA bottles are widely used in chemical labs and industry (e.g. trace analytic) because of minimum of interaction of the material with the chemicals inside. However, because of showing better performance at testing conditions PP bottles were used for further bottle tests, not only for the reason that they are much cheaper than PFA bottles.

Table 23: Conductivity before and after PFA and PP bottle test 1 (Test protocol: DI water @ 90 °C, 2 weeks); compensation: T25-lin

Sample	κ_{begin} [μS/cm] @ 23.5 °C	κ_{end} [μS/cm] @ 24.8 °C
R1 (PFA)	2.53±0.05	9.41±0.19
R2 (PFA)	2.54±0.05	9.55±0.19
R3 (PFA)	2.52±0.05	6.40±0.13
R4 (PP)	2.47±0.05	1.92±0.04

Table 24: Conductivity before and after PP and PFA bottle test 2 (Test protocol: DI water @ 90 °C, 3 days); compensation: T25-lin

Sample	κ_{begin} [μS/cm] @ 23.5 °C	κ_{end} [μS/cm] @ 24.2 °C
R1 (PP)	1.84±0.04	1.87±0.04
R2 (PP)	1.84±0.04	1.88±0.04
R3 (PP)	1.84±0.04	1.82±0.04
R4 (PP)	1.84±0.04	1.83±0.04
R5 (PP)	1.84±0.04	1.94±0.04
R6 (PFA)	1.84±0.04	3.22±0.06
R7 (PFA)	1.84±0.04	3.04±0.06

(a) Bottle R1

(b) Bottle R2

(c) Bottle P1

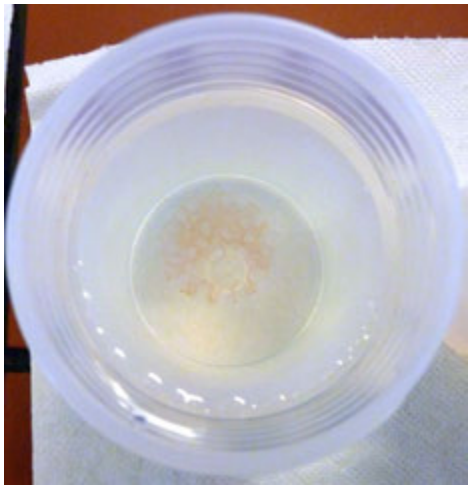

(d) Bottle P2

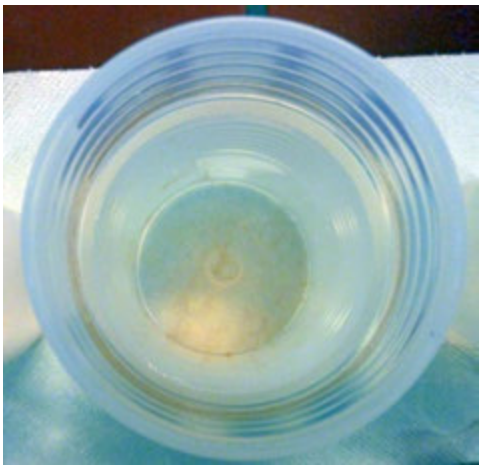

(e) Bottle P3

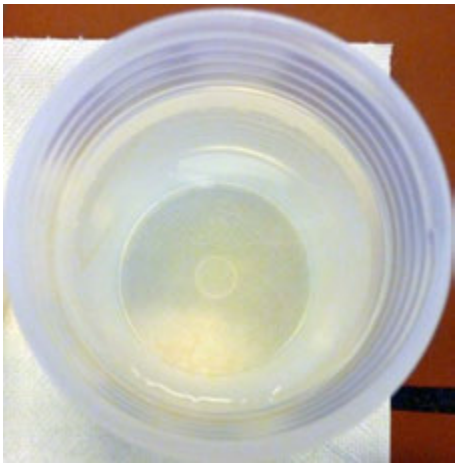

(f) Bottle P4

Figure 43: Corrosion products at the bottom of the bottles can bee seen at figures (c), (d), (e) and (f). Figure (a) and (b) show the reference bottles.

5 Analytical investigations

5.1 ICP-OES analysis and ion chromatography

Leachant solutions were analyzed via inductively coupled plasma optical emission spectroscopy (ICP-OES). In Figure 44 the comparison of a reference measurement of the test system (TB-Ref) to the test of samples P1-TB-7D and S5-TB-7D in the testbed is shown. The higher conductivity of S5-TB-7D is reflected by the total concentration of detected species (ICP Total) of 146 ppm compared to 44 ppm for P1-TB-7D. ICP Total of S5-6W (38 ppm) is much lower although tested for six weeks. The elements Al, B, Ca and Si can be related to glass reinforcement (alumino-borosilicates and soda lime) which can also be seen in Figures 45 and 46 [12]. The samples of the one week leaching test S1, S2 and S3 are shown in Figure 45 where S2 has the highest ICP Total. The elemental analysis matches with the analysis data found in literature [12]. In Figure 47 the results of ion chromatography are shown. The species found can be associated to fillers and additives and this species also were found in the published database [35, 13].

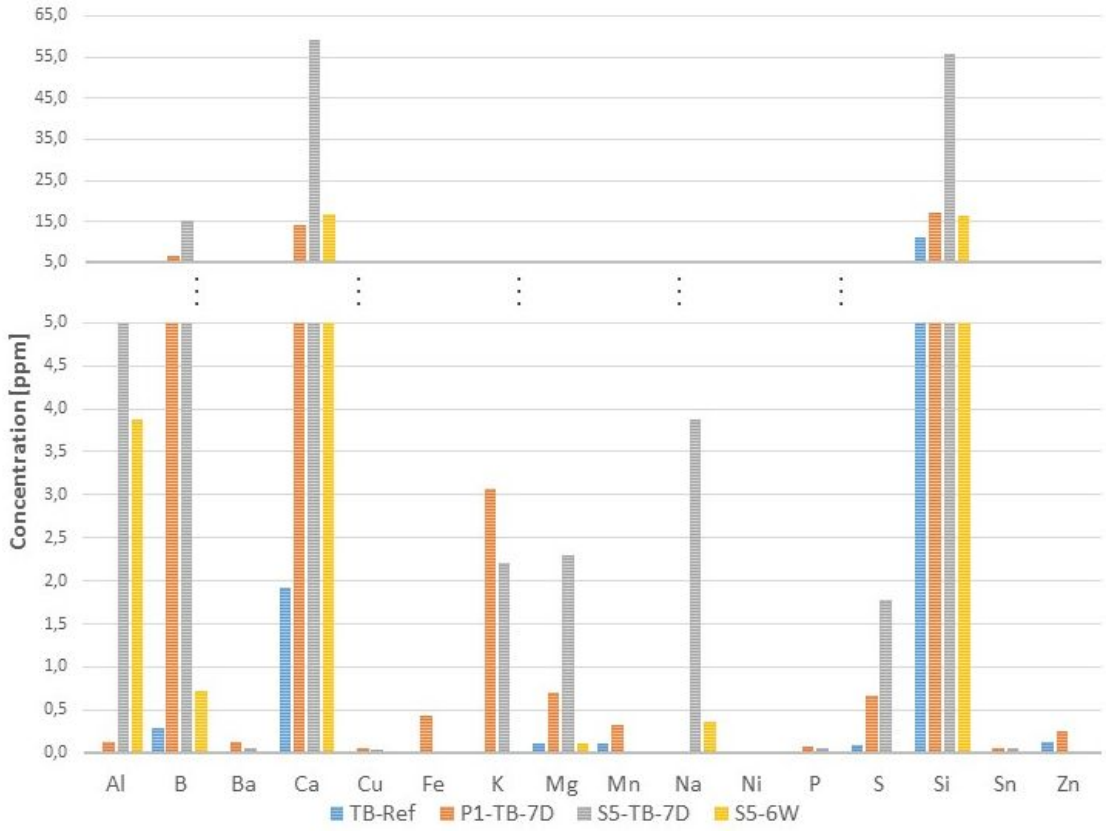

Figure 44: Analysis results ICP-OES of reference, P1, S5 (testbed) and S5 (6 weeks leaching test)

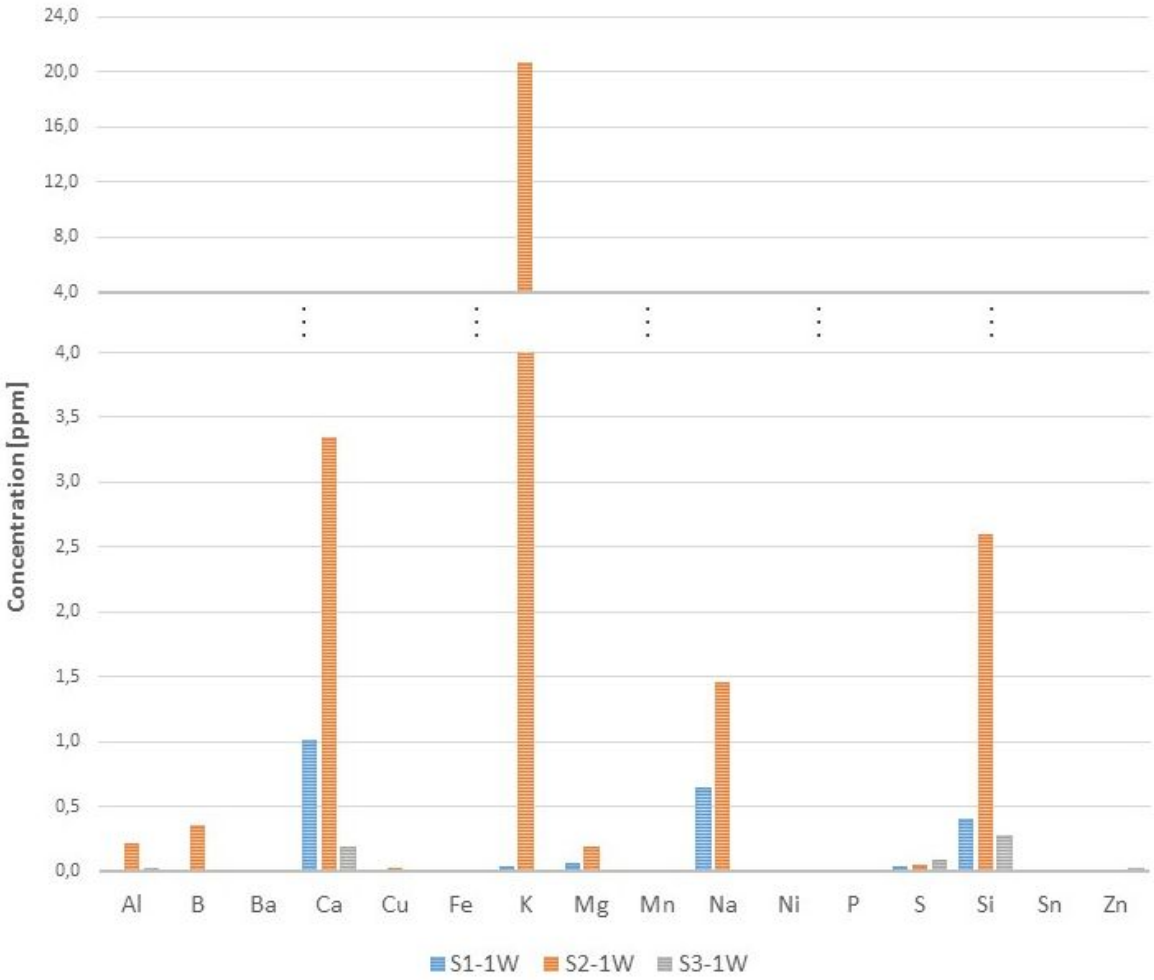

Figure 45: Analysis results ICP-OES of S1, S2 and S3 (one week leaching test)

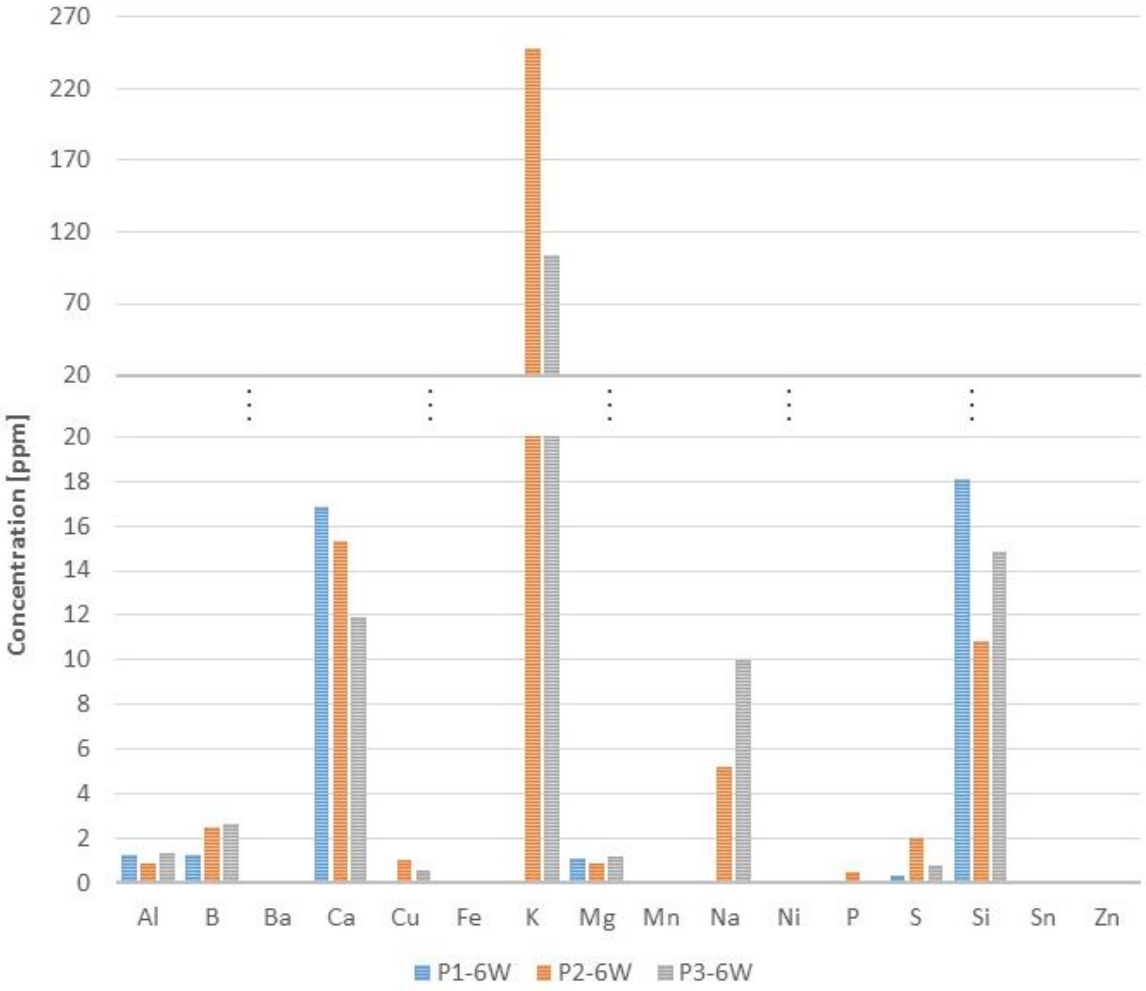

Figure 46: Analysis results ICP-OES of P1, P2 and P3 (six weeks leaching test)

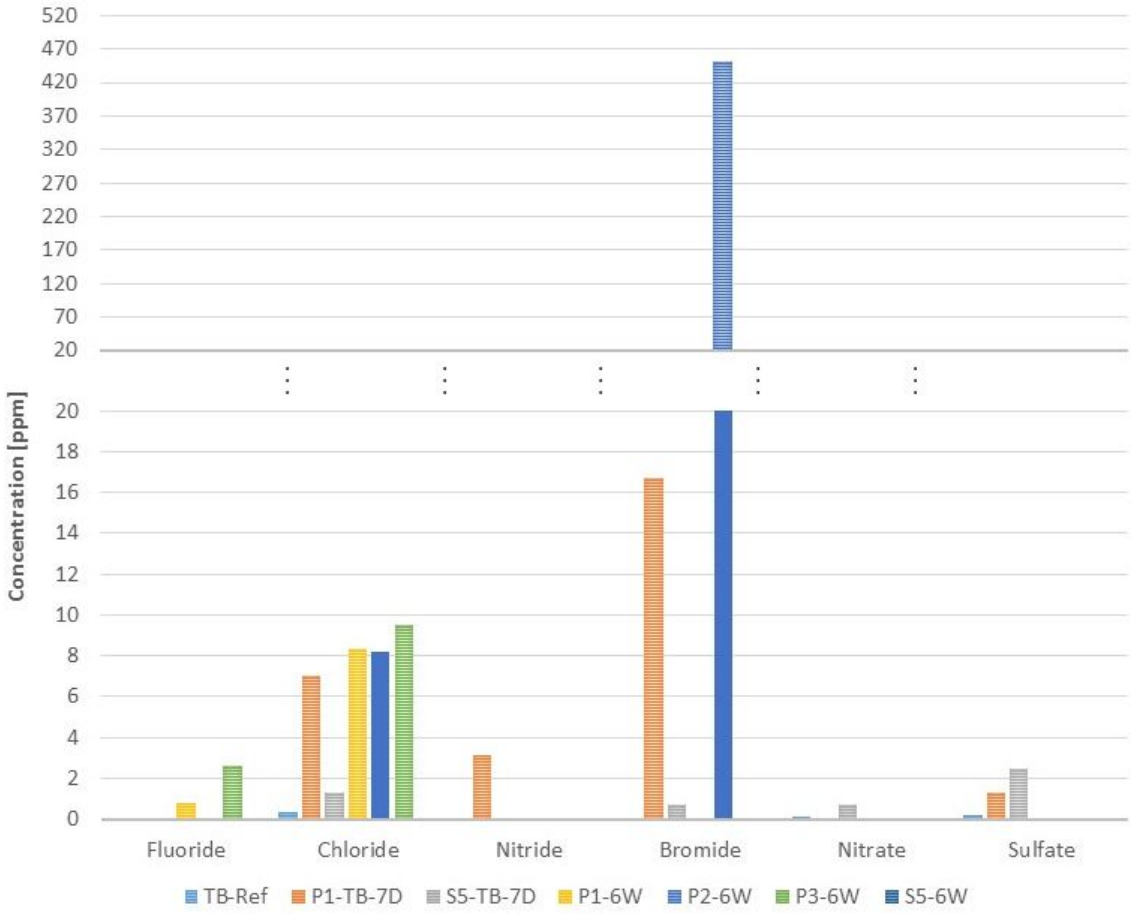

Figure 47: Results of ion chromatography

6 Optical investigations

The polyamide materials PLS90G30DR BK099 (P1), PLS95G35DH1 BK549 (P2) and 70G30HSLR BK099 (P3) shown also in Table 9 were investigated by microscope to get a more detailed insight in changes of surface morphology caused by leach out effects. At all samples visible (to the naked eye) changes were seen after the leaching tests in the beaker as well as in the Testbed. For P2 a very mat (leached out) surface could be seen after the tests which was also described in Section 4.1.3 and 3.5, for samples P1 and P2 this effect was much less.

6.1 Microscope pictures of DuPont polyamide materials before and after test in the Testbed

In Figure 48 microscope pictures of the rough side of sample P1 are shown before and after the leaching test within the Testbed. At a magnification of 50x in Figure 48(a) and (b) no significant changes can be seen. At a magnification of 200x in Figure 48(d) bright stripes can be seen which are shown in more detail in Figure 48(f) at a magnification of 500x. This stripes are very likely to be the glass fiber reinforcement of the polymer which contains 30 % glass fibers and which cannot be seen in the pictures of the sample before the test. Also the pictures of the smooth side in Figure 49(d) and (f) show this bright stripes. Additionally the surface does also show an increased density of structuring which indicates higher roughness after the test.
Although containing 35 % glass fiber reinforcement this effect was not seen at sample P2. The pictures of the rough side in Figure 50(b), (d) and (f) show a scratch at the leached out sample which is not very likely to be an effect of the leaching test. Beside this scratch the pictures (d) and (f) in Figure 50 have an washed-out appearance compared to (c) and (d). This effect can be seen even more clearly in Figure 51(b), (d) and (f). This surface was glossy before and mat after the test which can also be seen on the microscope pictures in the form of an increase in roughness.
The rough side of sample P3 (see Figure 52) didn´t show changes in surface roughness after the test but at a magnification of 500x again white stripes were found, see Figure 52. Also this sample contains 30 % glass fibers which were not visible on the surface before the test. The smooth side of sample P2 shows an increased density of structuring after the test similar to P1, indicating an increase in roughness which can be seen in Figure 53.

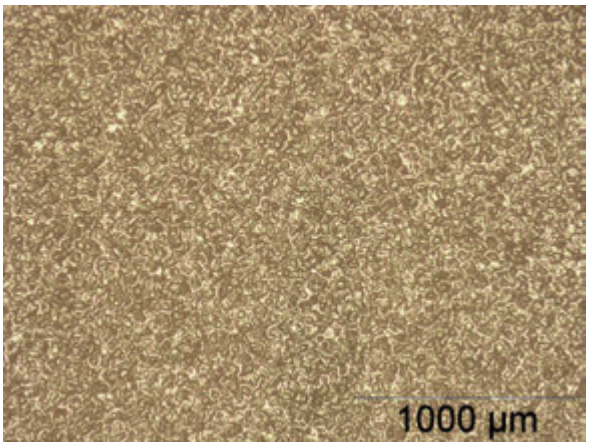

(a) Sample P1 as received; magnification 50x

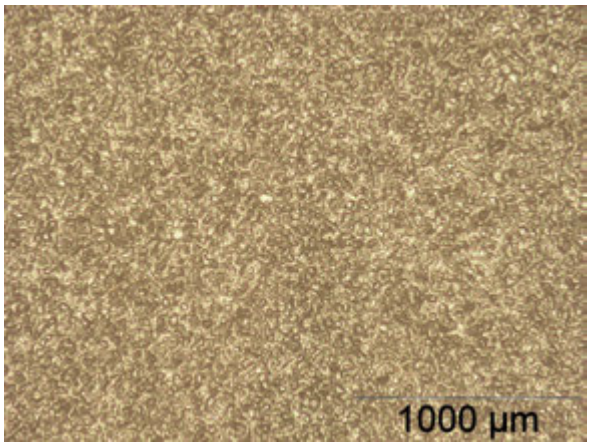

(b) Sample P1 leached out; magnification 50x

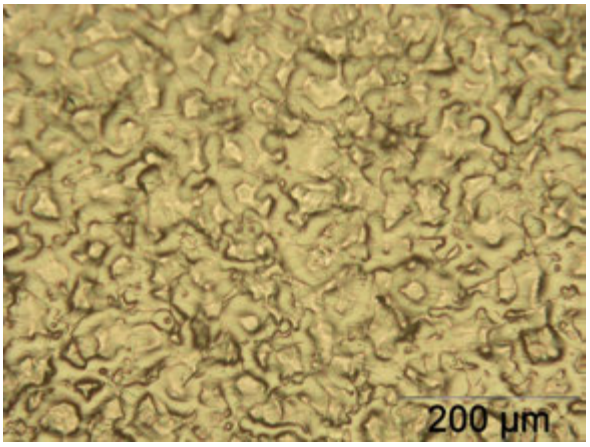

(c) Sample P1 as received; magnification 200x

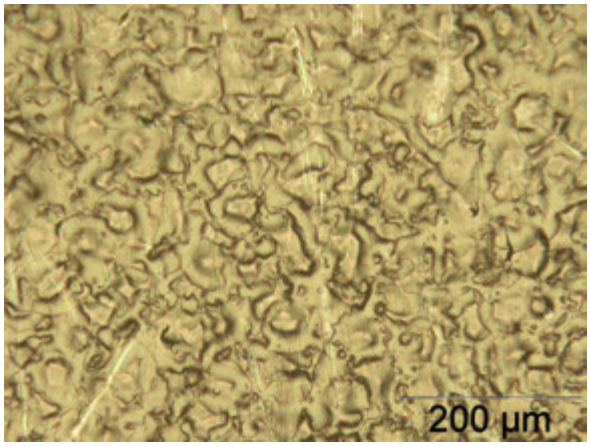

(d) Sample P1 leached out; magnification 200x

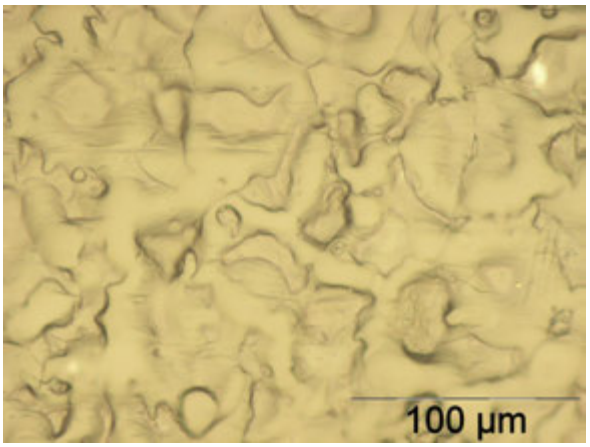

(e) Sample P1 as received; magnification 500x

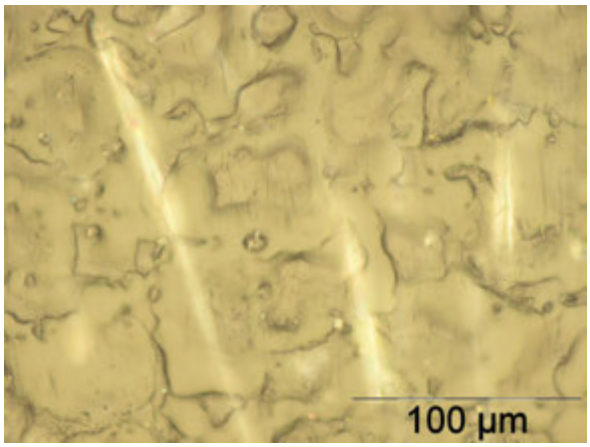

(f) Sample P1 leached out; magnification 500x

Figure 48: Comparison of the rough side of polymer sample P1: PLS90G30DR BK099 from DuPont before (left) and after (right) leaching test within the Testbed

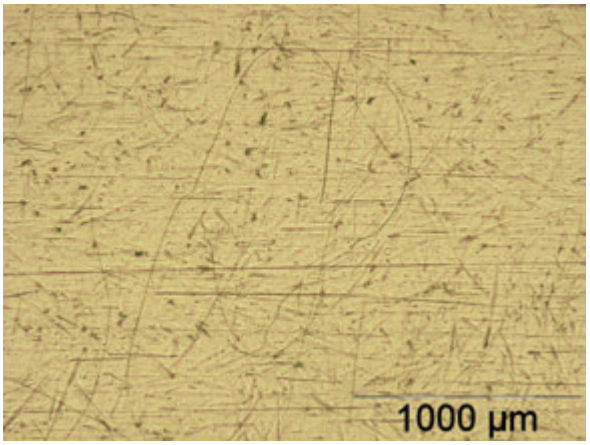

(a) Sample P1 as received; magnification 50x

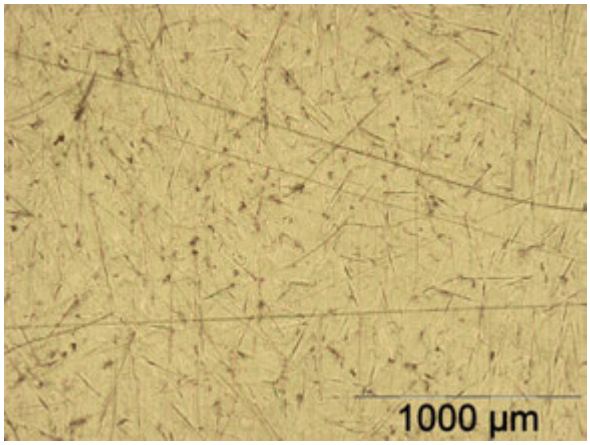

(b) Sample P1 leached out; magnification 50x

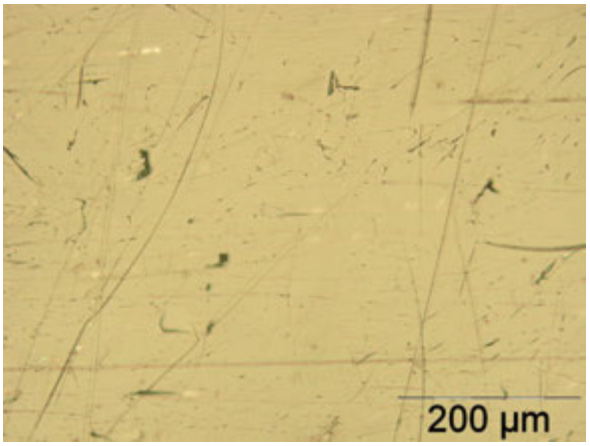

(c) Sample P1 as received; magnification 200x

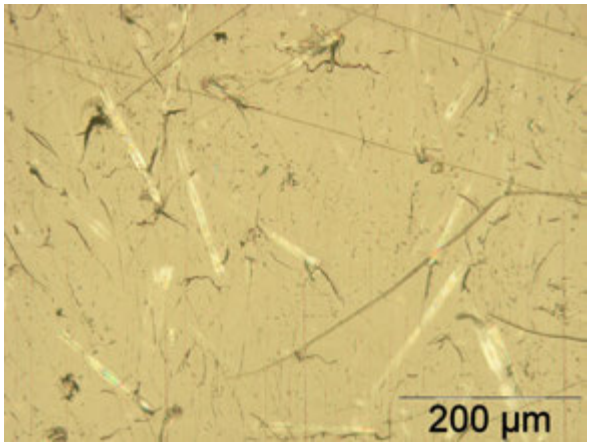

(d) Sample P1 leached out; magnification 200x

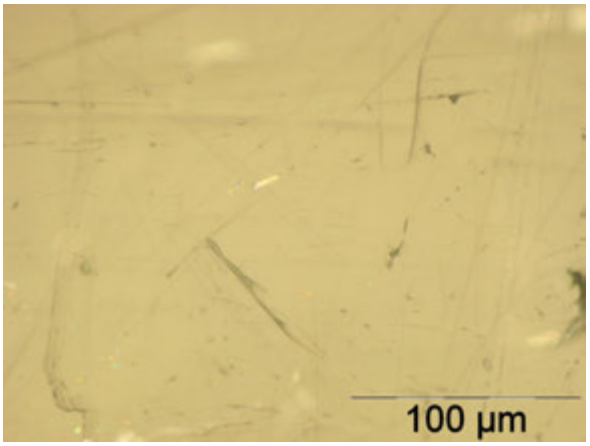

(e) Sample P1 as received; magnification 500x

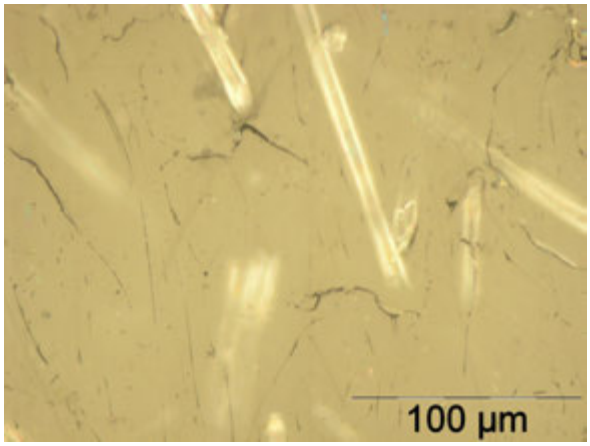

(f) Sample P1 leached out; magnification 500x

Figure 49: Comparison of the smooth side of polymer sample P1: PLS90G30DR BK099 from DuPont before (left) and after (right) leaching test within the Testbed

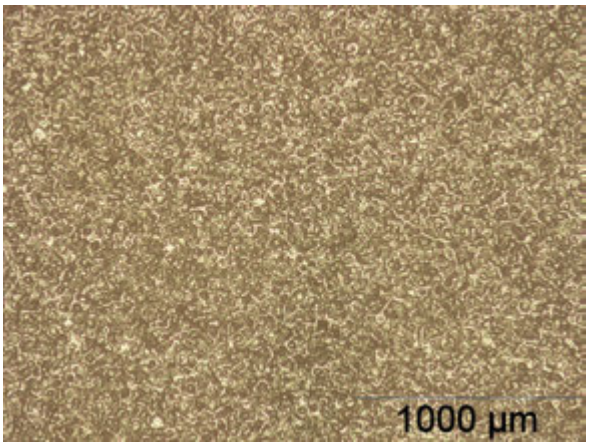

(a) Sample P2 as received; magnification 50x

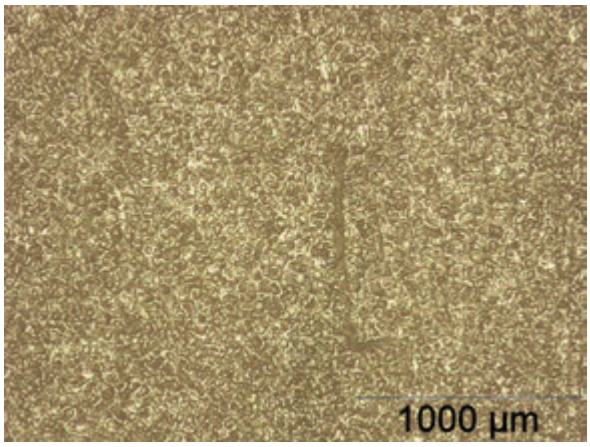

(b) Sample P2 leached out; magnification 50x

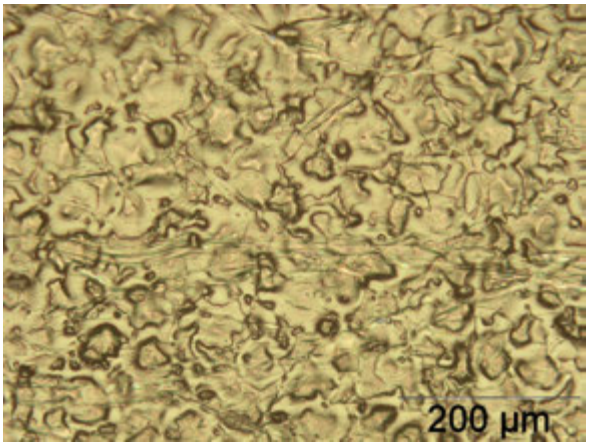

(c) Sample P2 as received; magnification 200x

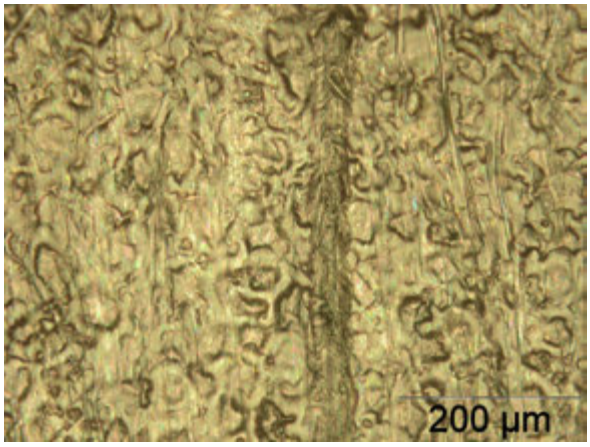

(d) Sample P2 leached out; magnification 200x

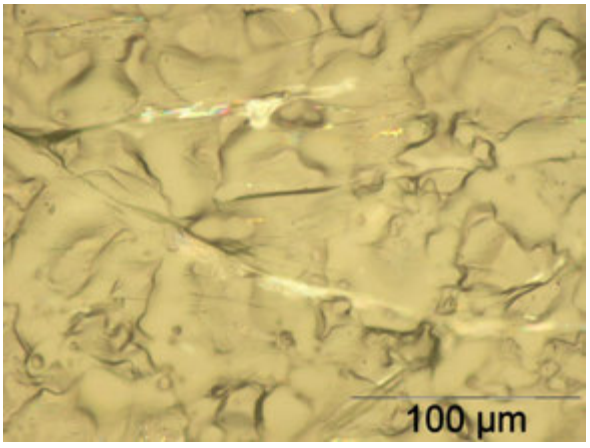

(e) Sample P2 as received; magnification 500x

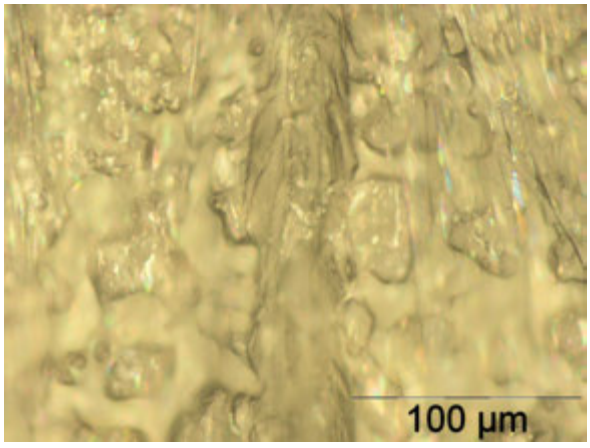

(f) Sample P2 leached out; magnification 500x

Figure 50: Comparison of the rough side of polymer sample P2: PLS95G35DH1 BK549 from DuPont before (left) and after (right) leaching test within the Testbed

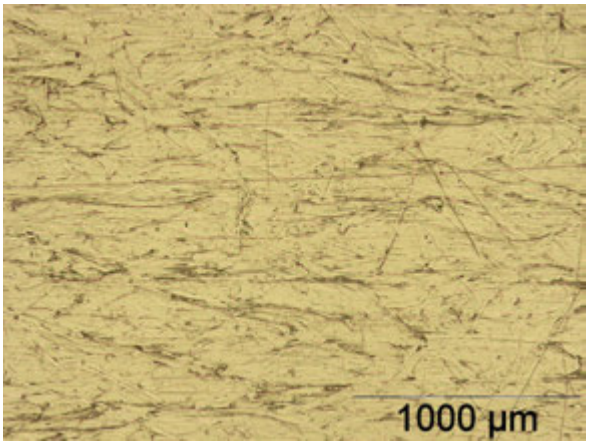

(a) Sample P2 as received; magnification 50x

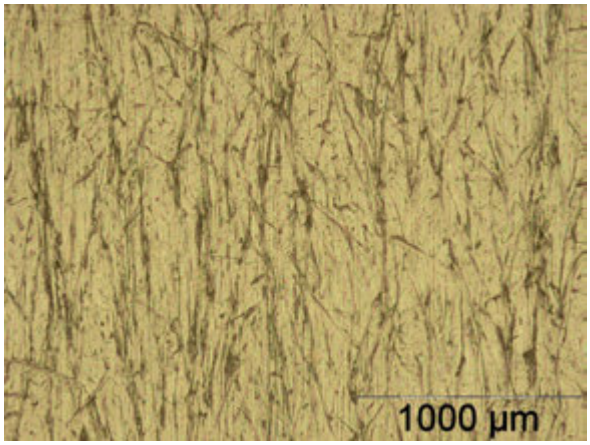

(b) Sample P2 leached out; magnification 50x

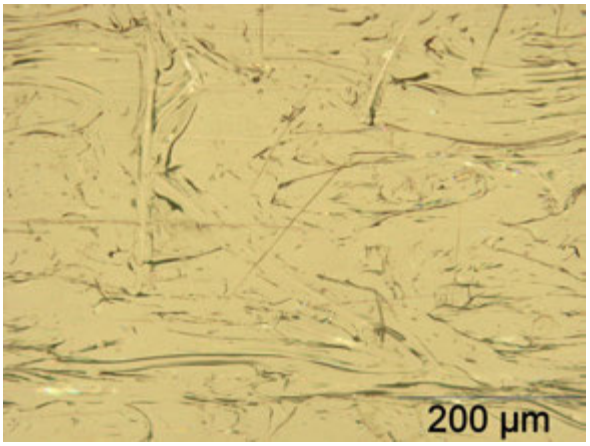

(c) Sample P2 as received; magnification 200x

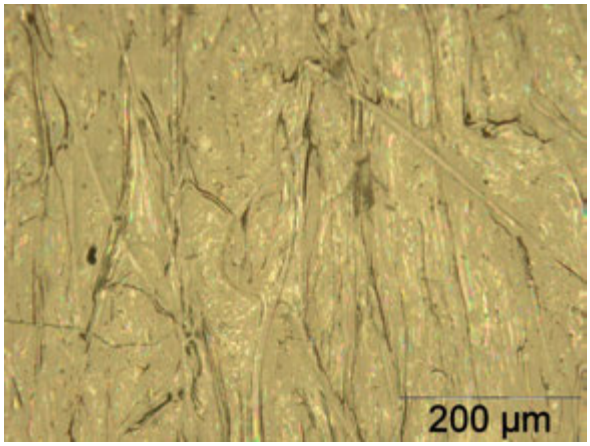

(d) Sample P2 leached out; magnification 200x

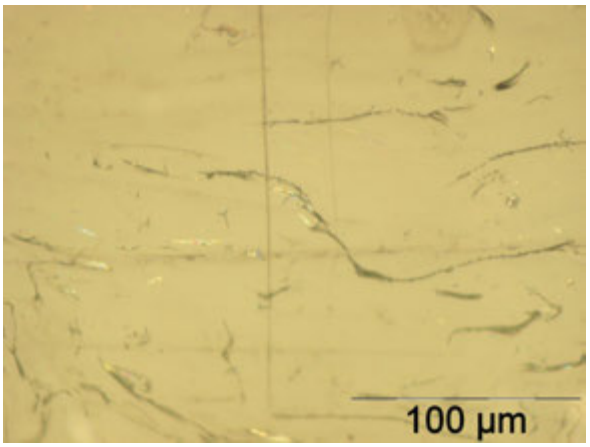

(e) Sample P2 as received; magnification 500x

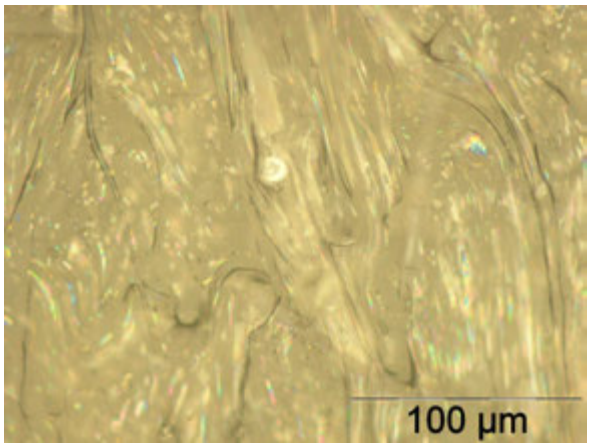

(f) Sample P2 leached out; magnification 500x

Figure 51: Comparison of the smooth side of polymer sample P2: PLS95G35DH1 BK549 from DuPont before (left) and after (right) leaching test within the Testbed

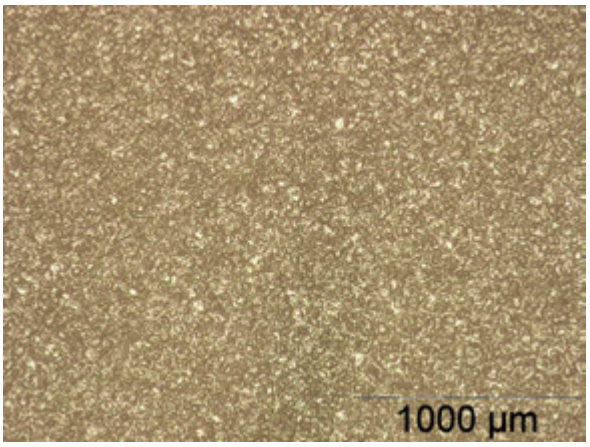

(a) Sample P3 as received; magnification 50x

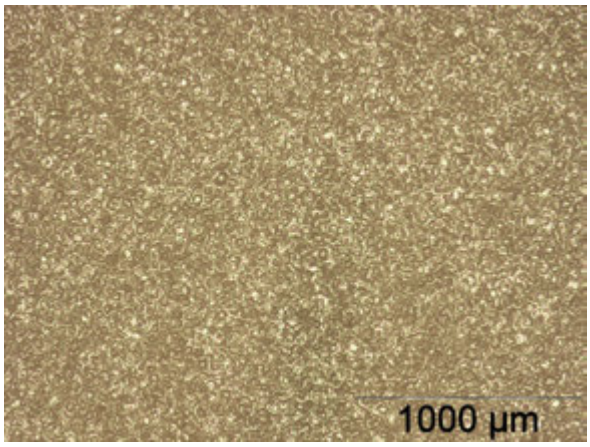

(b) Sample P3 leached out; magnification 50x

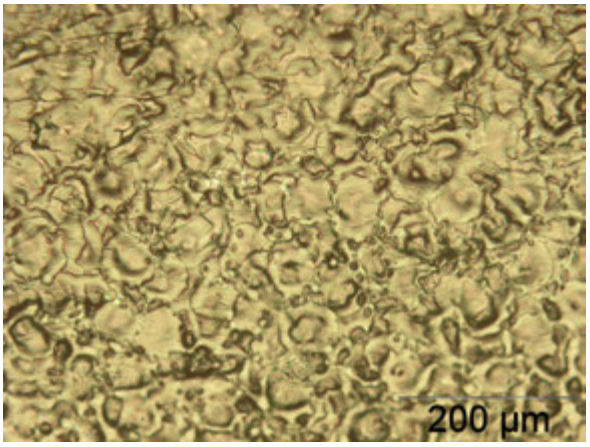

(c) Sample P3 as received; magnification 200x

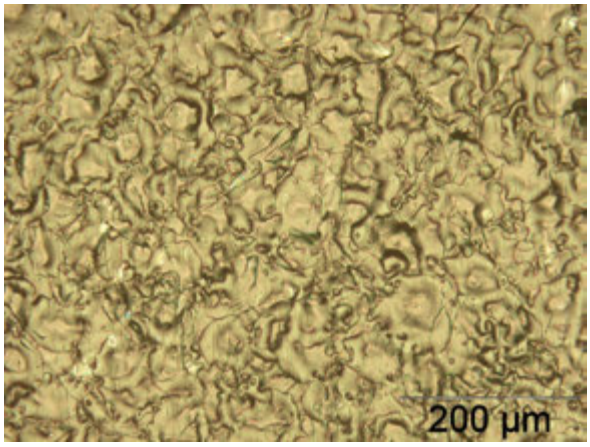

(d) Sample P3 leached out; magnification 200x

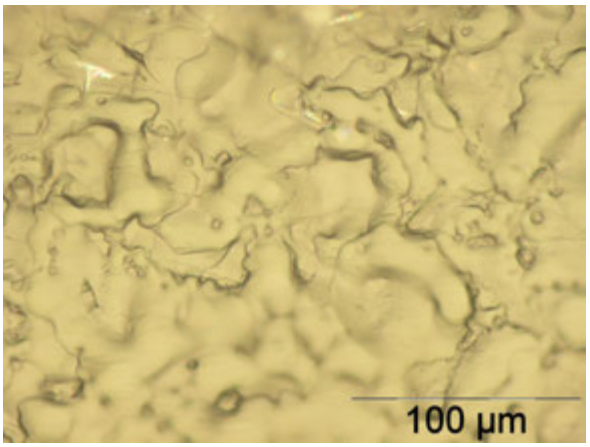

(e) Sample P3 as received; magnification 500x

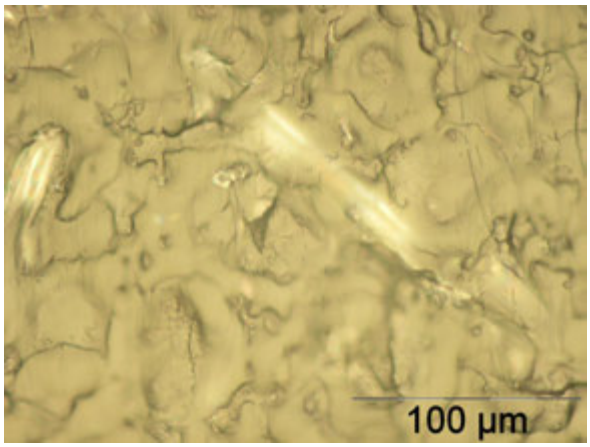

(f) Sample P3 leached out; magnification 500x

Figure 52: Comparison of the rough side of polymer sample P3: 70G30HSLR BK099 from DuPont before (left) and after (right) leaching test within the Testbed

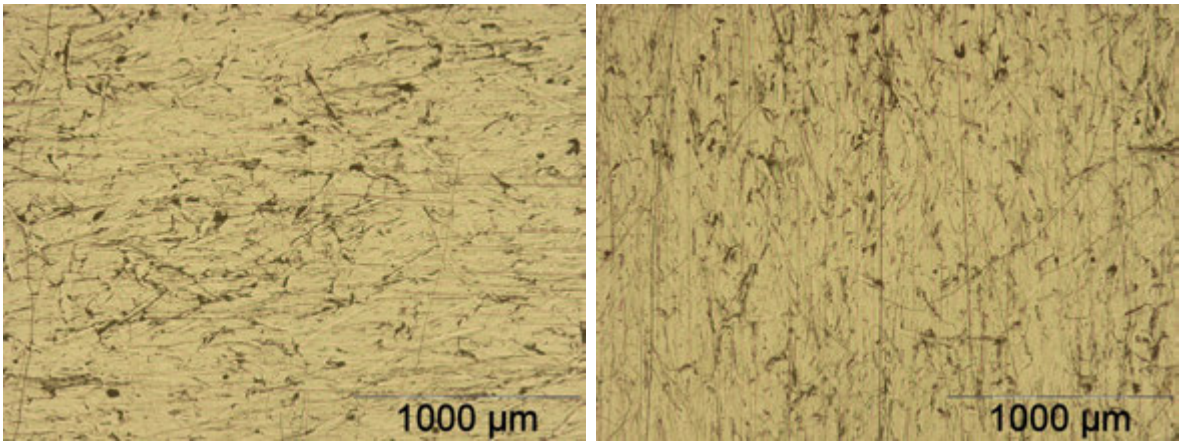

(a) Sample P3 as received; magnification 50x (b) Sample P3 leached out; magnification 50x

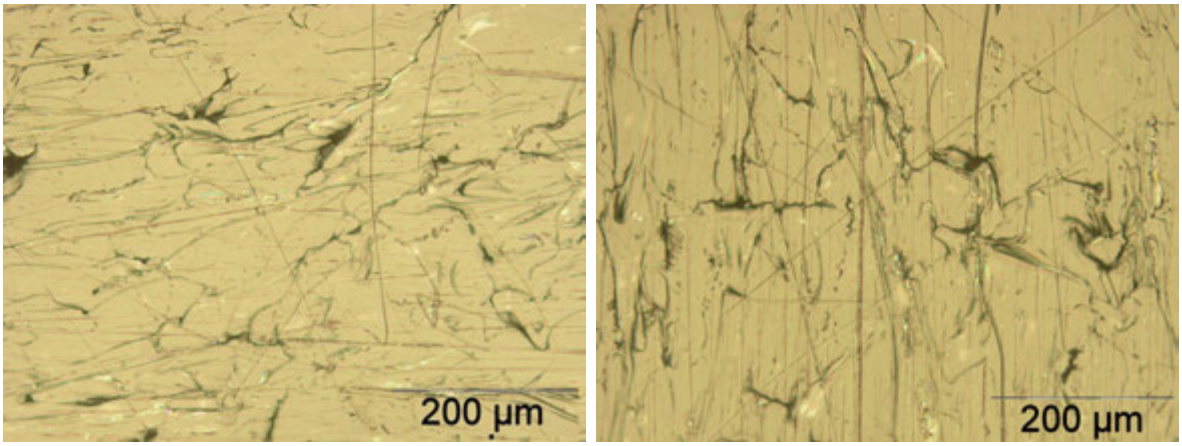

(c) Sample P3 as received; magnification 200x (d) Sample P3 leached out; magnification 200x

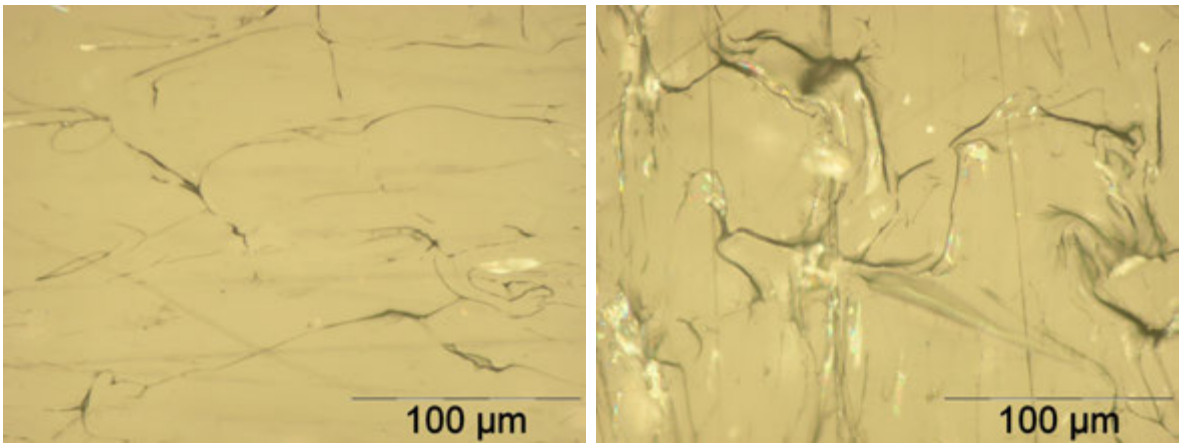

(e) Sample P3 as received; magnification 500x (f) Sample P3 leached out; magnification 500x

Figure 53: Comparison of the smooth side of polymer sample P3: 70G30HSLR BK099 from DuPont before (left) and after (right) leaching test within the Testbed

7 Outlook: Test system for the gas circuits

Outgoing from the testbed for the cooling circuit, one major question occurs in thinking about the design of such a test system: Does it make sense to stay in the liquid phase or should be tested in the gas phase? In the liquid phase with DI water as medium for testing one would assume higher contamination rates as in a dry gas atmosphere. On the other hand if there are hot condensing conditions the amount of species leached out of polymers might be similar or below the liquid phase at comparable temperature. But in case of corrosion it might be worse. Steam condensate which is able to absorb oxygen from air is known to be very corrosive to steel surfaces. Highly aggressive differential aeration cells can be created above 50 °C (pitting corrosion) [16]. This may also be enhanced stress conditions for other metal surfaces. While the latter issue is related to components in proximity of the cathode compartment, the situation is different at the anode side where hydrogen is present. Further, pH values of 2-4 are known to be present in fuel cell stacks [38]. Product water pH ranges from of 3-7 [39] and can even reach lower values depending on operating conditions. Therefore pH value of the condensing water is a parameter which may be addressed. Because of the fundamental difference between the liquid and the gaseous phase especially in combination with humidified hydrogen or air it would make more sense to stay in the gas phase for this test system. In the case of testing only polymeric materials the liquid phase might be an option.

7.1 Proposal for design and testing procedure gas phase

In this section a more qualitative description is given about a possible design and testing procedure. Basically the system would contain of a closed loop according to proposals for enhancement of the coolant testbed in Section 3.6. Main components within the loop are: heater, circulation pump, humidifier, sensors (temperature, volume flow, pressure) and actuators (valves). Further components may be: (1) conductivity measurement of condensate, (2) extraction unit for water analysis, (3) elements for partial cooling of system components (e.g. test object, conductivity measurement) to cause condensation like a cold trap, (4) analysis unit (see below), (5) DI water barrel and pump for system purge and humidification, (6) gas bottles with hydrogen / oxygen and pressure regulation, (7) unit for pH value regulation,

To achieve accelerated testing conditions the temperature level should be chosen close to the upper limit of possible temperatures in the gas circuits, as well as humidity and pressure. The following parameters could possibly be modified:

- Test medium: hydrogen / oxygen / air
- Humidity: medium / high / condensing
- pH value: acidic / neutral
- Duration of test
- Flow rate, pressure, temperature

Therefore the output of this test system would be a list of materials/components with possible applications and positions in a fuel cell system. The test objects may be classified as (i) applicable for gas loops under condensing (100 % R.H.) conditions or (ii) applicable for gas loops under dry or low humidity conditions.

7.2 Analytic methods versus mass loss

At the end of the test there will be an amount of condensate which has to be analyzed. Conductivity can be measurement in any case and can give a first insight in the order of magnitude of contamination. As shown by the comparison of "real mass loss" and calculated TDS values in Section 3.5, the amount of non-ionic species can exceed the amount of ionic species significantly. This is also confirmed by literature data [13], where conductivity and total organic carbon (TOC) was measured. In some cases samples showed low conductivities while the TOC value was high. Therefore a characterizing index for leaching properties of polymers was defined as the sum of TOC and solution conductivity. It was shown, that this "leaching index" correlated with voltage loss [40]. It is also proposed as a quick an easy screening method for fuel cell developers to check their BOP materials [40]. Therefore evaluation of leaching index seems to be a reasonable method for screening polymer materials. However, an alternative to the leaching index would be the mass loss of the samples. Therefore the materials can be just weighed before and after the leaching test and the corresponding mass loss can be evaluated as shown in Section 3.5. In case of a test component the evaluation of mass loss may be not possible, therefore the TDS value of the solution could be evaluated by gravimetry whereas the latter needed to be evaluated if applicable. For more precise characterization additional analysis methods have to be applied to identify all involved species. Usually several analytic methods are used to characterize polymers and their contamination potential. For example inductively coupled plasma optical emission spectroscopy (ICP-OES) for elemental analysis, liquid gas chromatography mass spectrometry (GCMS) for analysis of organic compounds and ion chromatography (IC) to identify ionic species. Then the

next step would be to compare the species with a database of known species effecting low temperature PEM fuel cell performance, which can be a problem for organic substances due to their large variety. Various organic species were found in leachant solutions and isolated model compounds where studied. These show less voltage loss than the combination with other species as typically found in leachant solutions [12, 41]. This indicates that detailed analysis of the contamination potential of a certain material can be very complex.

8 Summary

The function principle of a low temperature PEM fuel cell (LT-PEM-FC) was described. An overview of a PEM fuel cell system which includes balance of plant (BOP) components was given. LT-PEM-FCs and contamination was introduced which includes contamination sources, impacts and mechanisms for the cooling circuit as well as for the gas circuits. Basics of conductivity measurements including proton transport in aqueous solutions and CO_2 induced conductivity increase were described. A model for calculating the contribution of various ambient concentrations of CO_2 to conductivity of pure water was used. The design of a test system for material compatibility for the coolant loop of a LT-PEM-FC system its measurement procedure and evaluation method were described. Analysis of the reference measurements in combination with after treatment of possible ion sources in the system was done and showed a slightly decrease in variation of conductivity increase rates. Residual amounts of BASF coolant in fresh DI water showed high conductivity increase rates up to $4.5\,\mu$S/cm/day. The average value over of conductivity increase rates decreased from $3.7\,\mu$S/cm/day to $1.5\,\mu$S/cm/day over 53 reference measurements. A CO_2 degassing procedure was implemented and showed reproducible shape of reference measurements with pure DI water. Reference measurement with BASF coolant showed upward bending over time period of one week which was not understood completely. Evaluation of the testbed by reference materials showed that the values $\kappa_{end}^{nrel-corr}$ of samples PLS90G30DR BK099 (P1) and 70G30HSLR BK099 (P3) are smaller than the literature values by a factor of about 3-4, HR5330HF BK503 (S1) by a factor of 11 and HTN51G35HSLR BK420 (S2) by a factor of 5. The values κ_{end}^{nrel} of samples P1, P3, S1 and S2 by a factor of abut 2. Both values of sample PLS95G35DH1 BK549 (P2) exceed the literature value by a factor of about 3 for sample R7-120 BL (S5) by a factor of 11. The high conductivity value of S5 is assumed to be caused by a crack of the sample which increased its surface area significantly. This can be concluded as a poor match. For sample 6130 NC010 (S3) the values fit better, especially $\kappa_{end}^{nrel-corr}$. The literature value of R4-200 BL (S4) also shows a better fit. The relative mass loss of the test in the testbed was 0.47 % for P1, 1.7 % for P2 and 0.56 % for P3. The conductivity after the one hour boiling test was $15.7\,\mu$S/cm the relative mass loss was 0.018 %. The six weeks leaching tests showed conductivities which were lower than literature by a factor of about 2 for P1, P3 and S2. S1 is smaller by a factor of 9. P2 and S3 exceeded literature by a factor of 3. A good match was found for S4 and S5. The relative mass loss of the six weeks leaching test was 0.63 % for P1, 2.46 % for P2 and 0.71 % for P3. The relative mass loss of S1-S5 indicated insufficient drying conditions. The conduc-

tivities of the one week leaching tests were lower for all samples compared to the six weeks leaching tests. The conductivities of another batch was reproducible for P1 and P2. The second batch of P3 was not reproducible. Changes of surface area to volume of water ratio showed a linear behavior. For BASF coolant the increase in conductivity was lower. Non-colored materials show the influence of additives. Degassing tests of DI water decreases conductivity by 1.5 μS/cm. Traces of ethylene glycol effect the CO_2 degassing and back-diffusion process. In stainless steel corrosion tests in DI water no effect of bimetallic corrosion was found, but corrosion related to the surface quality was found. PFA bottles contribute to conductivity in DI water at 90 °C. Analytic results were comparable to literature and could be attributed to glass reinforcement, additives and fillers. Optical investigations of P1-P3 showed higher roughness of the surfaces after the extraction tests.

9 List of used materials an equipment

- Lab balance: Sartorius Entris ENTRIS224I-1S; Reproducibility 0.1 mg, Linearity 0.2 mg
- Microscope: Olympus BX-51
- Conductivity meter: WTW Multi 3410 SET E + measuring cell LR 925/01
- pH meter: WTW Multi 3410 SET E + pH-Sensor SenTix® 980, accuracy < 5 % RD
- Conductivity meter: XS Instruments Cond 70, accuracy < 1 % FS (Scales 0...200, 200...2000)
- Conductivity measurement in testbed: Mettler Toledo M300 ISM 1K 1/4 DIN Thornton Transmitter + measuring cell ISM 1/2" NPT 0,1C Ti 29mm, accuracy < 5 % RD
- Deionized water: received from AVL fuel cell lab (Apparatus TKA-LAB-UPW)
- BASF fuel cell coolant: Glysantin® FC G 20-00/50; Composition: 45-55 % (mono) ethylene glycol with inhibitors in DI water
- ICP-OES 5100 Agilent Technologies
- HPLC (HP1050, Agilent 1100)

10 Appendix

10.1 Uncertainty analysis

Section 4.1.2 and 4.1.3:

The measurement error of the scale Δ_{scale} is 0.2 mg. The uncertainties (maximum error) for the relative mass loss and the theoretical dry sample mass can be calculated by

$$\Delta_{\Delta m_{Ref}^{rel}} = \left| \frac{1}{m_{Ref,dry}} \right| \Delta_{scale} + \left| \frac{m_{Ref,new}}{(m_{Ref,dry})^2} \right| \Delta_{scale} \tag{43}$$

$$\Delta_{m_{Sample,dry}^{theoretical}} = \left| \frac{1}{\Delta m_{Ref}^{rel}} \right| \Delta_{scale} + \left| \frac{m_{new}}{(\Delta m_{Ref}^{rel})^2} \right| \Delta_{\Delta m_{Ref}^{rel}} \tag{44}$$

the uncertainty for the corrected mass loss is

$$\Delta_{\Delta m_{Corr}} = \Delta_{m_{Sample,dry}^{theoretical}} + \Delta_{scale} \tag{45}$$

and for the relative corrected mass loss

$$\Delta_{m_{Corr}^{rel}} = \frac{\Delta_{\Delta m_{Corr}}}{m_{Sample,dry}^{theoretical}} \cdot 100 \tag{46}$$

10.2 Measurement protocols of tested polyamide materials

Measurement protocols of tested polyamide materials can be seen in Figures 54, 55, 56, 57, 58, 59, 60

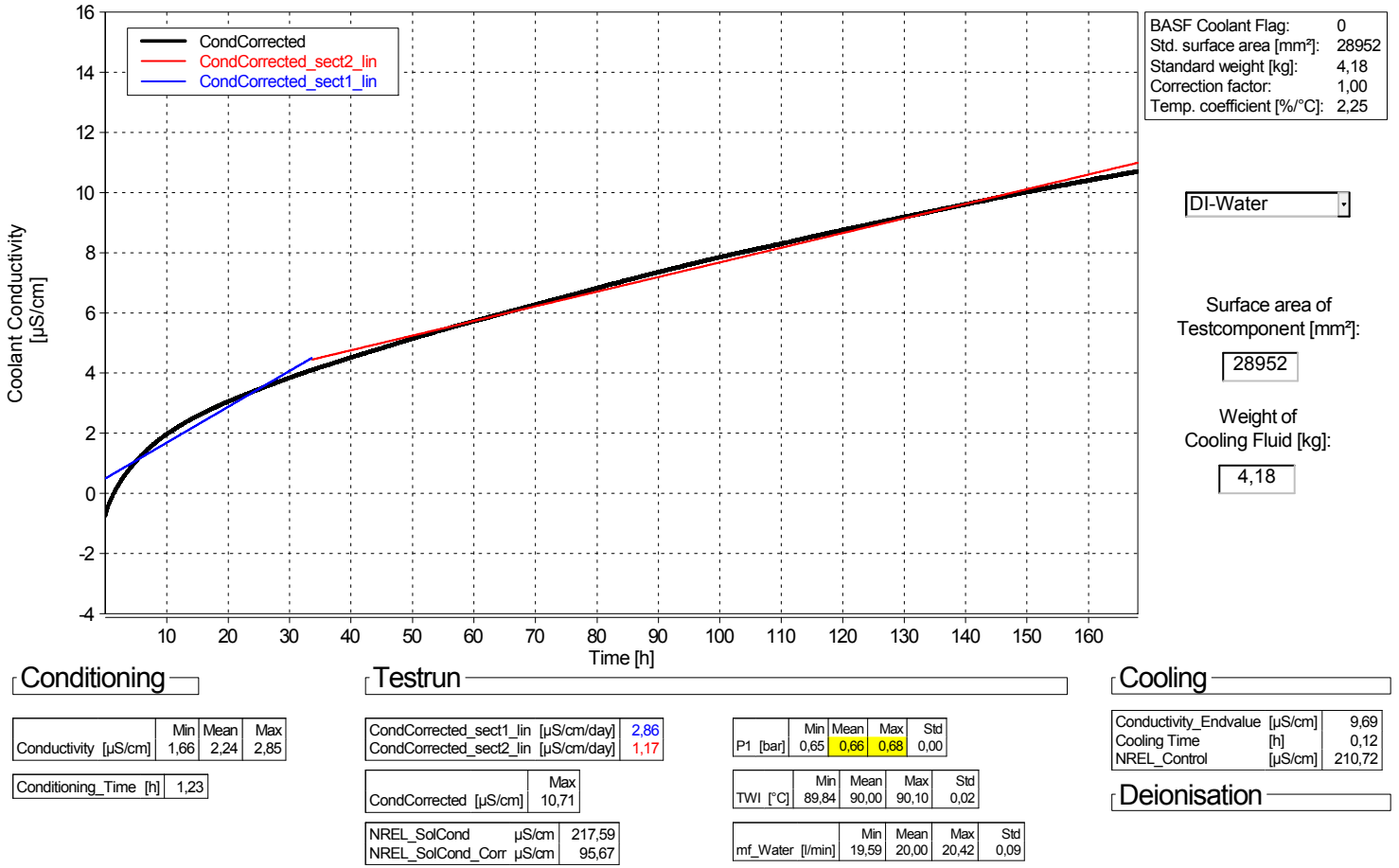

Test Object Parameters

Component / Material
Polyamide
Manufacturer / Supplier
DuPont
Grade / ID Number.Meas ID
PLS90G30DR BK099.861

Test Parameters

Duration of Test
168 (h)
Beginning Date
2016-03-22
System Parameters
SYS_FC_Conditioning_TB_V03
TFP_FC_Conditioning_TB_V2
Cooling_TB_14

Figure 54: Measurement protocol of polyamide sample P1

MEASUREMENT PROTOCOL MATERIALCOMPATIBILITY

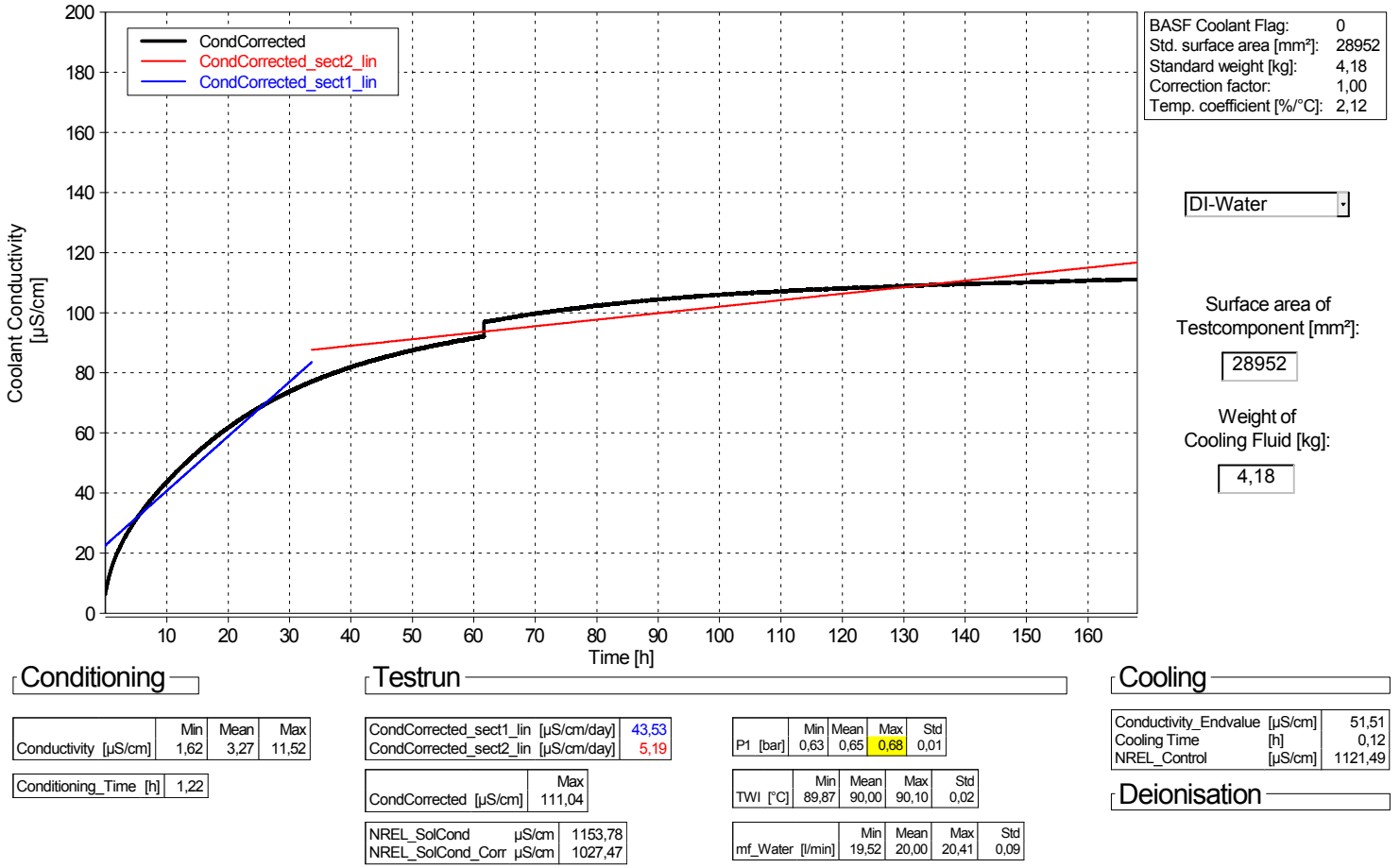

BASF Coolant Flag:	0
Std. surface area [mm²]:	28952
Standard weight [kg]:	4,18
Correction factor:	1,00
Temp. coefficient [%/°C]:	2,12

DI-Water

Surface area of Testcomponent [mm²]:

28952

Weight of Cooling Fluid [kg]:

4,18

Test Object Parameters

Component / Material
Polyamide
Manufacturer / Supplier
DuPont
Grade / ID Number.Meas ID
PLS95G35DH1 BK549.864

Test Parameters

Duration of Test
168 (h)
Beginning Date
2016-03-30
System Parameters
SYS_FC_Conditioning_TB_V03
TFP_FC_Conditioning_TB_V2
Cooling_TB_14

Conditioning

	Min	Mean	Max
Conductivity [µS/cm]	1,62	3,27	11,52

Conditioning_Time [h]	1,22

Testrun

CondCorrected_sect1_lin [µS/cm/day]	43,53
CondCorrected_sect2_lin [µS/cm/day]	5,19

	Max
CondCorrected [µS/cm]	111,04

NREL_SolCond	µS/cm	1153,78
NREL_SolCond_Corr	µS/cm	1027,47

	Min	Mean	Max	Std
P1 [bar]	0,63	0,65	0,68	0,01

	Min	Mean	Max	Std
TWI [°C]	89,87	90,00	90,10	0,02

	Min	Mean	Max	Std
mf_Water [l/min]	19,52	20,00	20,41	0,09

Cooling

Conductivity_Endvalue	[µS/cm]	51,51
Cooling Time	[h]	0,12
NREL_Control	[µS/cm]	1121,49

Deionisation

Figure 55: Measurement protocol of polyamide sample P2

MEASUREMENT PROTOCOL MATERIALCOMPATIBILITY

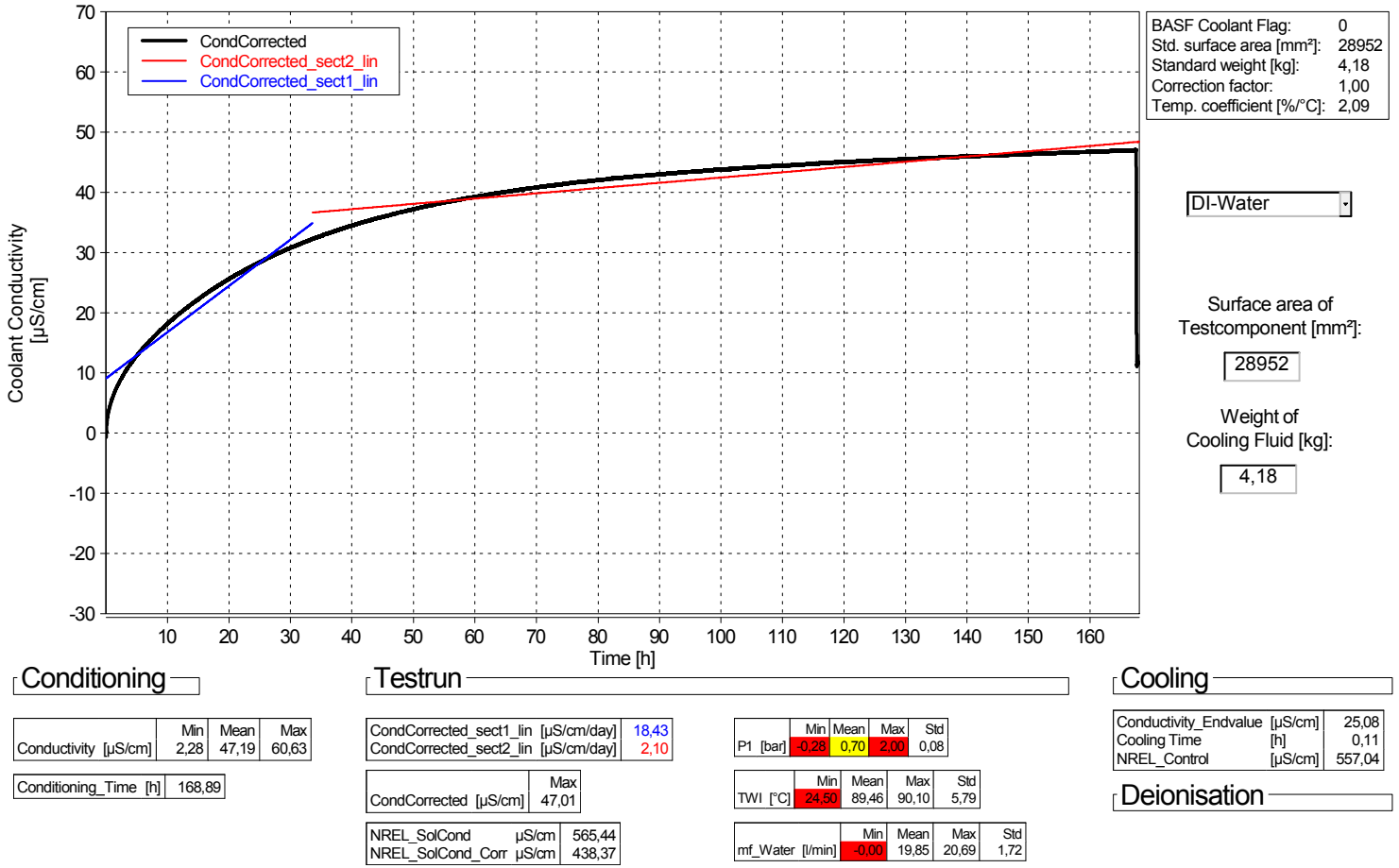

BASF Coolant Flag:	0
Std. surface area [mm²]:	28952
Standard weight [kg]:	4,18
Correction factor:	1,00
Temp. coefficient [%/°C]:	2,09

DI-Water

Surface area of Testcomponent [mm²]:
28952

Weight of Cooling Fluid [kg]:
4,18

Test Object Parameters

Component / Material
Polyamide
Manufacturer / Supplier
DuPont
Grade / ID Number.Meas ID
70G30HSLR BK099.871

Test Parameters

Duration of Test
169 (h)
Beginning Date
2016-04-11
System Parameters
SYS_FC_Conditioning_TB_V03
TFP_FC_Conditioning_TB_V2
Cooling_TB_14

Conditioning

	Min	Mean	Max
Conductivity [µS/cm]	2,28	47,19	60,63

Conditioning_Time [h]	168,89

Testrun

CondCorrected_sect1_lin [µS/cm/day]	18,43
CondCorrected_sect2_lin [µS/cm/day]	2,10

	Max
CondCorrected [µS/cm]	47,01

NREL_SolCond µS/cm	565,44
NREL_SolCond_Corr µS/cm	438,37

	Min	Mean	Max	Std
P1 [bar]	-0,28	0,70	2,00	0,08

	Min	Mean	Max	Std
TWI [°C]	24,50	89,46	90,10	5,79

	Min	Mean	Max	Std
mf_Water [l/min]	-0,00	19,85	20,69	1,72

Cooling

Conductivity_Endvalue	[µS/cm]	25,08
Cooling Time	[h]	0,11
NREL_Control	[µS/cm]	557,04

Deionisation

Figure 56: Measurement protocol of polyamide sample P3

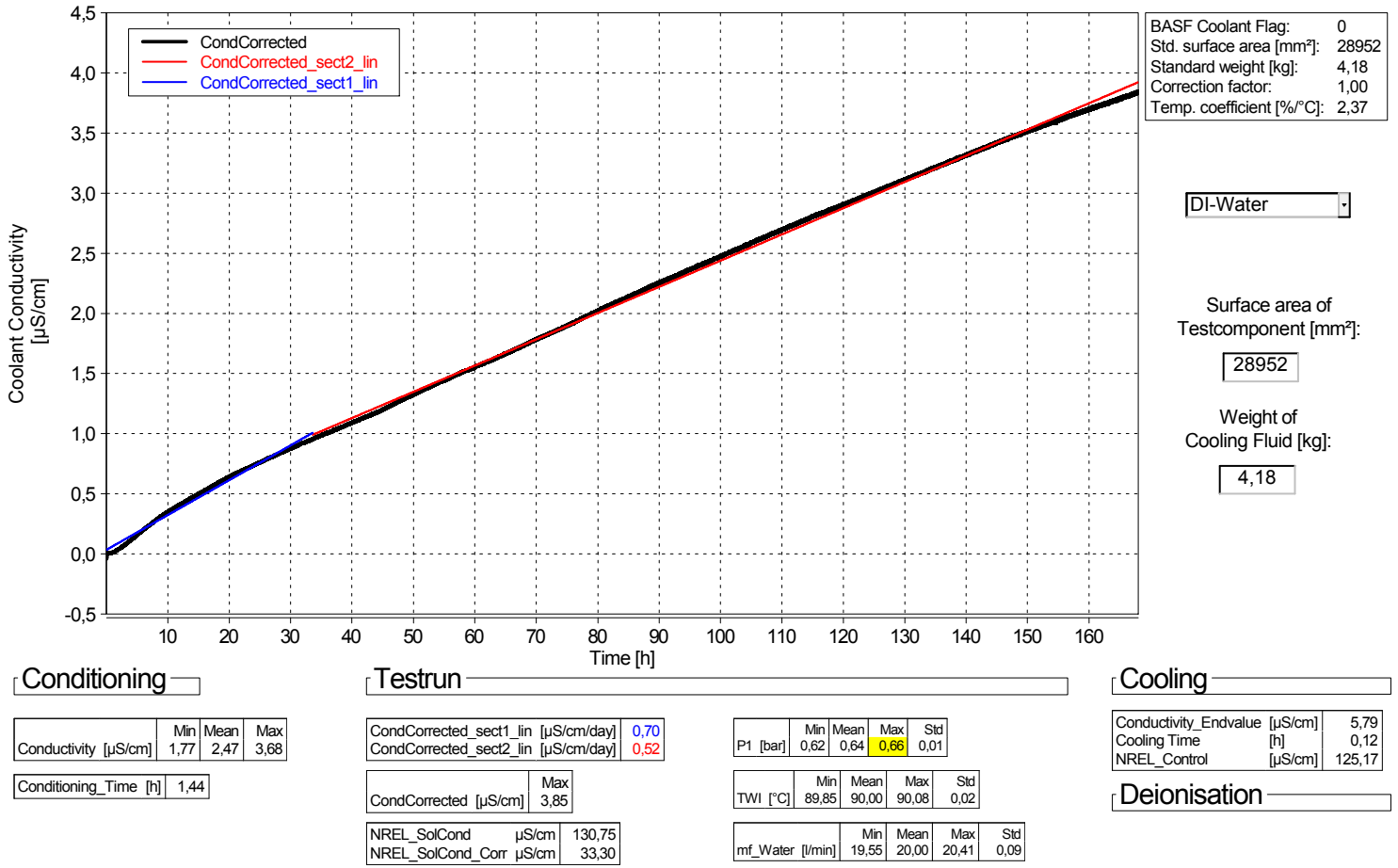

BASF Coolant Flag:	0
Std. surface area [mm²]:	28952
Standard weight [kg]:	4,18
Correction factor:	1,00
Temp. coefficient [%/°C]:	2,37

DI-Water

Surface area of Testcomponent [mm²]: 28952

Weight of Cooling Fluid [kg]: 4,18

Test Object Parameters

Component / Material
PBT (Crastin)
Manufacturer / Supplier
DuPont
Grade / ID Number.Meas ID
HR5330HF BK503.880

Test Parameters

Duration of Test
168 (h)
Beginning Date
2016-04-22
System Parameters
SYS_FC_Conditioning_TB_V03
TFP_FC_Conditioning_TB_V2
Cooling_TB_14

Conditioning

	Min	Mean	Max
Conductivity [µS/cm]	1,77	2,47	3,68

Conditioning_Time [h]	1,44

Testrun

CondCorrected_sect1_lin [µS/cm/day]	0,70
CondCorrected_sect2_lin [µS/cm/day]	0,52

	Min	Mean	Max	Std
P1 [bar]	0,62	0,64	0,66	0,01

	Max
CondCorrected [µS/cm]	3,85

	Min	Mean	Max	Std
TWI [°C]	89,85	90,00	90,08	0,02

NREL_SolCond µS/cm	130,75
NREL_SolCond_Corr µS/cm	33,30

	Min	Mean	Max	Std
mf_Water [l/min]	19,55	20,00	20,41	0,09

Cooling

Conductivity_Endvalue	[µS/cm]	5,79
Cooling Time	[h]	0,12
NREL_Control	[µS/cm]	125,17

Deionisation

Figure 57: Measurement protocol of polyamide sample S1

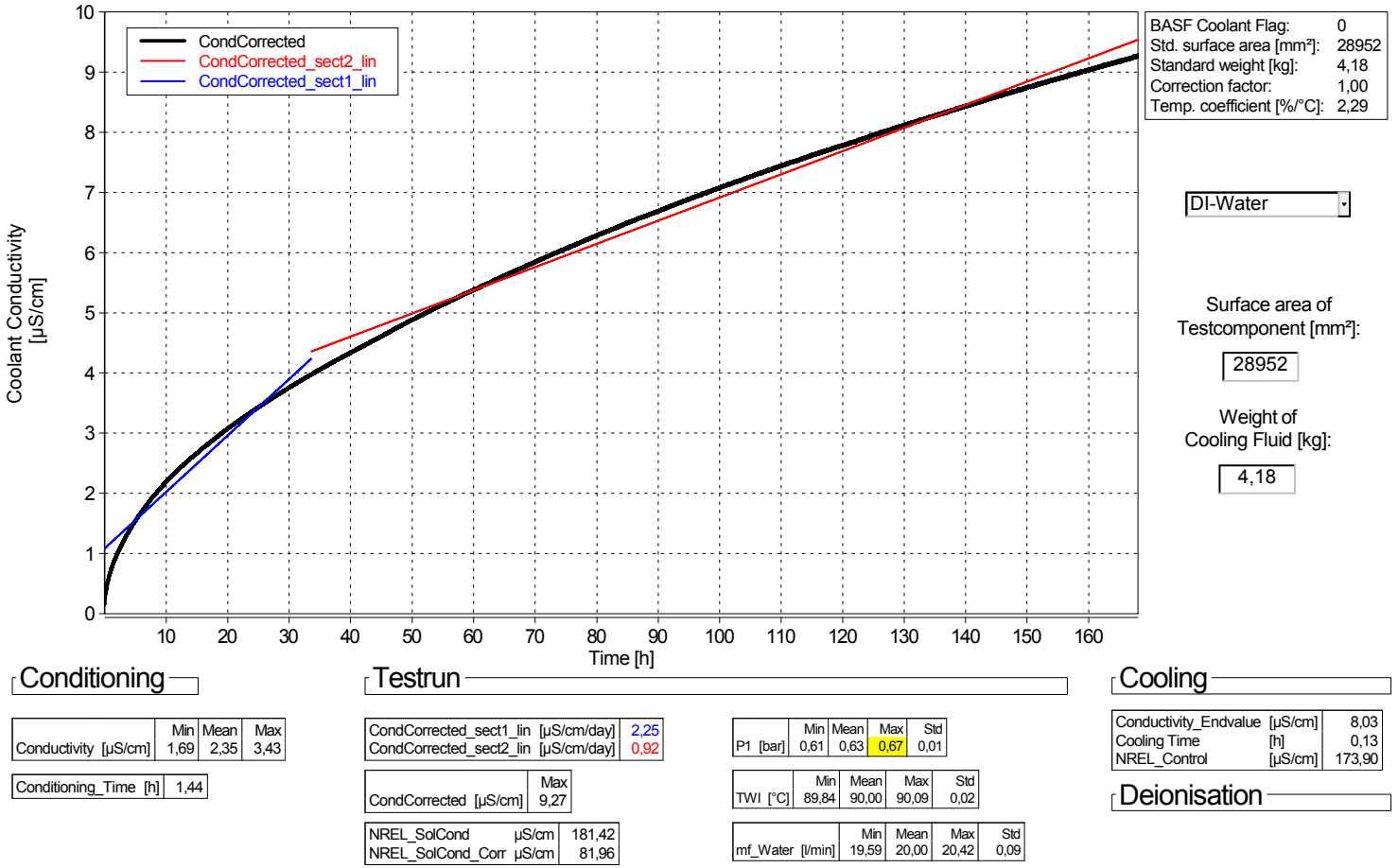

Test Object Parameters

Component / Material
PPA (Zytel)
Manufacturer / Supplier
DuPont
Grade / ID Number.Meas ID
HTN51G35HSLR BK420.887

Test Parameters

Duration of Test
168 (h)
Beginning Date
2016-05-02
System Parameters
SYS_FC_Conditioning_TB_V03
TFP_FC_Conditioning_TB_V2
Cooling_TB_14

Figure 58: Measurement protocol of polyamide sample S2

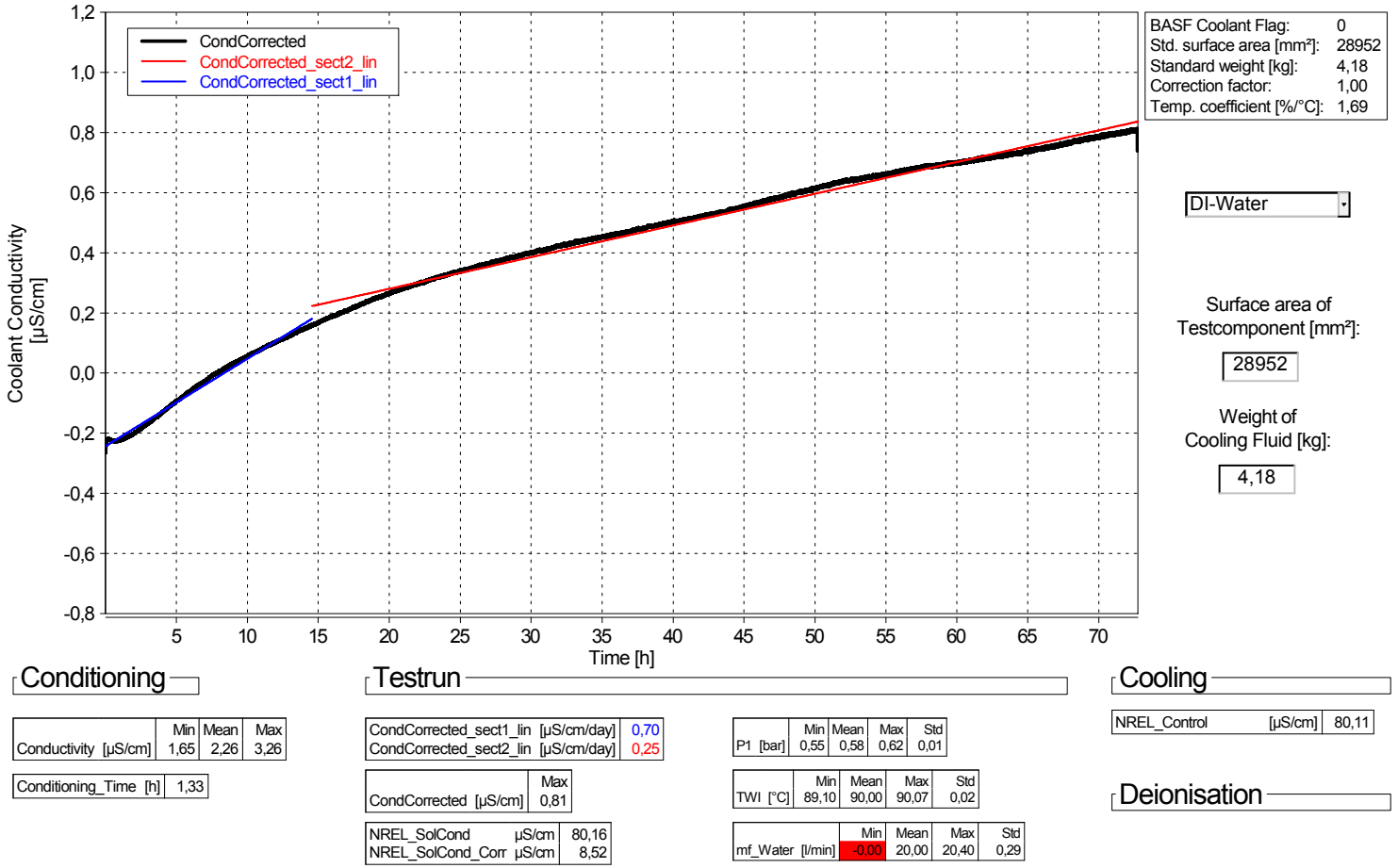

BASF Coolant Flag:	0
Std. surface area [mm²]:	28952
Standard weight [kg]:	4,18
Correction factor:	1,00
Temp. coefficient [%/°C]:	1,69

DI-Water

Surface area of Testcomponent [mm²]: 28952

Weight of Cooling Fluid [kg]: 4,18

Test Object Parameters

Component / Material
PBT (Crastin)
Manufacturer / Supplier
DuPont
Grade / ID Number.Meas ID
6130 NC010.892

Test Parameters

Duration of Test
73 (h)
Beginning Date
2016-05-10
System Parameters
SYS_FC_Conditioning_TB_V03
TFP_FC_Conditioning_TB_V2
Cooling_TB_14

Conditioning

	Min	Mean	Max
Conductivity [µS/cm]	1,65	2,26	3,26

Conditioning_Time [h]	1,33

Testrun

CondCorrected_sect1_lin [µS/cm/day]	0,70
CondCorrected_sect2_lin [µS/cm/day]	0,25

	Max
CondCorrected [µS/cm]	0,81

NREL_SolCond µS/cm	80,16
NREL_SolCond_Corr µS/cm	8,52

	Min	Mean	Max	Std
P1 [bar]	0,55	0,58	0,62	0,01

	Min	Mean	Max	Std
TWI [°C]	89,10	90,00	90,07	0,02

	Min	Mean	Max	Std
mf_Water [l/min]	-0,00	20,00	20,40	0,29

Cooling

NREL_Control [µS/cm]	80,11

Deionisation

Figure 59: Measurement protocol of polyamide sample S3/1

MEASUREMENT PROTOCOL MATERIALCOMPATIBILITY

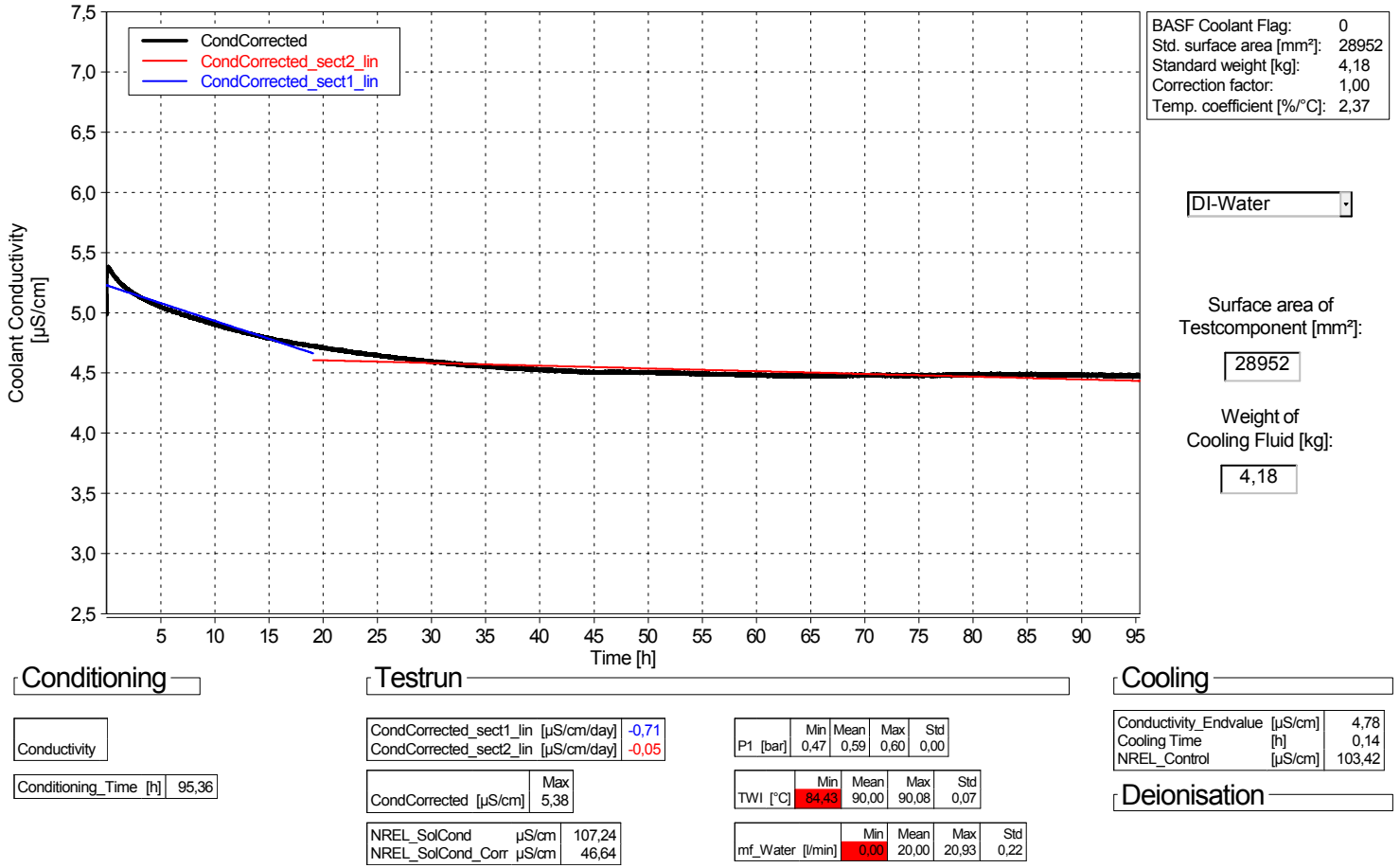

Test Object Parameters

Component / Material
PBT (Crastin)
Manufacturer / Supplier
DuPont
Grade / ID Number.Meas ID
6130 NC010.893

Test Parameters

Duration of Test
95 (h)
Beginning Date
2016-05-13
System Parameters
SYS_FC_Conditioning_TB_V03
TFP_FC_Conditioning_TB_V2
Cooling_TB_14

Figure 60: Measurement protocol of polyamide sample S3/2

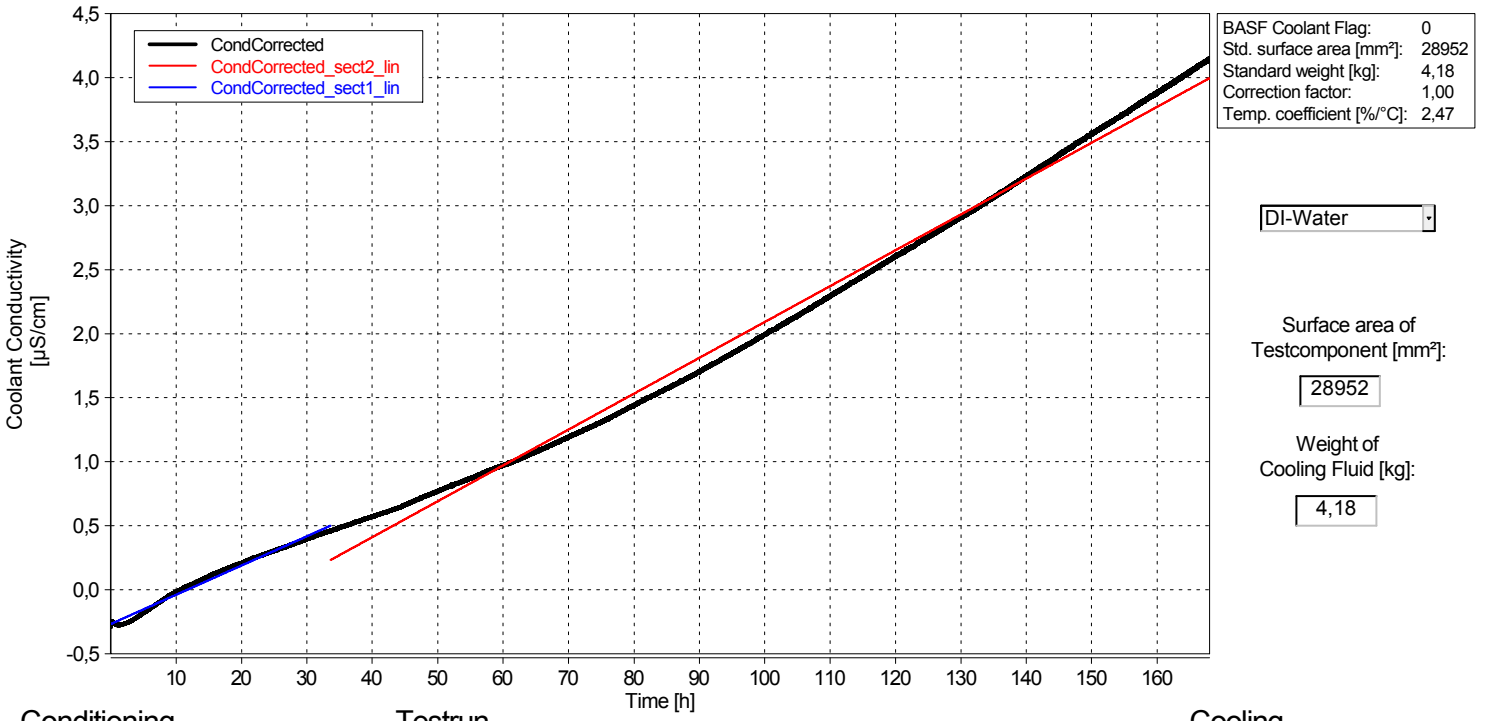

BASF Coolant Flag:	0
Std. surface area [mm²]:	28952
Standard weight [kg]:	4,18
Correction factor:	1,00
Temp. coefficient [%/°C]:	2,47

DI-Water

Surface area of Testcomponent [mm²]: 28952

Weight of Cooling Fluid [kg]: 4,18

Test Object Parameters

Component / Material
PPS (Ryton)
Manufacturer / Supplier
Chevron Phillips
Grade / ID Number.Meas ID
R4-200 BL.897

Test Parameters

Duration of Test
168 (h)
Beginning Date
2016-05-17
System Parameters
SYS_FC_Conditioning_TB_V03
TFP_FC_Conditioning_TB_V2
Cooling_TB_14

Conditioning

	Min	Mean	Max
Conductivity [µS/cm]	1,58	2,17	3,12

Conditioning_Time [h]	1,32

Testrun

CondCorrected_sect1_lin [µS/cm/day]	0,55
CondCorrected_sect2_lin [µS/cm/day]	0,67

	Max
CondCorrected [µS/cm]	4,15

NREL_SolCond	µS/cm	129,92
NREL_SolCond_Corr	µS/cm	34,99

	Min	Mean	Max	Std
P1 [bar]	0,61	0,63	0,70	0,02

	Min	Mean	Max	Std
TWI [°C]	89,84	90,00	90,10	0,02

	Min	Mean	Max	Std
mf_Water [l/min]	19,57	20,00	20,43	0,09

Cooling

Conductivity_Endvalue	[µS/cm]	5,73
Cooling Time	[h]	0,13
NREL_Control	[µS/cm]	123,43

Deionisation

Figure 61: Measurement protocol of polyamide sample S4

MEASUREMENT PROTOCOL MATERIALCOMPATIBILITY

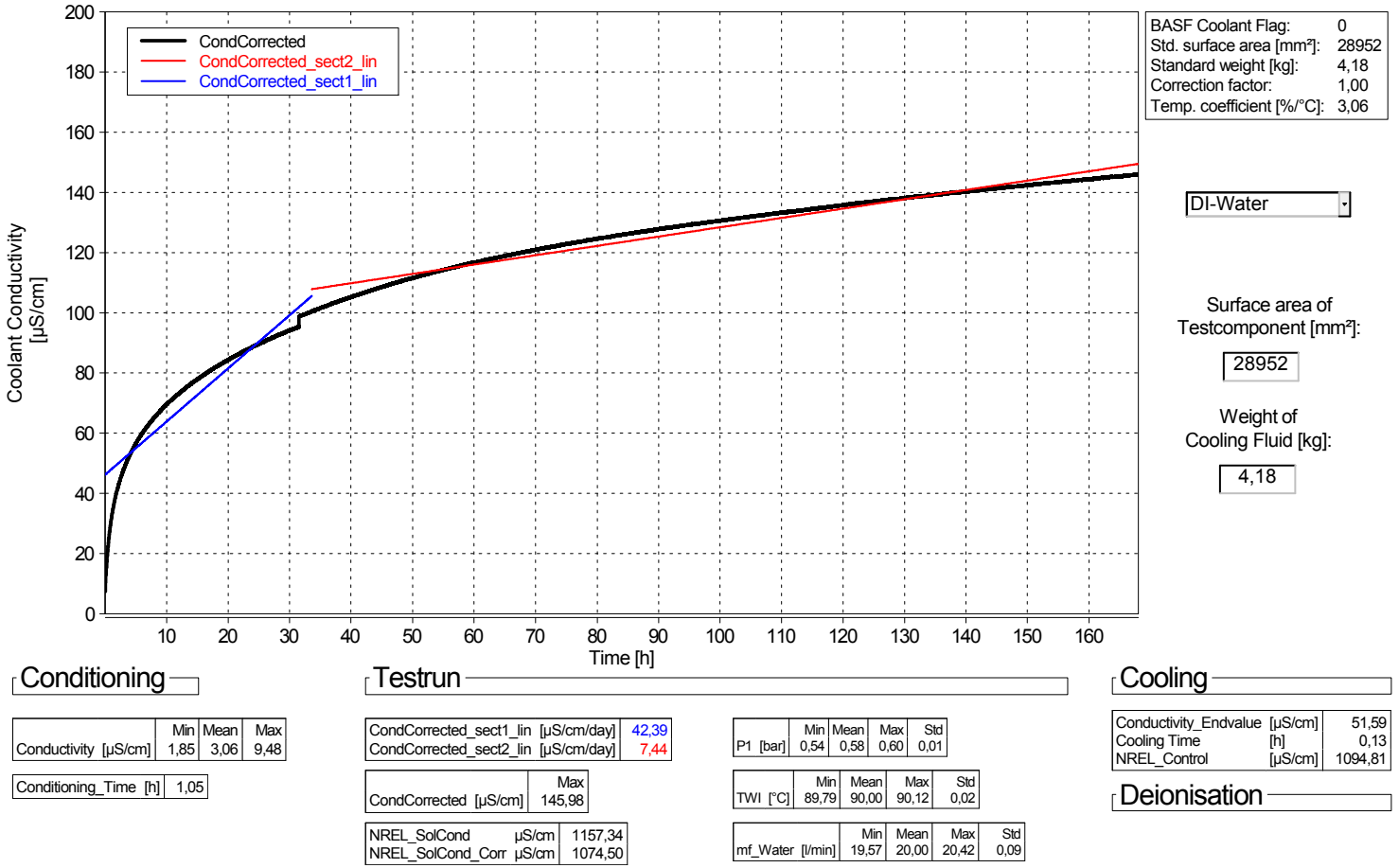

BASF Coolant Flag:	0
Std. surface area [mm²]:	28952
Standard weight [kg]:	4,18
Correction factor:	1,00
Temp. coefficient [%/°C]:	3,06

DI-Water

Surface area of Testcomponent [mm²]:

28952

Weight of Cooling Fluid [kg]:

4,18

Test Object Parameters

Component / Material
PPS (Ryton)
Manufacturer / Supplier
Chevron Phillips
Grade / ID Number.Meas ID
R7-120 BL.900

Test Parameters

Duration of Test
168 (h)
Beginning Date
2016-05-24
System Parameters
SYS_FC_Conditioning_TB_V03
TFP_FC_Conditioning_TB_V2
Cooling_TB_14

Conditioning

	Min	Mean	Max
Conductivity [µS/cm]	1,85	3,06	9,48

Conditioning_Time [h]	1,05

Testrun

CondCorrected_sect1_lin [µS/cm/day]	42,39
CondCorrected_sect2_lin [µS/cm/day]	7,44

	Max
CondCorrected [µS/cm]	145,98

NREL_SolCond	µS/cm	1157,34
NREL_SolCond_Corr	µS/cm	1074,50

	Min	Mean	Max	Std
P1 [bar]	0,54	0,58	0,60	0,01

	Min	Mean	Max	Std
TWI [°C]	89,79	90,00	90,12	0,02

	Min	Mean	Max	Std
mf_Water [l/min]	19,57	20,00	20,42	0,09

Cooling

Conductivity_Endvalue	[µS/cm]	51,59
Cooling Time	[h]	0,13
NREL_Control	[µS/cm]	1094,81

Deionisation

Figure 62: Measurement protocol of polyamide sample S5

References

[1] Guangsheng Zhang and Satish G. Kandlikar, "A critical review of cooling techniques in proton exchange membrane fuel cell stacks," *International journal of hydrogen energy*, 2011.

[2] M. R. Islam, B. Shabani, G. Rosengarten, and J. Andrews, "The potential of using nanofluids in pem fuel cell cooling systems: A review," *Renewable and Sustainable Energy Reviews*, vol. 48, pp. 523–539, 2015.

[3] Kabza A., "PEMFC - proton exchange membrane fuel cell: Informationen zum Thema Brennstoffzelle." `http://pemfc.de/`, 2015.

[4] S. G. Kandlikar and Z. Lu, "Thermal management issues in a pemfc stack – a brief review of current status," *Applied Thermal Engineering*, vol. 29, no. 7, pp. 1276–1280, 2009.

[5] P. Corbo, F. Migliardini, and O. Veneri, *Fuel Cells for Automotive Applications*. Springer-Verlag London, 2011.

[6] F. Barbir, *PEM fuel cells: Theory and practice*. Waltham, MA: Academic Press, 2nd ed. ed., 2013.

[7] Xuan Cheng, "A review of pem hydrogen fuel cell contamination: Impacts, mechanisms, and mitigation," *Elsevier*, 2007.

[8] Pyoungho Choi, "Thermodynamics and proton transport in nafion: Ii. proton diffusion mechanisms and conductivity," *Journal ofThe Electrochemical Society*, no. 152, pp. E123–E130, 2005.

[9] P. Corbo, F. Migliardini, and O. Veneri, *Design of Hydrogen Fuel Cell Systems for Road Vehicles*. Springer-Verlag London, 2011.

[10] B. D. James, J. A. Kalinoski, and K. N. Baum, "Mass production cost estimation for direct h2 pem fuel cell systems for automotive applications. 2009 update," 2010.

[11] H. Dominghaus, P. Elsner, P. Eyerer, and T. Hirth, eds., *Kunststoffe: Eigenschaften und Anwendungen ; mit 275 Tabellen*. VDI-Buch, Heidelberg u.a: Springer, 8., neu bearb. und erw. aufl. ed., 2012.

[12] Huyen Dinh and National Renewable Energy Laboratory, "Effect of system contaminants on pemfc performance and durability - doe hydrogen and fuel cells program fy 2012 annual progress report," *DOE Hydrogen and Fuel Cells Program*, 2012.

[13] Huyen Dinh, "Material screening data tool." `http://www.nrel.gov/hydrogen/system_contaminants_data/`, 09.12.2014.

[14] DAVID M. GRAY, "A comprehensive look at conductivity measurement in steam and power generation waters," 2006.

[15] C. H. Hamann and W. Vielstich, *Elektrochemie*. Weinheim: Wiley-VCH, 4., vollst. überarb. und aktualisierte aufl. ed., 2005.

[16] D. A. Jones, *Principles and prevention of corrosion*. Upper Saddle River, NJ: Prentice Hall, 2. ed. ed., 1996.

[17] Wikipedia, "Molare Leitfähigkeit." `https://de.wikipedia.org/wiki/Molare_Leitf%C3%A4higkeit`, 25. Juli 2015.

[18] E. Codorniu-Hernández and P. G. Kusalik, "Probing the mechanisms of proton transfer in liquid water," *Proceedings of the National Academy of Sciences of the United States of America*, vol. 110, no. 34, pp. 13697–13698, 2013.

[19] Wikipedia, "Grotthuss mechanism." `https://en.wikipedia.org/wiki/Grotthuss_mechanism`, 1 October 2015.

[20] R. Pawlowicz, "Calculating the conductivity of natural waters," *Limnology and Oceanography: Methods*, vol. 6, pp. 489–501, 2008.

[21] A. Mettler-Toledo AG, "Ein Leitfaden für Leitfähigkeitsmessungen: Theorie und Praxisanwendungen," 2014.

[22] Dr. Pieter Tans, "Trends in atmospheric carbon dioxide." `http://www.esrl.noaa.gov/gmd/ccgg/trends/`, November 5, 2015.

[23] Truman S. Light, "The conductivity of low concentrations of co2 dissolved in ultrapure water from 0-100°c: Paper presented at the 209th american chemical society national meeting, anaheim, ca," 1995.

[24] V. R. Gajevskiy, "Electric conductivity of carbon dioxide aqueous solutions," *Ukrainian Journal of Physics*, vol. 60, no. 3, pp. 258–262, 2015.

[25] R. Sander, "Compilation of henry's law constants (version 4.0) for water as solvent," *Atmospheric Chemistry and Physics*, vol. 15, no. 8, pp. 4399–4981, 2015.

[26] E. Kouril, "Conductivity measurement in high purity water samples below 10 μsiemens/cm." `www.iccontrols.com/files/4-2.pdf`, 2012.

[27] A. H. England, A. M. Duffin, C. P. Schwartz, J. S. Uejio, D. Prendergast, and R. J. Saykally, "On the hydration and hydrolysis of carbon dioxide," *Chemical Physics Letters*, vol. 514, no. 4-6, pp. 187–195, 2011.

[28] Michael Falk, "Infrared spectrum of carbon dioxide in aqueous solution," *Vibrational Spectroscopy*, 1992.

[29] Md. Opu, "Understanding the effects of pemfc contamination from balance of plant assembly aids materials: In situ studies," *Journal of The Electrochemical Society*, 2015.

[30] "Oberflächen von Edelstahlrohren." http://www.tps-technitube.com/downloads/inosindt/inosindt_oberflaechen_de_26.pdf, 2010.

[31] U. Bobe and G. Wildbrett, "Anforderungen an Werkstoffe und Werkstoffoberflächen bezüglich Reinigbarkeit und Beständigkeit," *Chemie Ingenieur Technik*, vol. 78, no. 11, pp. 1615–1622, 2006.

[32] Erica Tran (UCD), Dennis Liu (UCD), "Solubility and factors affecting solubility." http://chemwiki.ucdavis.edu/Core/Physical_Chemistry/Equilibria/Solubilty/Solubility_and_Factors_Affecting_Solubility.

[33] F. S. Serpa, "Solubility of carbon dioxide in ethane-1,2-diol–water mixtures," *Journal of Chemical & Engineering Data*, vol. 58, no. 12, pp. 3464–3469, 2013.

[34] Walter J. ROSSITER, "An investigation of the degradation of aqueous ethylene glycol and propylene glycol solutions using ion chromatography," *Solar Energy Materials*, no. 11, pp. 455–467, 1985.

[35] Huyen Dinh, "An overview of nrel's online data tool for fuel cell system-derived contaminants," 2014.

[36] Huyen Dinh and National Renewable Energy Laboratory, "Effect of system contaminants on pemfc performance and durability - doe hydrogen and fuel cells program fy 2011 annual progress report," *DOE Hydrogen and Fuel Cells Program*, 2011.

[37] Dr. Dmitry Breslavsky, "European steel and alloy grades." http://www.steelnumber.com/.

[38] R. A. Antunes, M. C. L. Oliveira, G. Ett, and V. Ett, "Corrosion of metal bipolar plates for pem fuel cells: A review," *International journal of hydrogen energy*, vol. 35, no. 8, pp. 3632–3647, 2010.

[39] K.H. Hou, "Analysis on the corrosion behavior of al-alloy bipolar plate and ph value of water product for the pemfc," *IPCBEE*, no. 8, pp. 313–317, 2011.

[40] Huyen Dinh and National Renewable Energy Laboratory, "Effect of system contaminants on pemfc performance and durability - doe hydrogen and fuel cells program fy 2014 annual progress report," *DOE Hydrogen and Fuel Cells Program*, 2014.

[41] H. Wang, C. Macomber, and H.N. Dinh: NREL, "Evaluation of pemfc system contaminants on the performance of pt catalyst via cyclic voltammetry: Preprint," *PRIME*, 2012.